CCM-82-05

FIBER ORIENTATION IN CURVILINEAR FLOW

JAMES LINDSAY YORK

CENTER FOR COMPOSITE MATERIALS

College of Engineering
University of Delaware
Newark, Delaware

Date: 7/11/95 Time: 5:21:17PM

Page: 1 Document Name: untitled

1 OF 1

DTIC DOES NOT HAVE THIS ITEM

1 - AD NUMBER: D436986
6 - UNCLASSIFIED TITLE: FIBER ORIENTATION IN CURVILINEAR FLOW,
10 - PERSONAL AUTHORS: YORK,J. L. ;
11 - REPORT DATE: DEC , 1982
12 - PAGINATION: 153P
14 - REPORT NUMBER: CCM-82-05
20 - REPORT CLASSIFICATION: UNCLASSIFIED
21 - SUPPLEMENTARY NOTE: M.S. THESIS SUBMITTED TO THE UNIVERSITY OF DELAWARE.
22 - LIMITATIONS (ALPHA): APPROVED FOR PUBLIC RELEASE; DISTRIBUTION UNLIMITED. AVAILABILITY: CENTER FOR COMPOSITE MATERIALS, UNIVERSITY OF DELAWARE, 208 EVANS HALL, NEWARK, DE. 19711.
33 - LIMITATION CODES: 1 24

END Y FOR NEXT ACCESSION END

FIBER ORIENTATION IN CURVILINEAR FLOW

By

James Lindsay York

Center for Composite Materials
University of Delaware
Newark, Delaware

Sponsored by the

University-Industry Research Program
"Application of Composite Materials
to Industrial Products"

A thesis submitted to the Faculty of the University of Delaware in partial fulfillment of the requirements for the degree of Master of Mechanical and Aerospace Engineering.

December 1982

ABSTRACT

It is well recognized that the material properties in fiber reinforced components are strongly dependent on the fiber orientation. In mold filling processes involving short fiber reinforced composites, fiber orientation occurs as a result of the flow induced stresses. It is important to be able to predict this flow induced orientation.

A numerical method has been developed previously to predict the in-plane fiber orientation in plane flow. This scheme is refined to enable predictions for fiber orientation in axisymmetric flow. The numerical method is verified by comparing numerical and analytical solutions for fiber orientation in Poiseuille flow.

The fiber orientation may be described by certain orientation parameters, which relate the degree of collimation to the material properties. These orientation parameters are incorporated into both the plane and axisymmetric flow algorithms, thus providing a link to available structural analysis routines.

Several numerical examples of practical importance are presented. A prediction for the fiber orientation near molded holes is established by determining the fiber orientation resulting from flow around a circular inclusion. In a further example, the process for molding an axisymmetric disk is simulated to determine the numerically predicted fiber orientation.

TABLE OF CONTENTS

NOMENCLATURE

Roman Symbols

a_3	Coefficient of skewness
b_i	Axes of ellipsoid of revolution
d_{ij} , $\bar{d}_{ij}$	Components of rate of deformation tensor
e_{ijk}	Permutation symbol
g_{ij}	Metric tensor components
f_a	Orientation parameter
f_p	Orientation parameter
g_a	Orientation parameter
g_p	Orientation parameter
H	Height
k	Number of intervals
L	Length
m_i	Number of fibers in i^{th} interval
M_2	Second moment
M_3	Third moment
n	Orientation density function

N	Number of fibers
P_i	i^{th} stream point
r, $\bar{r}$	Radial components of cylindrical coordinate system
R	Radius
r_p	Aspect ratio
u_i , $\bar{u}_i$	Velocity components
x_i , $\bar{x}_i$	Cartesian coordinate components
x_i^o	Fiber axes
y^i	Cylindrical coordinate components
z, $\bar{z}$	Axial components of cylindrical coordinate system
z_i , $\bar{z}_i$	Vorticity components

Greek Symbols

α	Orientation angle
α_i	Orientation angle associated with i^{th} fiber
α°	Mode angle
β	Orientation angle
β_i	Orientation angle associated with i^{th} fiber
δ	Offset angle
γ	Angle descriptor for orientation density function
Γ	Strain rate

ψ	Stream function
ψ_i	Stream function value
ϕ_1	Orientation angle
ϕ_{1_i}	Orientation angle associated with i^{th} fiber
ϕ_1°	Mode angle
$<\phi_1>$	Mean of a continuous distribution
$\bar{\phi}_1$	Mean of the orientations of a finite number of fibers
θ, $\bar{\theta}$	Cylindrical coordinates
θ_1	Orientation angle
τ_{ij}	Shear stress components
ω_{ij} , $\bar{\omega}_{ij}$	Vorticity components
ζ	Angle descriptor for orientation density function

LIST OF ILLUSTRATIONS

LIST OF TABLES

CHAPTER 1. INTRODUCTION

Composite materials are becoming widely used, especially for aerospace applications where stiff, strong lightweight materials are required. However, traditional hand lay-up methods for fabricating composite materials are expensive and time-consuming and, hence, can only be used when increased structural performance outweighs cost requirements. With the advent of less expensive fabrication techniques, composites are becoming sound economic alternatives for many other applications.

One promising inexpensive fabrication method is injection molding, a process in which a plasticized charge is forced under pressure into the cavity of a closed die where it (the charge) is formed into the shape of that cavity. During this mold filling process, fiber alignment occurs due to fluid stresses induced by the flow. Since the material properties and strength of the resulting component part are strongly dependent on the orientation of the fibers, it is essential to be able to predict this flow induced fiber orientation.

An early attempt to predict flow-induced orientation was performed by Jeffery [9]. Jeffery developed equations describing the motion of a single ellipsoidal particle immersed in a Newtonian fluid. Goldsmith and Mason [7] have used Jeffery's equations to solve for the orientation of ellipsoidal particles in both Couette and hyperbolic radial flows. Based on Goldsmith and Mason's predictions for orientation in hyperbolic radial flow, Goettler et al. [6] presented a new manufacturing concept for producing short fiber reinforcement in extruded rubber hoses in a one-step fabrication process. Their idea was to alter the die design such that a constriction of the flow occurs at some intermediate point, followed by an expansion to form the dimensions of the final product. In the region of expansion, fiber orientation occurs in the hoop direction, thus providing the necessary reinforcement. The work by Goettler et al. represents one of the early attempts to control the orientation in short fiber molded components based on analytical techniques.

Givler [5] has developed a numerical method to predict in-plane fiber orientation in plane flow. The method consists of solving the flow equations via the finite element method and, subsequently, numerically integrating Jeffery's equations to determine fiber orientation. Givler's work represents a first attempt to develop a

general method for determining fiber orientation, although it is restricted to in-plane fibers in plane flow.

Once the fiber orientation is determined, material properties may be predicted. Using the "aggregate model," McCullough et al. [13] have shown that two orientation parameters are needed to relate the degree of orientation to the material properties for planar fiber orientation distributions, if the orientation distribution is symmetric about the mode of the distribution. This mode orientation angle serves to isolate the local principal material axes.

The first objective of this work is to determine the orientation parameters and mean orientation angle for the in-plane fiber distributions in plane flow from Givler's numerical orientation scheme, thus linking Givler's algorithm to available structural analysis programs to form a complete numerical system capable of evaluating the influence of mold designs on the performance of molded parts.

The second objective of this work is to determine fiber orientation in axisymmetric flow. In the axisymmetric development, the assumption of planar orientation is lifted. Again, the ultimate goal is to portray the fiber orientation in terms of orientation parameters. A new set of orientation parameters is needed in view of the non-planar distribution assumption. McGee [14] has determined

that four orientation parameters are necessary to compute the material properties for non-planar distributions. It is these four orientation parameters which are determined in the axisymmetric scheme.

The contents of this thesis are organized in the following manner: Chapter 2 introduces Jeffery's orientation equations and briefly summarizes the various assumptions made in the development of these equations. The analysis involved in determining fiber orientation from Jeffery's equations is then explained. Chapter 3 reviews Givler's numerical method for determining the in-plane fiber orientation in plane flow, and introduces algorithms for determining the mean orientation angle and the orientation parameters. Several numerical examples are presented. Chapter 4 develops the numerical method for determining fiber orientation in axisymmetric flow and, subsequently, devises the scheme for computing the non-planar orientation parameters. As in Chapter 3, several numerical examples are included. Results and conclusions, as well as suggestions for further research, are presented in Chapter 5.

CHAPTER 2. GENERAL ORIENTATION EQUATIONS

In this chapter, orientation equations developed by Jeffery [9] are incorporated to solve for fiber orientation. Jeffery formulated equations to determine the motion of a single rigid ellipsoidal particle immersed in a viscous fluid subject to the following assumptions:

1. Apart from the local disturbance near the particle, the fluid motion is steady and varies in space on a scale that is large compared with the dimensions of the particle.

2. The fluid which surrounds the particle is incompressible and Newtonian.

3. The fluid velocity is low; hence, inertia terms may be neglected (creeping flow).

4. The particle is non-sedimenting.

A summary of Jeffery's analysis is presented here. For details, the interested reader is referred to the original reference.

One important conclusion drawn by Jeffery is that

under the above assumptions, the particle ultimately attains the velocity of the fluid which it displaces. This enables one to track the paths taken by particles simply by determining the flow streamlines.

To solve for the particle orientation, a rectangular Cartesian coordinate set of axes x_1^0 , x_2^0 , x_3^0 , fixed in the particle, is defined such that the surface of the ellipsoid is described by the expression:

$$\frac{(x_1^0)^2}{b_1^2} + \frac{(x_2^0)^2}{b_2^2} + \frac{(x_3^0)^2}{b_3^2} = 1$$

It is natural to determine the orientation of these axes relative to a set of axes $\bar{x}_1$, $\bar{x}_2$, $\bar{x}_3$ fixed in direction whose origin lies at the center of the particle. The relative orientation between the two sets of axes is described by the three Euler angles. If the particle is an ellipsoid of revolution, however, only two of the three Euler angles are needed to fully describe its orientation, as shown in Figure 2.1. A fiber may be modelled as an ellipsoid of revolution.

Jeffery found expressions relating the hydrodynamic torque acting on the particle to the spins about its axes. With the assumption of creeping flow, the torque vanishes, and by relating the spins about the axes to the Euler angles

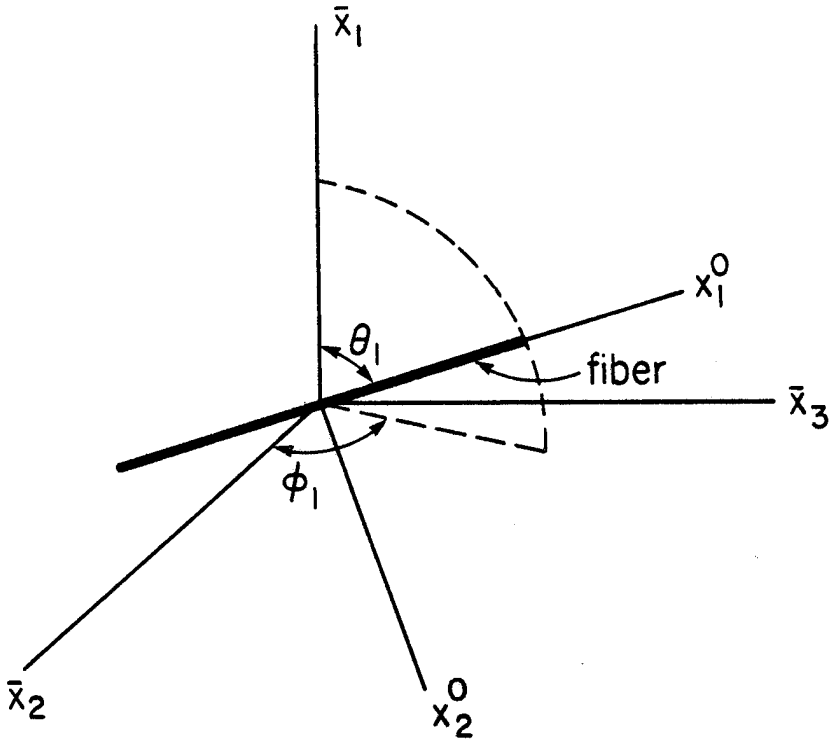

Figure 2.1 Fiber orientation relative to a coordinate system whose axes are fixed in direction

for an ellipsoid of revolution, the following expressions result [7]:

$$\frac{\partial \phi_1}{\partial t} = \bar{z}_1 - \bar{z}_2 \cos\phi_1 \cot\theta_1 - \bar{z}_3 \sin\phi_1 \cot\theta_1$$

$$+ B\left[-\bar{d}_{12} \sin\phi_1 \cot\theta_1 + \bar{d}_{23} \cos 2\phi_1\right.$$

$$\left. + \bar{d}_{31} \cos\phi_1 \cot\theta_1 - \frac{1}{2}(\bar{d}_{22} - \bar{d}_{33}) \sin 2\phi_1\right] \qquad (2.1)$$

$$\frac{\partial \theta_1}{\partial t} = - \bar{z}_2 \sin\phi_1 + \bar{z}_3 \cos\phi_1 + B\left[\bar{d}_{12} \cos\phi_1 \cos 2\theta_1\right.$$

$$+ \frac{1}{2}\,\bar{d}_{23}\,\sin 2\phi_1\,\sin 2\theta_1 + \bar{d}_{31}\,\sin\phi_1\,\cos 2\theta_1$$

$$+ \frac{1}{4}(\bar{d}_{22} - \bar{d}_{33})\,\cos 2\phi_1\,\sin 2\theta_1$$

$$+ \frac{3}{4}(\bar{d}_{22} + \bar{d}_{33})\,\sin 2\theta_1\Big] \qquad (2.2)$$

where $\bar{z}_i$ and $\bar{d}_{ij}$ are the respective components of vorticity and rate of deformation defined by

$$\bar{z}_i = \frac{1}{2}(\bar{u}_{k,j} - \bar{u}_{j,k})\,e_{ijk}$$

$$\bar{d}_{ij} = \frac{1}{2}(\bar{u}_{i,j} + \bar{u}_{j,i})$$

and B is a function of the particle aspect ratio, r_p, given by

$$B = \frac{r_p^2 - 1}{r_p^2 + 1}$$

where $r_p = b_1/b_2$.

It is desirable to determine the orientation relative to an inertial reference frame since the fluid kinematics are most naturally defined relative to a fixed reference frame. For this purpose an inertial Cartesian coordinate system x_1 , x_2 , x_3 is introduced such that each x_i axis points in the same direction as the corresponding $\bar{x}_i$ axis. Obviously, the orientation of the particle axes relative to the inertial frame can be described by the same

Euler angles, ϕ_1 and θ_1 , used to describe the axes relative to the $\bar{x}_1$, $\bar{x}_2$, $\bar{x}_3$ system. In this new coordinate system, (2.1) and (2.2) are transformed to

$$\frac{D\phi_1}{Dt} = z_1 - z_2 \cos\phi_1 \cot\theta_1 - z_3 \sin\phi_1 \cot\theta_1 + B\left[- d_{12} \sin\phi_1 \cot\theta_1 + d_{23} \cos 2\phi_1 + d_{31} \cos\phi_1 \cot\theta_1 - \frac{1}{2}(d_{22} - d_{33}) \sin 2\phi_1\right] \quad (2.3)$$

$$\frac{D\theta_1}{Dt} = - z_2 \sin\phi_1 + z_3 \cos\phi_1 + B\left[d_{12} \cos\phi_1 \cos 2\theta_1 + \frac{1}{2} d_{23} \sin 2\phi_1 \sin 2\theta_1 + d_{31} \sin\phi_1 \cos 2\theta_1 + \frac{1}{4}(d_{22} - d_{33}) \cos 2\phi_1 \sin 2\theta_1 + \frac{3}{4}(d_{22} + d_{33}) \sin 2\theta_1\right] \quad (2.4)$$

where $\frac{D(\ )}{Dt} = \frac{\partial(\ )}{\partial t} + u_1 \frac{\partial(\ )}{\partial x_1} + u_2 \frac{\partial(\ )}{\partial x_2} + u_3 \frac{\partial(\ )}{\partial x_3}$

and z_i and d_{ij} are components of the vorticity and rate of deformation tensor relative to the x_1 , x_2 , x_3 coordinate system. Equations (2.3) and (2.4), or (2.1) and (2.2), enable one to fully determine the orientation of a fiber in flow fields under the restrictions stated above.

One final limitation of the above equations is that they were developed for a single particle; hence, they do not account for particle interactions in a fluid containing

many particles. Indeed, in typical mold filling operations, fiber volume fractions of 30-40% are common and fiber interations may become very significant. However, the analysis involved in dealing with such interactions is at the present time intractable; therefore, such interactions are not treated in this work.

2.1 Use of Jeffery's Equations to Determine Fiber Orientation

Upon inspection of (2.3) and (2.4), one notices the existence of vorticity and rate of deformation components. These components must first be determined and substituted into Jeffery's equations, which are then integrated to obtain the fiber orientation.

The solution to the flow equations must satisfy conservation of mass and momentum requirements, along with the constitutive approximation for the fluid. Conservation of mass and momentum are universal laws applicable to all fluids, but the constitutive relation is merely an approximation for modelling the behavior of each specific fluid. In this work, the "fluid" consists of a Newtonian fluid containing a concentration of suspended fibers. For a low volume fraction of fibers, the influence of the fibers on the behavior of the overall fluid is minimal, and the

Newtonian constitutive assumption is valid. However, a larger concentration of fibers exerts a considerable influence on the constitutive behavior of the suspension. Maschmeyer and Hill [10] have shown that when a high concentration of 3 mm fibers is mixed in a Newtonian fluid, the suspension becomes highly pseudoplastic. Thus a power law constitutive assumption appears valid for suspensions of high concentration.

The degree of orientation of the fibers can also be expected to have an influence on the constitutive properties of the suspension. One certainly anticipates different constitutive behavior in regions where fibers are highly aligned than in regions of random orientation. To include this effect, however, the relationship between viscosity and degree of orientation must first be determined. Thereafter, an iterative procedure is needed since the fluid mechanics has an effect on fiber orientation which in turn alters the fluid mechanics. However, for the remainder of this work, the vicosity dependence on fiber orientation is neglected.

CHAPTER 3. PLANE FLOW

This chapter deals with in-plane fiber orientation in plane flow. Numerically, the flow equations are easier to solve in plane flow since the flow is two-dimensional. Also, the fiber orientation equations simplify considerably, and in special cases, can be solved analytically. In Section 3.1, the appropriate simplifications are introduced into the fiber orientation equations. Furthermore, it is shown that in-plane fibers maintain their in-plane orientation and one of the orientation equations is eliminated. Section 3.2 present an analytical solution for fiber orientation in plane Poiseuille flow. This solution provides a basis for checking the numerical scheme. The numerical method is developed in Section 3.3. The orientation parameters which relate the degree of orientation to the material properties are introduced in Section 3.4 and a method for determining them as well as the mode of the distribution in terms of the orientations of a finite number of fibers is presented. Finally, in Section 3.5, a number of numerically determined solutions are presented. To check the numerical scheme, the fiber orientation in plane Poiseuille flow is

evaluated and the results are compared with the analytical solution in Section 3.2. Also, the fiber orientation in flow around a circular inclusion in both finite and infinite width channels is determined. The latter examples are of pragmatic importance because they provide predictions for the orientation around molded holes.

3.1 Orientation Equation for In-Plane Fibers in Plane Flow

Consider plane flow in which variations in the x_1 coordinate direction may be ignored. For this type of flow, several of the vorticity and rate of deformation tensor components are identically zero:

$$z_i = \begin{pmatrix} z_1 \\ 0 \\ 0 \end{pmatrix}$$

$$d_{ij} = \begin{bmatrix} 0 & 0 & 0 \\ 0 & d_{22} & d_{23} \\ 0 & d_{23} & d_{33} \end{bmatrix}$$

Inserting the appropriate simplifications into Equations (2.3) and (2.4) one obtains:

$$\frac{D\phi_1}{Dt} = z_1 + B[d_{23}\cos 2\phi_1 - \tfrac{1}{2}(d_{22}-d_{33})\sin 2\phi_1] \tag{3.1}$$

$$\frac{D\theta_1}{Dt} = \frac{B}{4}[2d_{23}\sin 2\phi_1 \sin 2\theta_1 + (d_{22}-d_{33})\cos 2\phi_1 \sin 2\theta_1 + 3(d_{22}+d_{33})\sin 2\theta_1] \tag{3.2}$$

Equation (3.1) clearly indicates that the in-plane response of a fiber is independent of the out-of-plane orientation. If one considers fibers initially oriented in the plane of the flow ($\theta_1=\pi/2$), then equation (3.2) reduces to $\frac{D\theta_1}{Dt} = 0$ which indicates that a fiber remains in-plane. The remainder of this chapter deals exclusively with in-plane fibers; hence, only the single differential equation (3.1) needs to be solved to completely determine the fiber orientation.

It is worthwhile to note for later reference that, under the above simplifications, Equations (2.1) and (2.2) reduce to the single differential equation:

$$\frac{\partial\phi_1}{\partial t} = \bar{z}_1 + B[\bar{d}_{23}\cos 2\phi_1 - \tfrac{1}{2}(\bar{d}_{22}-\bar{d}_{33})\sin 2\phi_1] \tag{3.3}$$

Although the above assumptions have considerably simplified the analysis, (3.1) and (3.3) are still

extremely difficult to solve analytically except for some very simple flows. The next section deals with a flow where an analytical solution does exist. Thereafter, a procedure is developed for numerically determing fiber orientation for more complicated flows.

3.2 Fiber Orientation in Plane Poiseuille Flow - Analytical Solution

Consider the pressure-driven, steady, creeping flow of an incompressible Newtonian fluid through a rectangular channel of very large aspect ratio as shown in Figure 3.1, where the flow is in the x_3 direction. The ratios H/w and H/L are small compared to unity and thus in regions away from the edges of the channel, the velocity variations occur only in the x_2 direction. The fiber orientation in this fully developed region is to be determined.

Under conditions of unit flow, the normalized velocity profile is

$$u_3 = \frac{3}{2}\left(1 - \frac{x_2^2}{H^2}\right)$$

$$u_1 = u_2 = 0$$

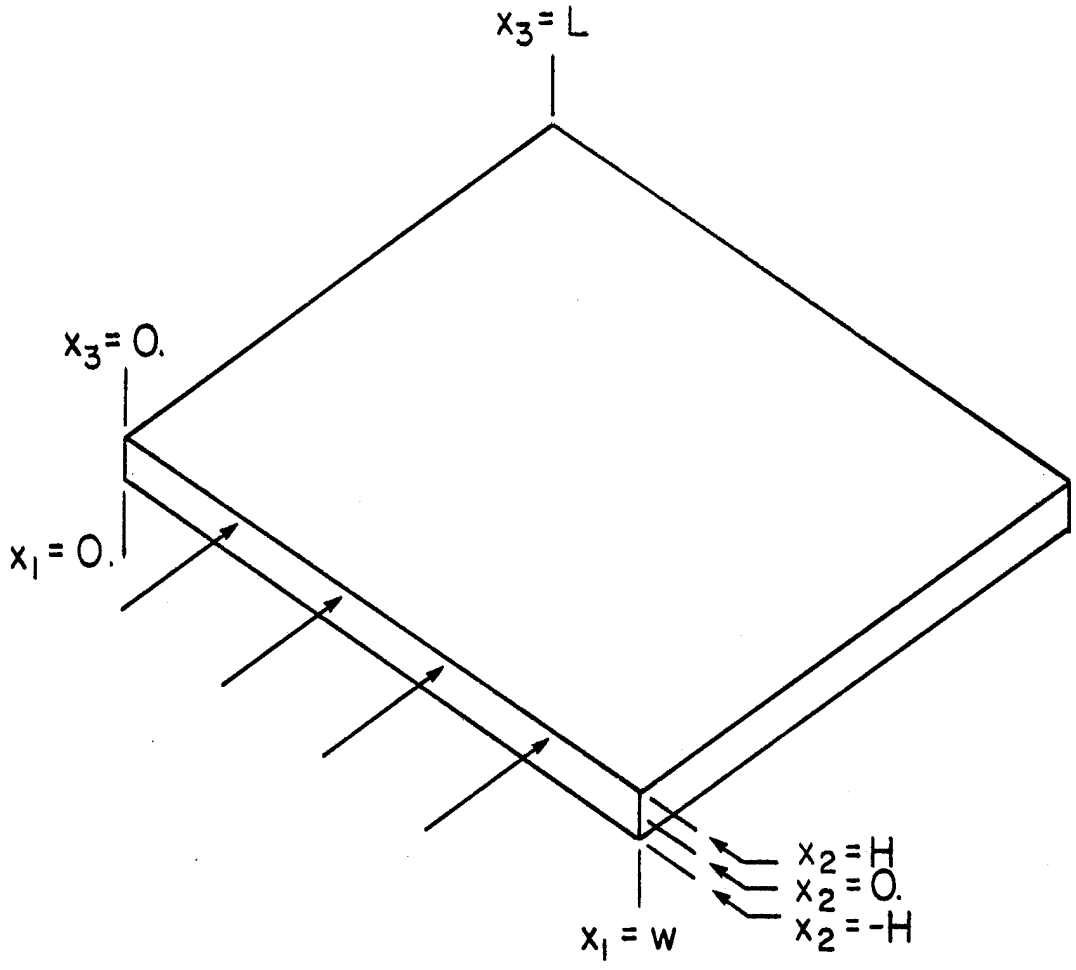

Figure 3.1 Geometry for plane Poiseuille flow

and the components of the vorticity and rate of deformation are computed to be

$$z_i = \begin{Bmatrix} \frac{1}{2}\Gamma \\ 0 \\ 0 \end{Bmatrix}$$

$$d_{ij} = \begin{bmatrix} 0 & 0 & 0 \\ 0 & 0 & \frac{1}{2}\Gamma \\ 0 & \frac{1}{2}\Gamma & 0 \end{bmatrix}$$

where $\Gamma = \frac{du_3}{dx_2} = -3x_2/H^2$

Substituting into Equation (3.1), one obtains:

$$\frac{\partial \phi_1}{\partial t} + u_3 \frac{\partial \phi_1}{\partial x_3} = \frac{\Gamma}{r_p^2+1}(r_p^2 \cos^2 \phi_1 + \sin^2 \phi_1) \qquad (3.4)$$

If one deals with fibers entering the domain perpendicular to the flow streamline (ie, ϕ_1=0. at x_3=0), then $\frac{\partial \phi_1}{\partial t} = 0$ and (3.4) reduces to

$$\frac{d\phi_1}{dx_3} = \frac{\Gamma}{u_3(r_p^2+1)} (r_p^2 \cos^2 \phi_i + \sin^2 \phi_1)$$

and the resulting solution is

$$\tan \phi_1 = r_p \tan \frac{\Gamma x_3/u_3}{r_p + 1/r_p}$$

or

$$\tan \phi_1 = r_p \tan\left[-\frac{2x_2x_3}{(H^2-x_2^2)(r_p+1/r_p)}\right] \qquad (3.5)$$

Assuming a fiber aspect ratio of 50, the fiber orientation is plotted in Figure 3.2 for H=1. One immediate observation to be made from the figure is that a distinct layer of fibers aligned parallel to the streamlines exists near the wall boundary. This alignment correlates well with experimental observations of fiber alignment near wall boundaries in short-fiber injection molded components.

Having attained an analytical solution, one may now proceed to develop a numerical scheme to predict fiber orientation. The known analytic solution in this section can be used to check the accuracy of the numerical method.

3.3 Numerical Method

Except for very few simple flow geometries, Equation (3.1) cannot be solved by analytical methods. However, one may wish to determine fiber orientation for complicated flow situations which exist in many molding processes. With this motivation, the necessity to develop a numerical scheme to determine fiber orientation is obvious. The majority of the material covered in this section was previously developed by Givler [5].

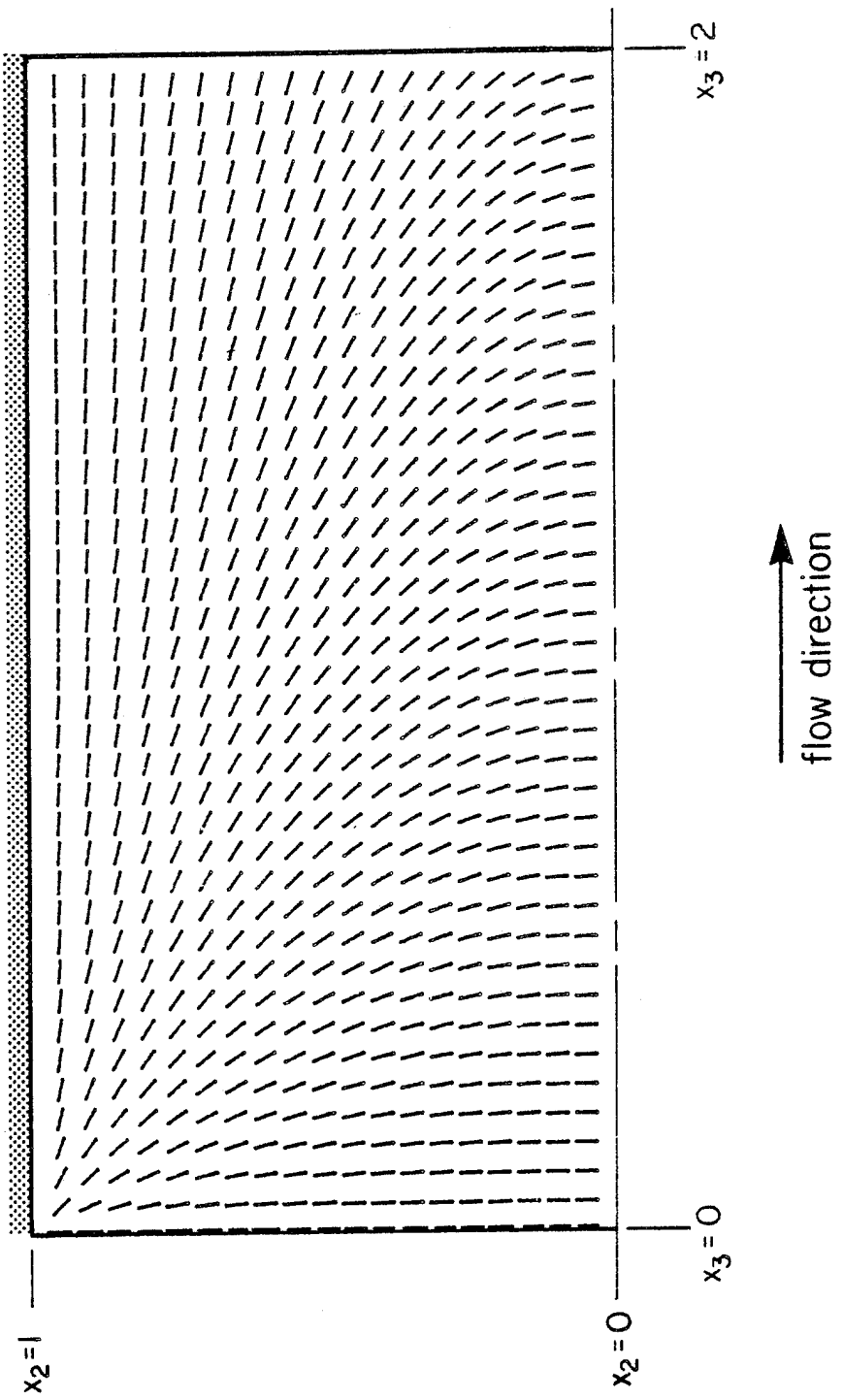

Figure 3.2 Fiber orientation in plane Poiseuille flow for fibers initially perpendicular to flow streamlines

As mentioned previously, the first step in solving for fiber orientation is to obtain the flow field. The finite element method has been used extensively in the literature to solve fluid mechanics problems with excellent results and consequently, is incorporated in this work. The details of the method employed herein are fully described in References 2 and 5. The analysis utilizes the six-node triangular element shown in Figure 3.3 to solve the plane and, later, axisymmetric flows. In the finite element analysis, the continuity, momentum, and constitutive equations are reduced to a set of algebraic equations via the Galerkin method and after solving this system of equations, a discretized solution is obtained.

From the discretized solution for the fluid mechanics, it remains to determine the fiber orientation. This is accomplished by determining the orientation of individual fibers as they traverse the flow streamlines.

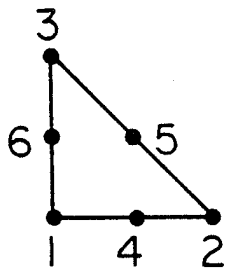

Figure 3.3 Six-node triangular element

Obviously, unless some collimation is evident, one cannot know precisely the initial orientations of all fibers. Indeed, if the initial orientations were known, it would not be feasible to track each fiber through the domain. An alternative approach is to select a number of streamlines which sensibly cover the domain in which the fiber orientation is to be determined. Then a finite number of fibers of varying initial orientations are allowed to traverse each streamline, and the orientation of each fiber is computed at various locations along the streamline. Thus information is obtained about the dispersion of fibers as well as the principal direction of orientation. Usually, an initially random orientation distribution is input. A random distribution will be defined in a later section.

To find the streamlines, one must first determine the stream function, ψ. From the numerical solution, the stream function values are known at the nodal points as shown in Figure 3.4. To isolate a streamline, the finite element grid is scanned element by element to identify nodal points having the particular values of the stream function, ψ_o , corresponding to the streamline. However, except in rare circumstances the streamline will not intersect an element boundary exactly at a nodal point. Therefore, linear interpolation is used to determine the locations at which the streamlines

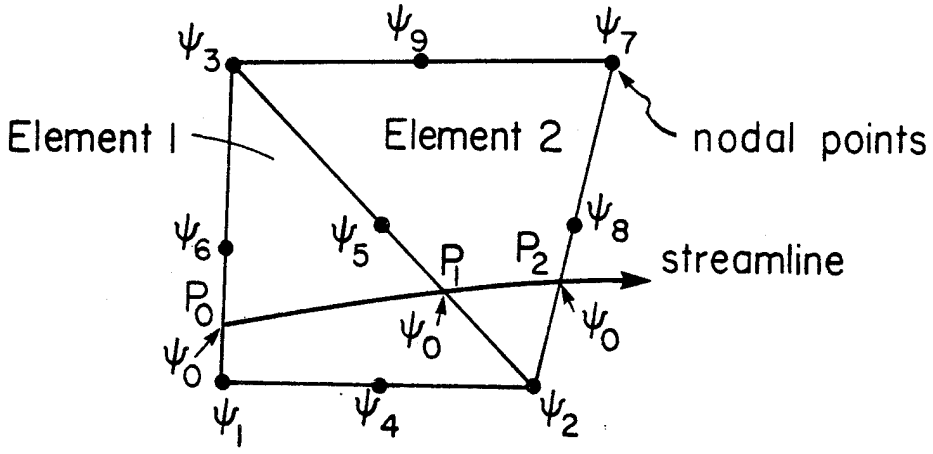

Figure 3.4 Determination of streamlines from numerical fluid mechanics solution

intersect the element boundaries. After scanning every element, a collection of coordinates is obtained which corresponds to locations where the streamline crosses the element boundaries. These points must next be placed in order, which is accomplished by noting that if a streamline crosses an element boundary, it must cross a second boundary in the same element. Thus, given the initial point of the streamline, shown as P_o in Figure 3.4, the neighbor to this point, P_1 , can be determined since it lies on a boundary to the same element. But P_1 is also a point of intersection for a second element. In fact, all stream points, with the exception of the first and last, mark the intersection of the streamline and the boundary of

two elements. Having found the second element containing P_1 , the next neighbor, P_2 , may be found since it lies in the same element as P_1 . This procedure continues until all the stream points are arranged in order, forming the streamline.

In the exceptional case where a streamline crosses an element boundary at a corner node, the stream point marks the intersection of the streamline and more than two elements (see Figure 3.5). However, simply disregarding the elements which the streamline does not pass through results in the stream point being contained by just two elements.

Having formed the strealines, it remains to numerically determine the orientations of fibers at selected locations along each streamline. To do this, the coordinate system whose axes remain fixed in direction and translate along the fiber center (the $\bar{x}_1$, $\bar{x}_2$, $\bar{x}_3$ axes in Figure 2.1) is adopted, and Equation (3.3) can be used to determine the fiber orientation relative to this system. The advantage of working with (3.3) is that differentiation is with respect to a single variable, time. To illustrate the procedure for integrating (3.3), suppose the initial fiber orientation is given at point P_o in Figure 3.4 and the fiber orientation at location P_1 is

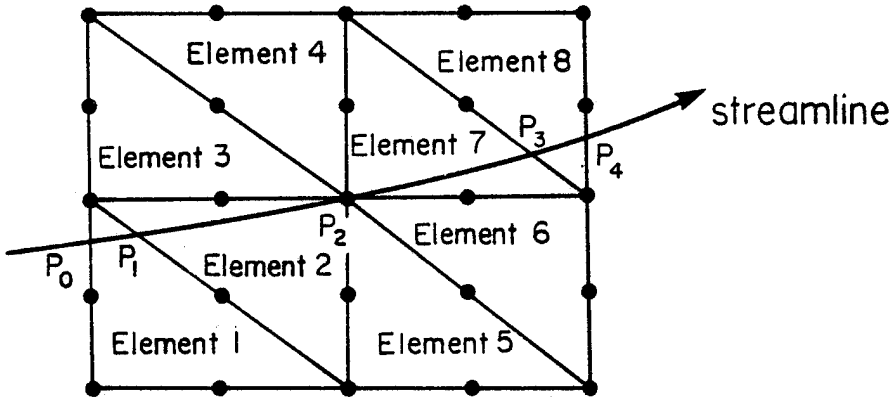

Figure 3.5 Streamline crossing corner node

desired. The time required for a fiber to travel from P_o to P_1 can be estimated by dividing the distance from P_o to P_1 by the velocity at P_o . This sets the time increment for evaluation of the fiber orientation in (3.3). The vorticity and rate of deformation components are approximated as constants over the length of the element equal to those values computed at P_o . With these approximations, a numerical differential equation solver using the Runge-Kutta-Verner fifth and sixth order method is adopted to solve (3.3). The differential equation solver is a subroutine available from International Mathematical and Statistical Libraries. The fiber orientation at subsequent stream points is obtained in an analogous manner.

The stream points provide an effective sampling region in which to plot fiber orientation provided that the elements are appropriately sized.

Under the above procedure for determining fiber orientation, it is obvious that the finer the mesh used, the more accurate the solution provided roundoff errors do not become significant. Questions of convergence of this scheme were addressed by Givler [5] who showed that this method yields sixth order convergence.

3.4 Orientation Parameters for Planar Fiber Distribution

To this point, the methodology for obtaining the orientations of individual fibers at discrete locations in the flow field has been developed. The number of locations containing prescribed fiber orientations depends on the fineness of the mesh and the number of streamlines. If fibers of varying initial orientations are input at the beginning of each streamline then an orientation distribution will result at locations downstream. It is well known that the material properties of a fiber-reinforced component are strongly dependent on the degree, as well as, the direction of fiber orientation. Since the ultimate interest is in determining material properties, it is necessary to develop parameters relating the degree of

orientation to the material properties.

In a given region, the distribution of fibers may be described by an orientation density function, n. For a planar distribution of fibers (see Figure 3.6), the orientation density is a function of the single angle, ϕ_1; viz,

$$n = n(\phi_1)$$

The orientation density function is periodic with period π since the angle $\phi_1 + \pi$ depicts the same orientation ϕ_1; hence,

$$n(\phi_1) = n(\phi_1+\pi)$$

It is essential to confine ϕ_1 to lie within an interval equal to π which isolates one period in the orientation density function.

For a symmetric orientation distribution about the mode, ϕ_1° , such as the distribution in Figure 3.7, one intuitively expects local orthotropic material properties with the mode angle defining a principal material direction. The validity of the symmetric distribution assumption is investigated for a real flow situation in Appendix 1, where it is determined that the symmetry assumption

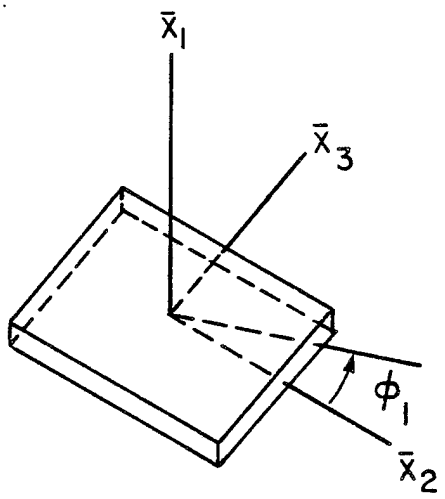

Figure 3.6 Planar fiber distribution

is valid. With this symmetry the orientation density function is normalized such that

$$\int_{\phi_1^\circ}^{\phi_1^\circ+\pi/2} n(\phi_1)d\phi_1 = 1 \tag{3.6}$$

In an interval centered at the mode, the mean, $<\phi_1>$, and the mode are equivalent.

McCullough et al. [13] have developed a technique for relating the microstructure in a short-fiber composite material to its material properties, which utilizes the concept of the "aggregate model." The microstructure is modelled as a collection of subregions, or grains, of

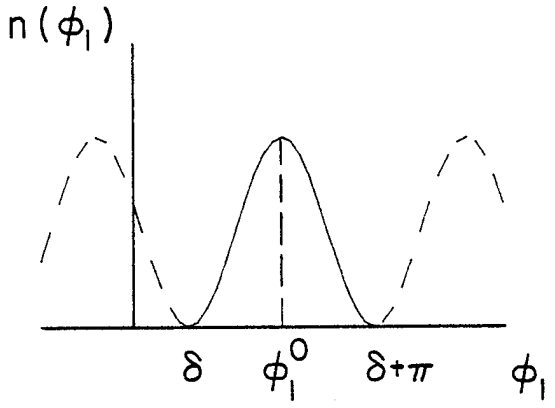

Figure 3.7 Symmetric orientation distribution about the mode

microlaminates of aligned fibers. McCullough assumed a symmetric distribution about the mode and introduced a new angle ζ which is measured from the mode (see Figure 3.8).

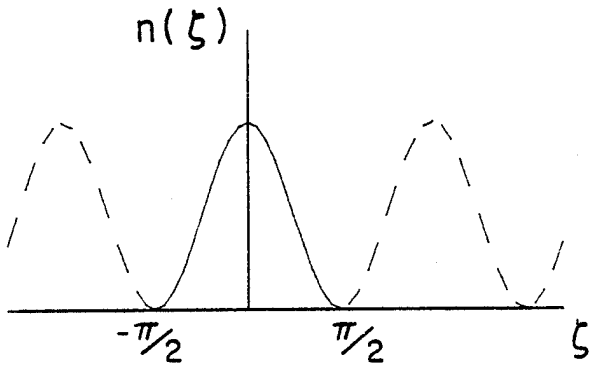

Figure 3.8 Orientation density as a function of ζ

Obviously, ϕ_1 and ζ are simply related through

$$\zeta = \phi_1 - \phi_1^\circ \tag{3.7}$$

Under this model, the material properties are related to the dispersion through two parameters, f_p and g_p, defined by

$$f_p = 2\langle\cos^2\zeta\rangle - 1 \tag{3.8}$$

$$g_p = \frac{1}{5}[8\langle\cos^4\zeta\rangle - 3] \tag{3.9}$$

where $\langle\cos^m\zeta\rangle = \int_o^{\pi/2} n(\zeta)\ \cos^m\zeta\ d\zeta$. The orientation parameters are constructed such that the degree of collimation can readily be interpreted. For $f_p = g_p = 1$, the fibers are perfectly aligned, whereas $f_p = g_p = 0$ signifies a random distribution. Intermediate values of f_p and g_p represent partial degrees of orientation. The orientation parameters may be expressed in terms of ϕ_1 by substituting (3.6) into (3.9) and (3.10):

$$f_p = 2\int_{\phi_1^\circ}^{\phi_1^\circ+\pi/2} n(\phi_1)\cos^2(\phi_1-\phi_1^\circ)d\phi_1 - 1 \tag{3.10}$$

$$g_p = \frac{1}{5}\left[8\int_{\phi_1^\circ}^{\phi_1^\circ+\pi/2} n(\phi_1)\cos^4(\phi_1-\phi_1^\circ)d\phi_1 - 3\right] \tag{3.11}$$

In order to obtain the orientation parameters from a distribution in ϕ_1 , the mode, ϕ_1° , must be determined.

In this work, an orientation density function is not explicitly developed; rather, the orientations of a finite number of fibers are determined, as explained previously. Hence, the orientation parameters must be expressed in terms of a finite number of fibers; this is accomplished in the next section. The subsequent section is concerned with the evaluation of ϕ_1° .

3.4.1 Determination of the Orientation Parameters from the Orientations of a Finite Number of Fibers

To be compatible with the numerical fiber orientation scheme developed earlier, the orientation parameters must be expressed in terms of the orientations of a finite number of fibers.

To determine the appropriate expression for f_p , one begins by dividing the integral in (3.10) into a finite number of intervals and approximating the behavior over each interval via

$$\int_{\phi_1^\circ}^{\phi_1^\circ+\pi/2} n(\phi_1)\cos^2(\phi_1-\phi_1^\circ)d\phi_1 \cong \sum_{i=1}^{k} n[(\phi_1)_i]\cos^2[(\phi_1)_i-\phi_1^\circ]\Delta\phi_1 \tag{3.12}$$

where k is the number of intervals and $(\phi_1)_i$ is the average value of ϕ_1 in the i^{th} interval. Defining m_i as the number of fibers whose oreintations lie in the i^{th} interval, it can be determined from the normalization condition (3.6) that

$$\frac{m_i}{N} = n[(\phi_1)_i]\Delta\phi_1 \tag{3.13}$$

where N is the total number of fibers. Substitution of (3.13) into (3.12) yields

$$\int_{\phi_1^\circ}^{\phi_1^\circ+\pi/2} n(\phi_1)\cos^2(\phi_1-\phi_1^\circ)d\phi_1 \cong \frac{1}{N}\sum_{i=1}^{k} m_i\cos^2[(\phi_1)_i-\phi_1^\circ]$$

or equivalently,

$$\int_{\phi_1^\circ}^{\phi_1^\circ+\pi/2} n(\phi_1)\cos^2(\phi_1-\phi_1^\circ)d\phi_1 \cong \frac{1}{N}\sum_{j=1}^{N} \cos^2(\phi_{1_j}-\phi_1^\circ) \tag{3.14}$$

where ϕ_{1_j} represents the orientation of the j^{th} fiber. Substituting (3.14) into (3.10), one obtains

$$f_p \cong \frac{2}{N}\sum_{i=1}^{N} \cos^2(\phi_{1_i}-\phi_1^\circ) - 1 \tag{3.15}$$

which is the desired expression relating f_p to the orientations of a finite number of fibers.

Following an analogous procedure, the following expression for g_p may be determined:

$$g_p \cong \frac{1}{5}\left[\frac{8}{N}\sum_{j=1}^{N}\cos^4(\phi_{1_j}-\phi_1^\circ)-3\right] \tag{3.16}$$

The expressions (3.15) and (3.16) are summarized in Table 3.1 for ease in reference.

With the above definitions of the orientation parameters, a random fiber distribution may be modelled from a finite number of fibers by adjusting the fiber orientations such that $f_p = g_p = 0$.

Inspection of (3.15) and (3.16) reveals that the mode, ϕ_1° , must be determined to compute the orientation parameters. The next section develops a method for determining the mode in terms of the orientations of a finite number of fibers.

Table 3.1

Orientation Parameters Expressed in Terms of the Orientation of a Finite Number of Fibers

$$f_p = \frac{2}{N}\sum_{i=1}^{N}\cos^2(\phi_{1_i}-\phi_1^\circ) - 1$$

$$g_p = \frac{1}{5}\left[\frac{8}{N}\sum_{i=1}^{N}\cos^4(\phi_{1_i}-\phi_1^\circ)-3\right]$$

3.4.2 Computation of the Mode

For a continuous distribution function, the computation of the mode angle is quite straightforward. One simply applies the definition of the mode:

$$\left.\frac{dn(\phi_1)}{d\phi_1}\right|_{\phi_1=\phi_1^\circ} = 0$$

Alternatively, in the case of symmetric distributions about the mode, the mode is equivalent to the mean in an interval centered about the mode; viz,

$$\phi_1^\circ = \int_{\phi_1^\circ-\pi/2}^{\phi_1^\circ+\pi/2} \phi_1 n(\phi_1) d\phi_1 = \langle\phi_1\rangle \qquad (3.17)$$

The condition (3.17) is easier to apply when dealing with distributions described in terms of the orientations of a finite number of fibers. The procedure to determine ϕ_1° using (3.17) is illustrated for continuous distributions and then extended to include distribution in terms of a discrete number of fibers.

Consider the continuous distribution in Figure 3.7. In order to determine the mode via (3.17), the period centered at the mode must be established. But this interval is unknown until the mode itself is determined. Hence, an iterative procedure is necessary where a mean is calculated based upon an initial guess for the interval. A new interval centered around the calculated mean is established, from which a new mean is calculated, leading to a new interval. The procedure continues until the difference between successively calculated mean values lies within some tolerance requirement. To illustrate the iterative scheme, the mode for the distribution in Figure 3.8 is determined iteratively in Figure 3.9.

These ideas are easily extended to cover distributions described by the orientations of a finite number of fibers. Consider, for example, the distribution depicted by the four fibers in Figure 3.10. Within the range $0 \leq \phi_1 < \pi$, the orientations of the four fibers are

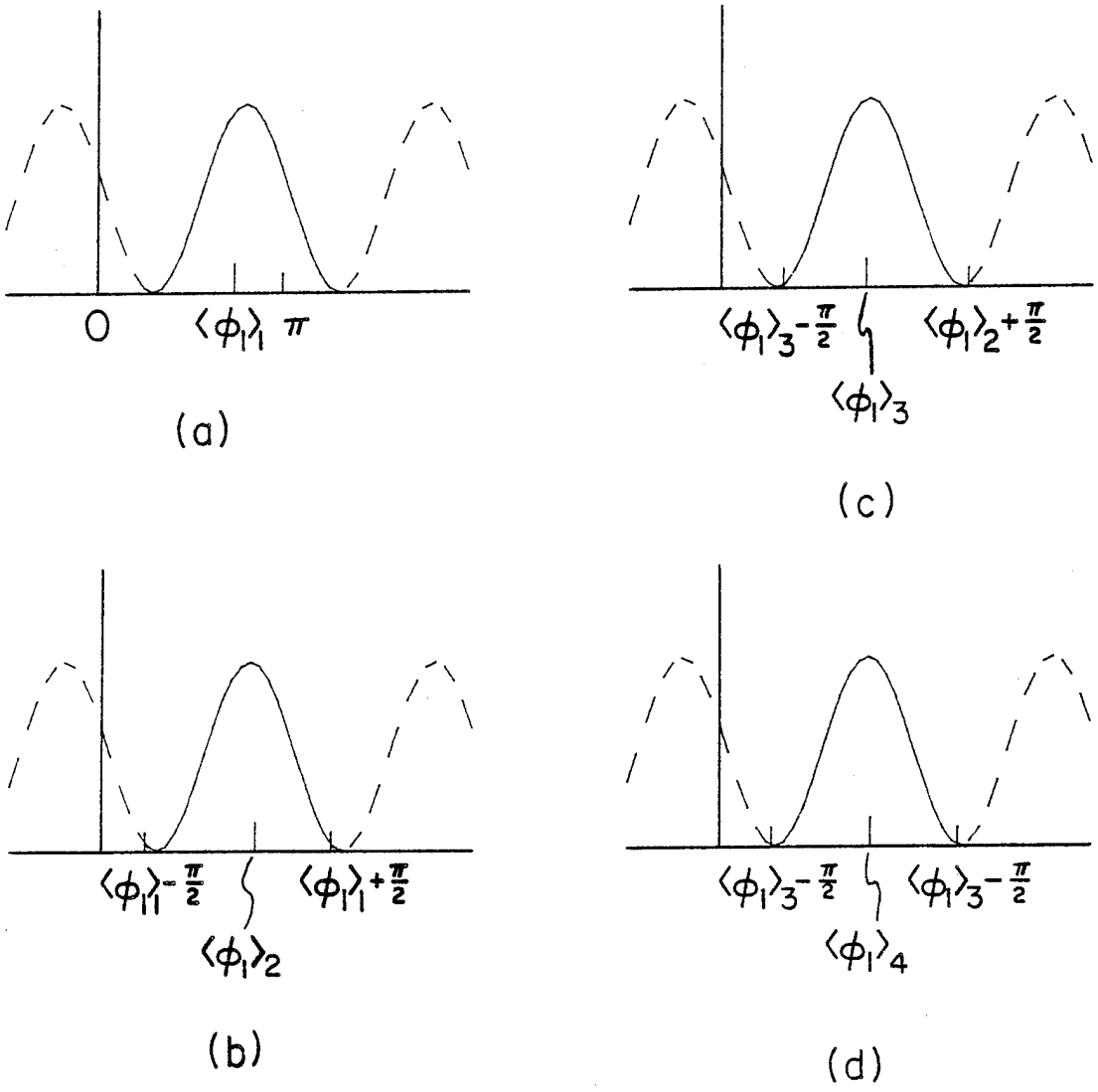

Figure 3.9 Determination of the mode via the iterative procedure. In (a) the mean angle, $\langle\phi_1\rangle_1$, is calculated in the interval $(0,\pi)$. A new interval centered about $\langle\phi_1\rangle_1$ is established in (b) from which a new mean, $\langle\phi_1\rangle_2$, is determined. This procedure continues until a close estimate for the mode is established in (d).

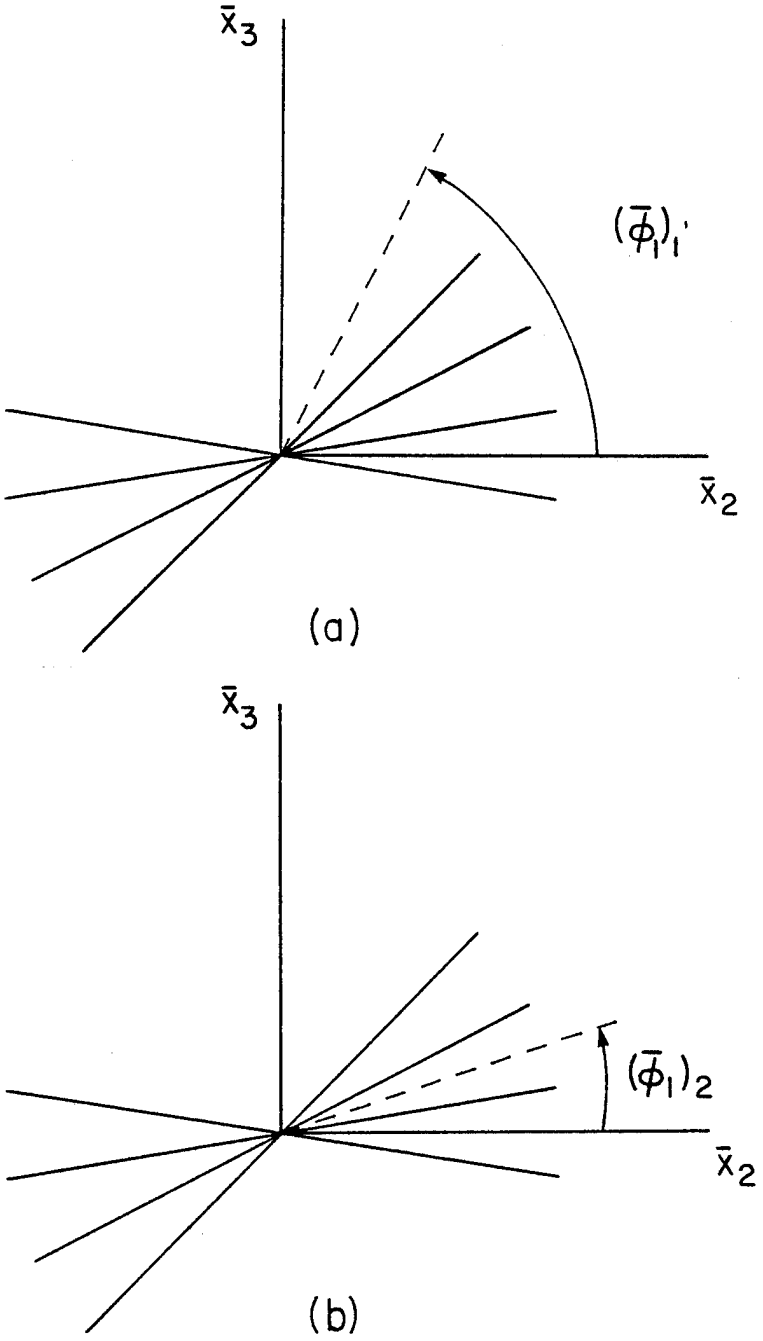

Figure 3.10 Determination of the mode from the orientations of a finite number of fibers via the iterative procedure

0.05π, 0.15π, 0.25π and 0.95π. Calculating the mean, $\bar{\phi}_1$ from the standard definition

$$\bar{\phi}_1 = \frac{1}{N} \sum_{i=1}^{N} \phi_{1_j}$$

where N is the total number of fibers and ϕ_{1_j} is the orientation of the j^{th} fiber, one obtains the mean angle depicted in Figure 3.10(a). Centering a new interval about the computed mean angle, the orientation of one of the fibers changes from 0.95π to -0.05π and a new mean results, which is shown in Figure 3.10(b). A further iteration does not change the mean value.

3.5 Numerical Solutions

In this section the numerical method is used to solve several example problems. The fiber orientation in plane Poiseuille flow is determined first, and the results are compared with the analytical solution developed in Section 3.2. Thereafter, several examples of pragmatic interest are presented.

3.5.1 Plane Poiseuille Flow

Consider again the wall-bounded, steady,

Newtonian flow in Figure 3.1. The analytical solution for the orientation of fibers initially perpendicular to the wall boundaries has been determined in Section 3.2. In the present example, the fiber orientation is determined numerically.

As previously stated, the first step in the numerical scheme is to solve the flow equations via the finite element method. Figure 3.11 depicts the finite element mesh and associated boundary conditions incorporated to solve the flow problem. Newtonian constitutive behavior is assumed.

The fluid mechanics results are presented in the form of contour plots. Stream function, pressure, and vorticity contours are plotted in Figures 3.12 through 3.14, respectively. It is, of course, possible to calculate these quantities analytically for this simple flow. Comparing the contour plots with the analytical solutions reveals that the numerical flow solution is accurate.

With the discretized solution to flow equations at hand, the fiber orientation may be determined. In Table 3.2, a comparison is made between the numerical and analytical solutions for the orientation of a fiber initially perpendicular to the wall boundary traversing the

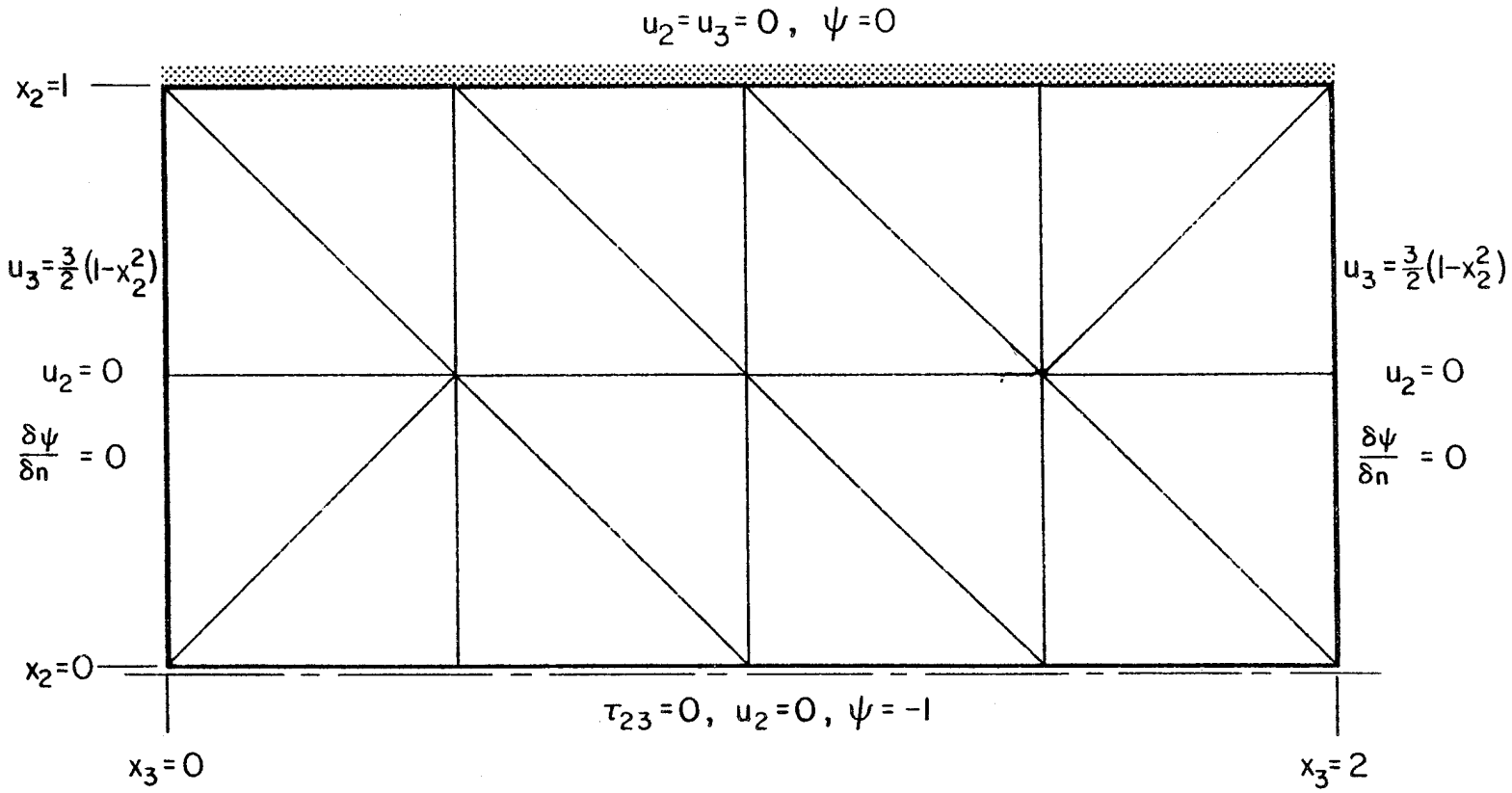

Figure 3.11 Finite element mesh and boundary conditions for solution of plane Poiseuille flow

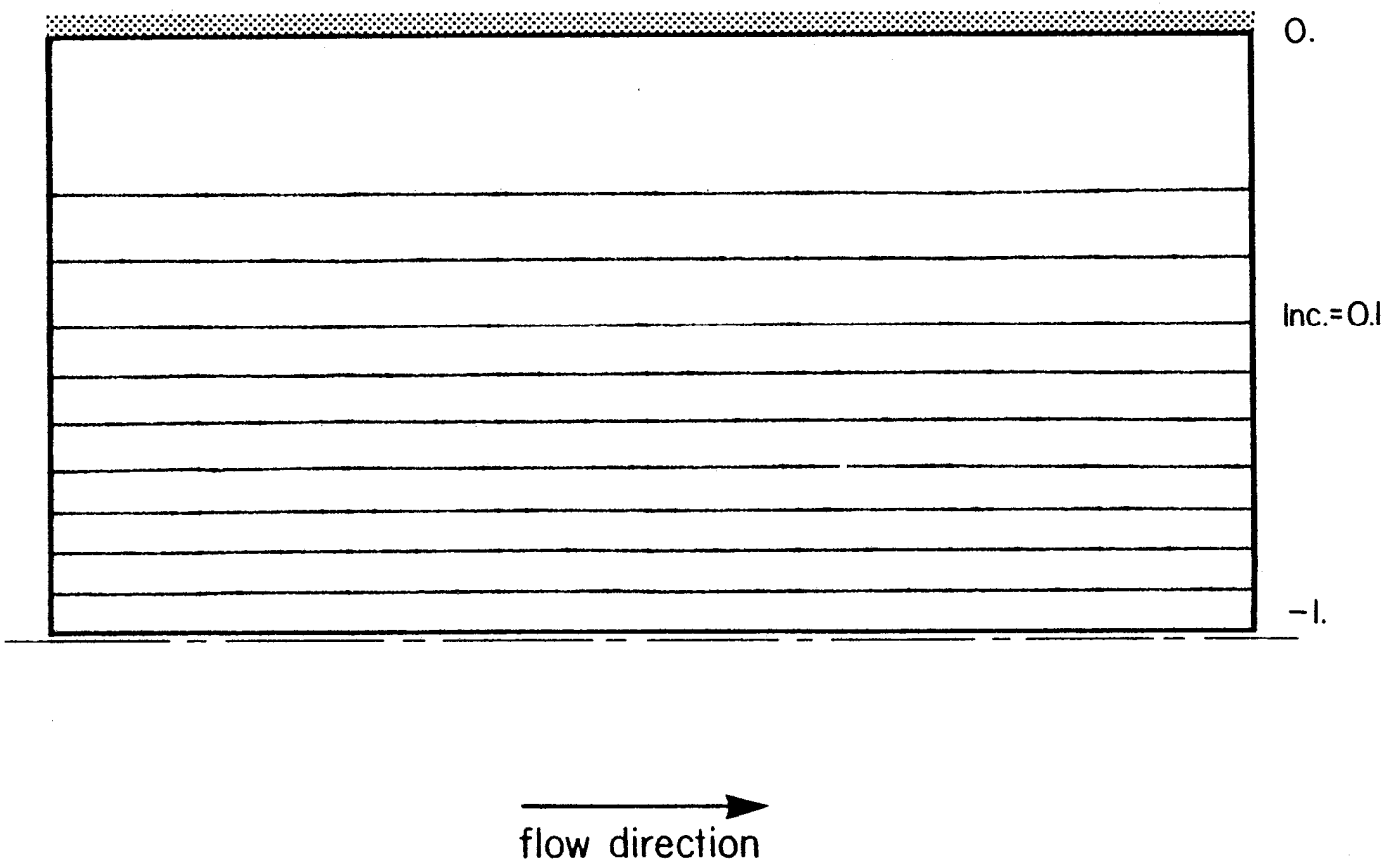

Figure 3.12 Stream function contours (streamlines) in plane Poiseuille flow

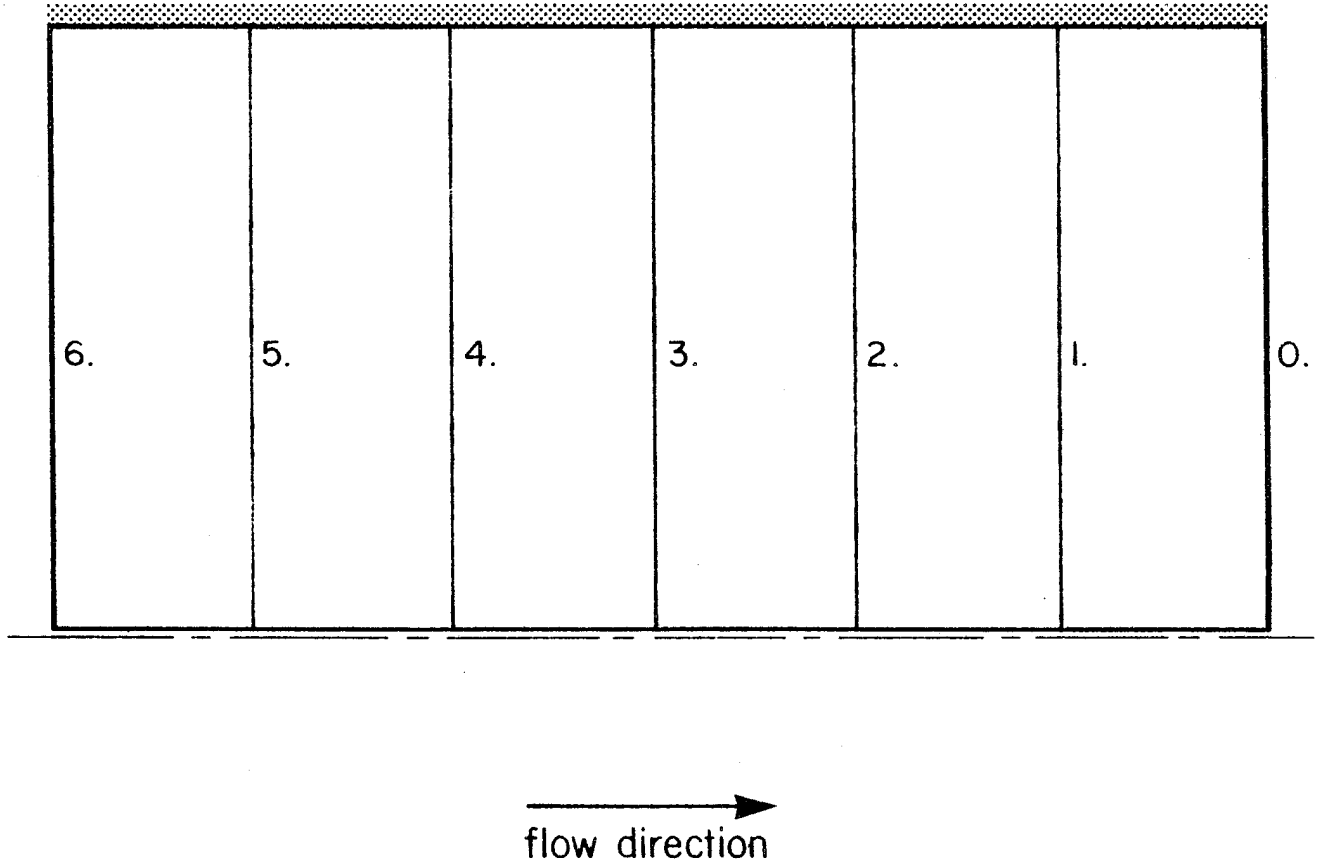

Figure 3.13 Pressure contours in plane Poiseuille flow

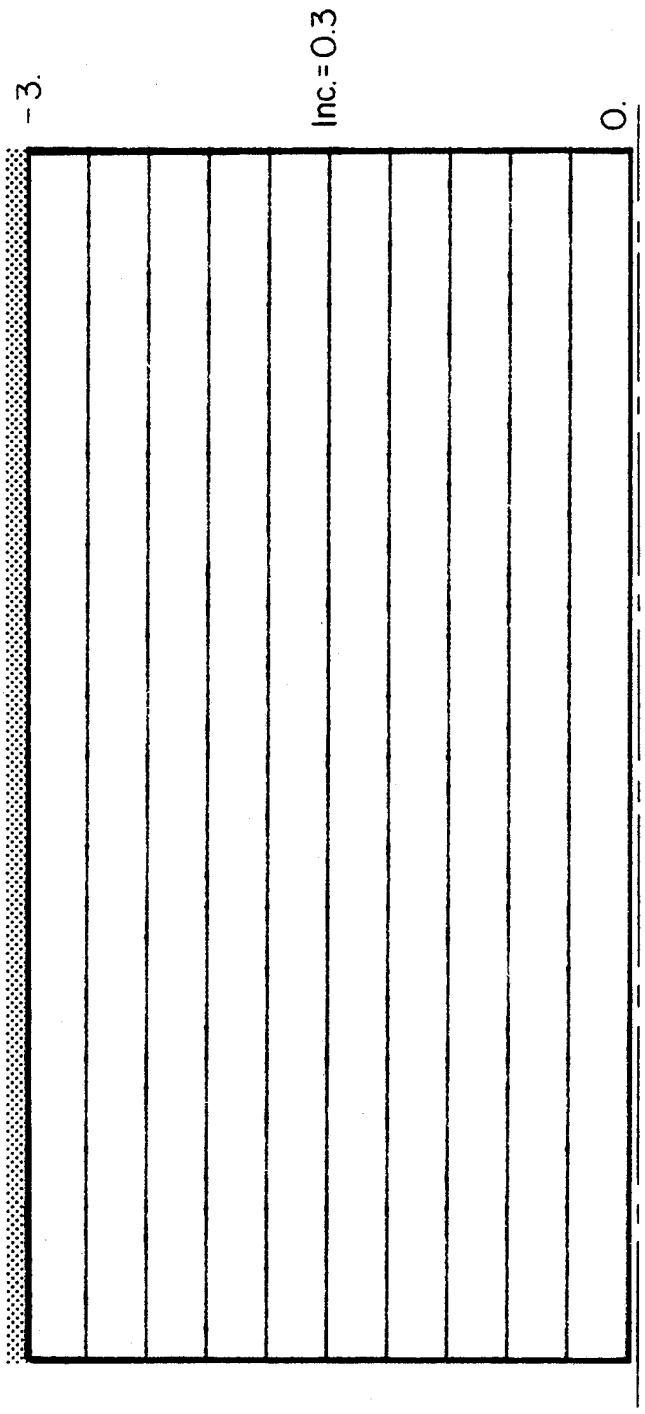

Figure 3.14 Shear stress contours in plane Poiseuille flow

streamline which traces the path $x_2 = 0.6$. It is seen that the numerical results compare favorably with the analytical predictions.

Table 3.2

Comparison of Analytical and Numerical Solutions in Plane Poiseuille Flow at x_2=0.6 for a Fiber Initially Perpendicular to the Wall Boundary

x_3	ϕ_1 analytical, rad	ϕ_1 numerical, rad
0.5	-0.753	-0.785
1.0	-1.08	-1.11
1.5	-1.23	-1.25

It is of interest to determine contours of the mode and orientation parameters for this flow. However, one must first determine the number of fibers needed to adequately portray the orientation distribution. This question is addressed in Appendix 2 where it is determined that as few as ten fibers give good estimates for both the mean fiber angle and orientation parameters.

A fiber plot, shown in Figure 3.15, reveals information about the direction of orientation, as well as, the degree of fiber alignment. It is readily

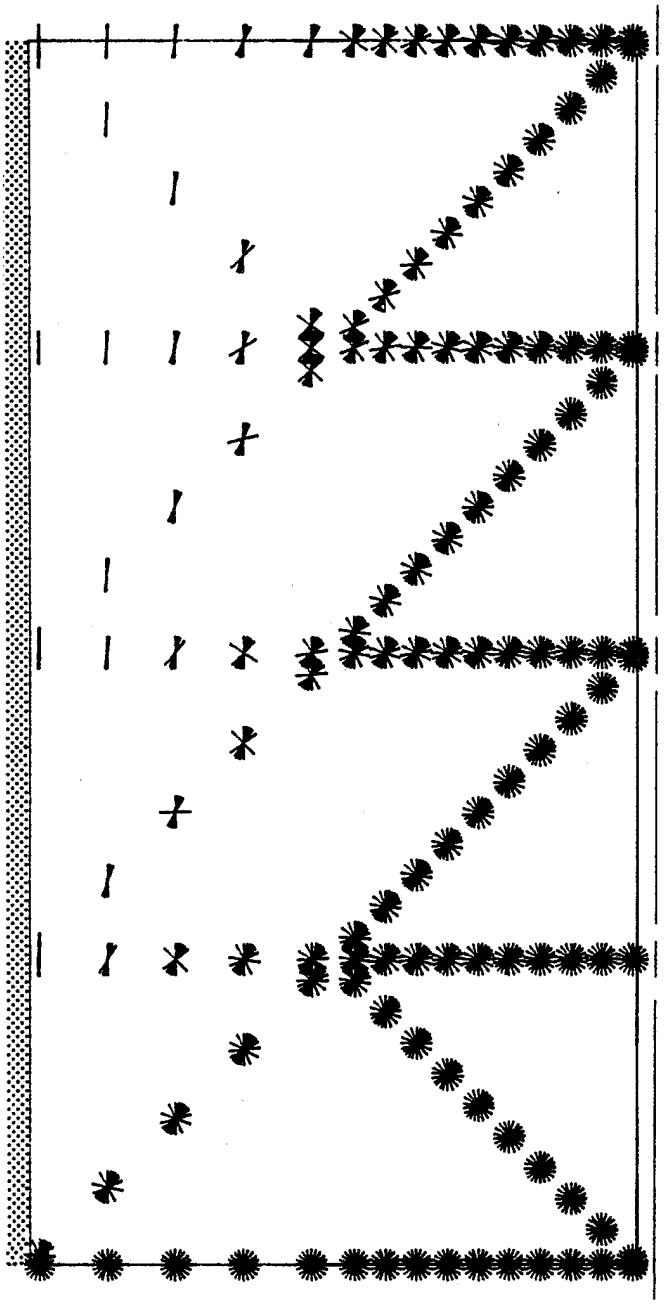

Figure 3.15 Fiber plot for initially random fiber orientation in plane Poiseuille flow

observed from the figure that a high degree of alignment is obtained in the wall region with the direction of collimation parallel to the wall. Near the centerline, the orientation is nearly random. These observations are reinforced in the mode angle and orientation parameter contour plots presented in Figures 3.16 through 3.18. Fiber alignment in the wall region in short-fiber molded components is a well known phenomenon.

It should be noted that, in the mode angle contour plot, contours are not plotted in highly dispersed regions (i.e., $f_p<0.4$) since the fibers do not have much directionality in these highly dispersed areas. The contours in the more oriented regions are easier to interpret since the "noise" imparted by plotting the contours in the dispersed regions has been eliminated. This condition is applied to all future mode angle plots.

3.5.2 Flow Around a Circular Inclusion in a Finite Width Channel

A problem of more pragmatic interest is the determination of fiber orientation in the region around a molded hole in a short-fiber injection molded component. The flow geometry consists of a finite width channel with a centered circular inclusion. In this example, the ratio of channel width to inclusion diameter is 10:1. The

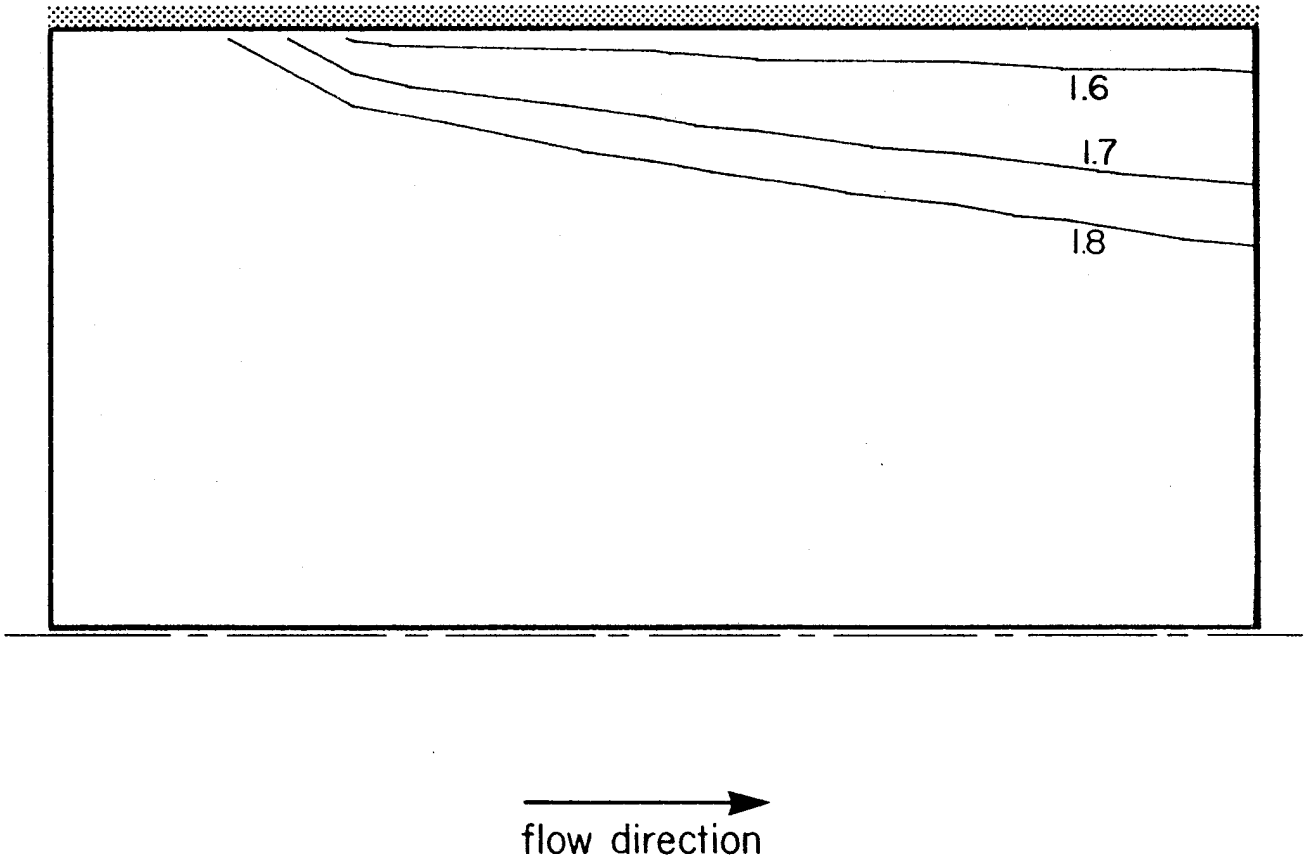

ϕ_1° is measured in radians

Figure 3.16 Mode angle contours for initially random fiber orientation in plane Poiseuille flow. ϕ_1° is measured clockwise with respect to the perpendicular to the flow direction.

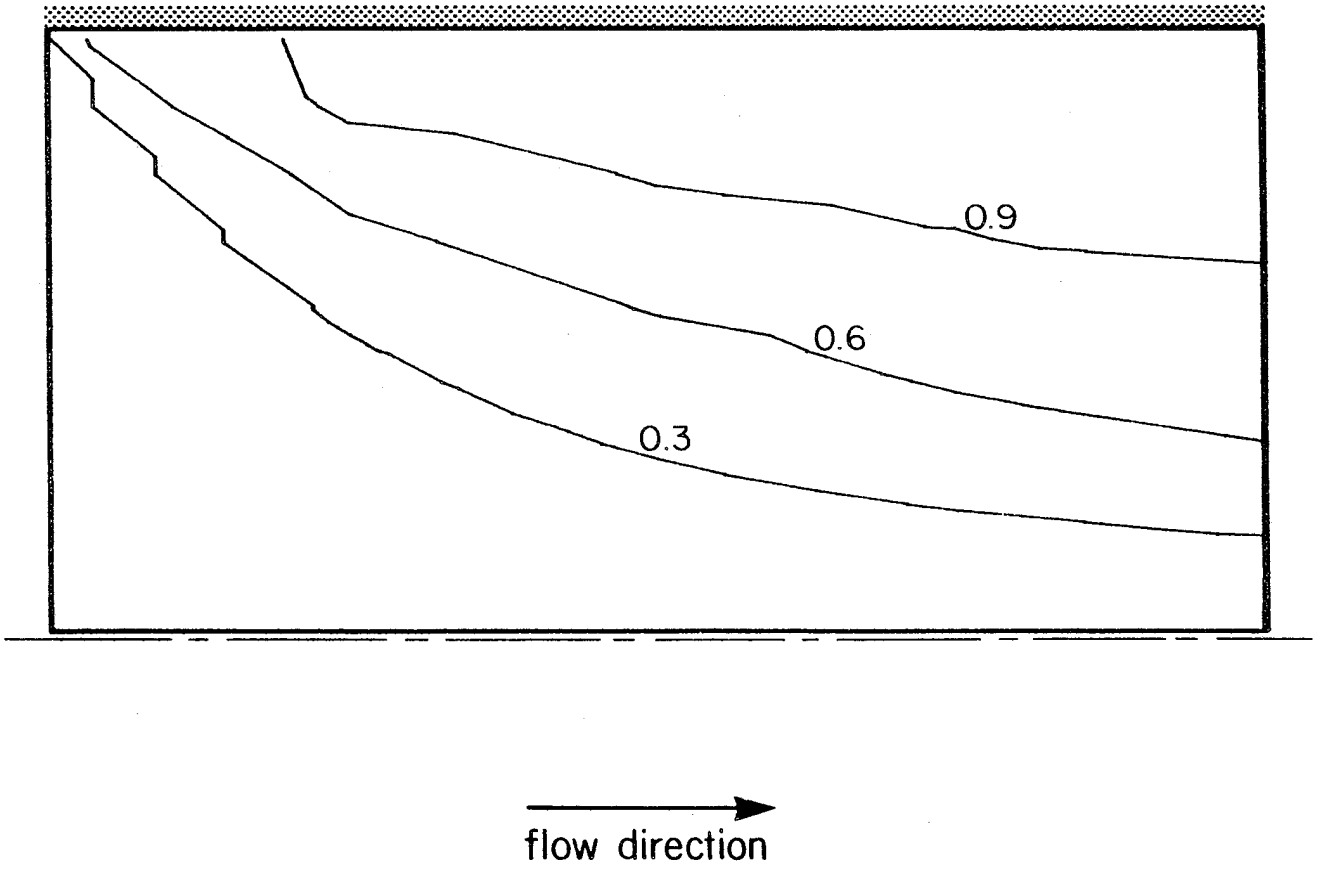

Figure 3.17 Contours of f_p for initially random fiber orientation in plane Poiseuille flow

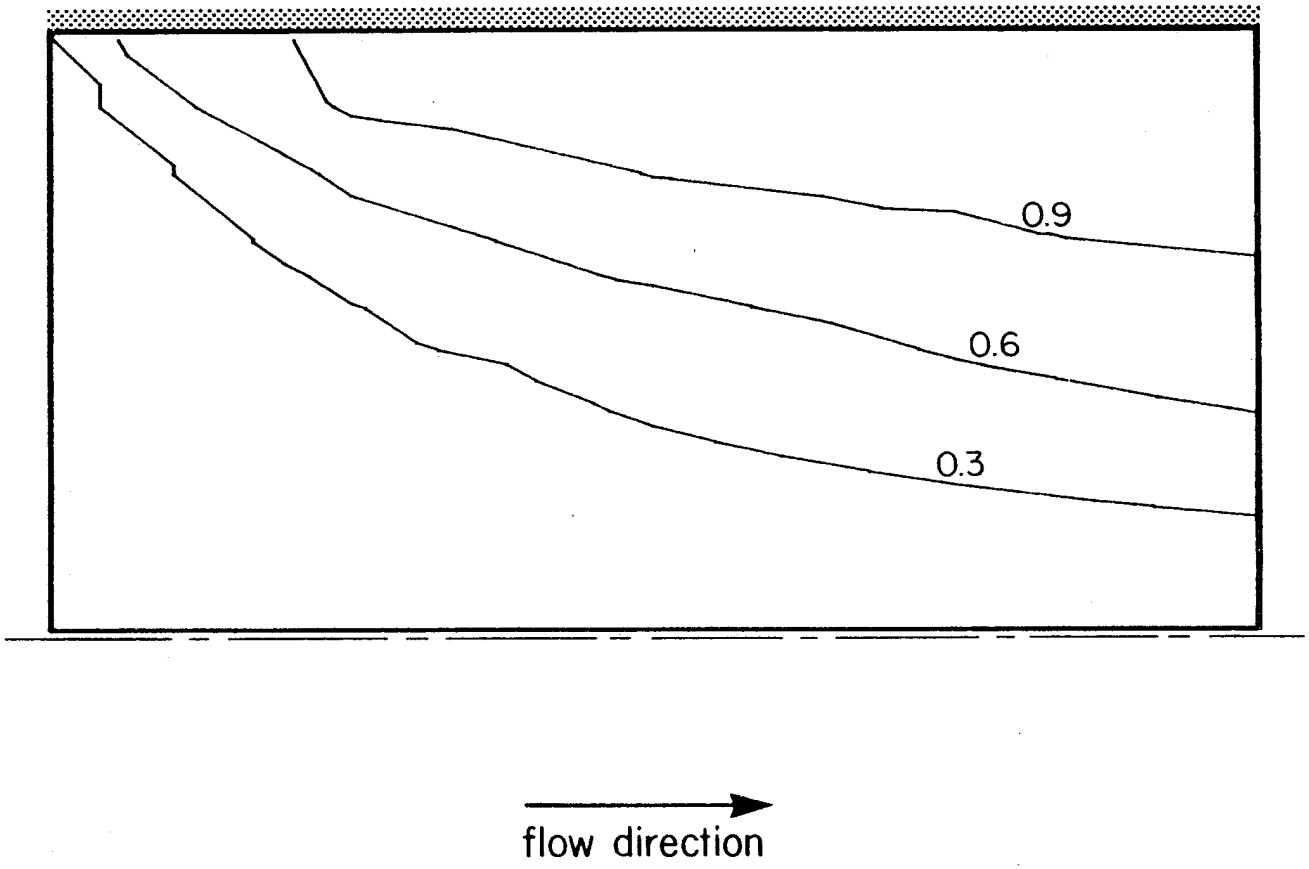

Figure 3.18 Contours of g_p for initially random fiber orientation in plane Poiseuille flow

finite element mesh and boundary conditions to determine the flow solution are depicted in Figure 3.19. Newtonian behavior is assumed.

The boundary conditions require explanation. Along the solid boundaries (i.e., the wall and inclusion boundaries), the normal no slip condition is assumed. On the centerline, adjacent to the inclusion, the shear stress and the x_2 component of velocity are both equal to zero. At the input and exit boundaries of the flow, it is assumed that the fluid is far enough away from the inclusion that the flow is unaffected by it; hence Poiseuille flow exists along these boundaries.

The resulting stream function, pressure, and shear stress contours are plotted in Figures 3.20 through 3.22, respectively. Here, an analytical solution is not available, thus one must be guided by intuition in interpreting the fluid mechanics solution. Inspection of the contour plots (especially the stream function contours) reveal that the flow solution is reasonable.

One next determines the fiber orientation. Guided by results in Appendix 2, ten randomly oriented fibers are input at the beginning of each streamline. The resulting orientation parameter and mode angle contours are depicted in Figures 3.23 through 3.25. Several interesting

observations can be made from these plots:

1) As before in the Poiseuille flow example, a distinct boundary layer of aligned fibers exists in the region near the wall.
2) A second boundary layer of collimated fibers is present resulting from flow around the insert. Downstream from the insert there is no mechanism available to misalign the fibers; consequently, the boundary layer propagates downstream.
3) A core of random fibers exists between the two boundary layers.

It has been mentioned previously that the presence of fibers leads to pseudoplastic fluid behavior, which may be portrayed by a power law constitutive assumption. Figures 3.26 through 3.34 present orientation parameter and mode angle contours for various power law indices under unit flow conditions. The primary observation to be made is that lowering the power law index leads to a larger core of random fibers.

3.5.3 Flow Around a Circular Inclusion in an Infinite Width Channel

In the previous example, the wall boundary played an important role in determining the fiber orientation.

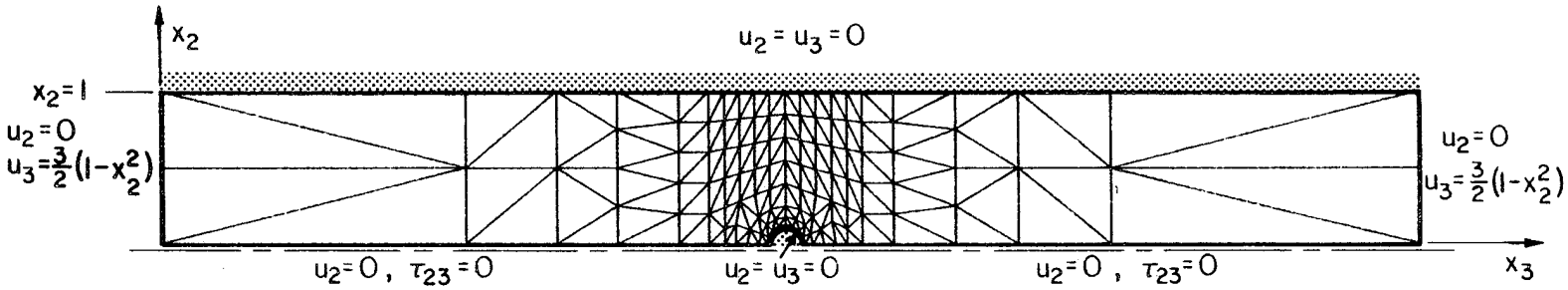

Figure 3.19 Finite element mesh and boundary conditions for determining Newtonian flow around a circular inclusion in a finite width channel

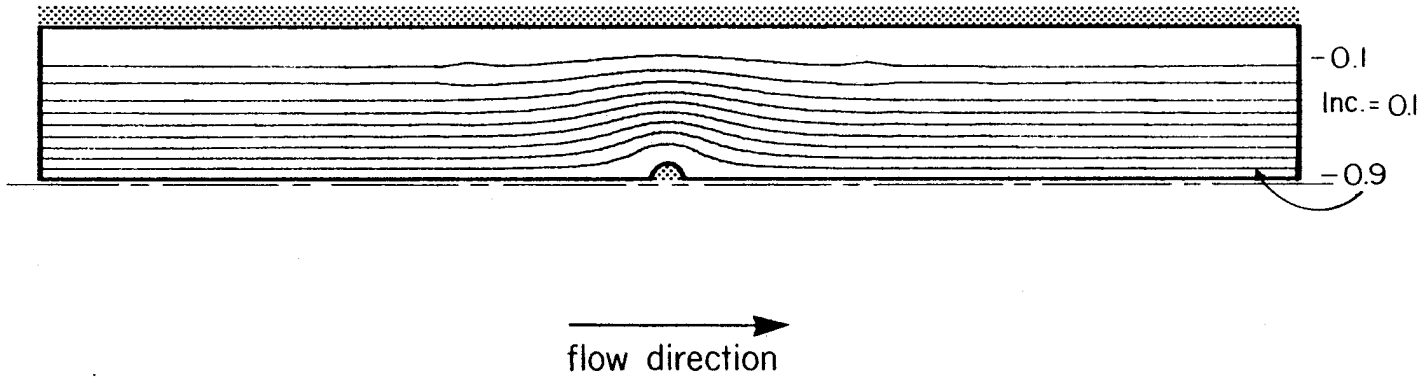

Figure 3.20 Stream function contours (streamlines) for Newtonian flow around a circular inclusion in a finite width channel

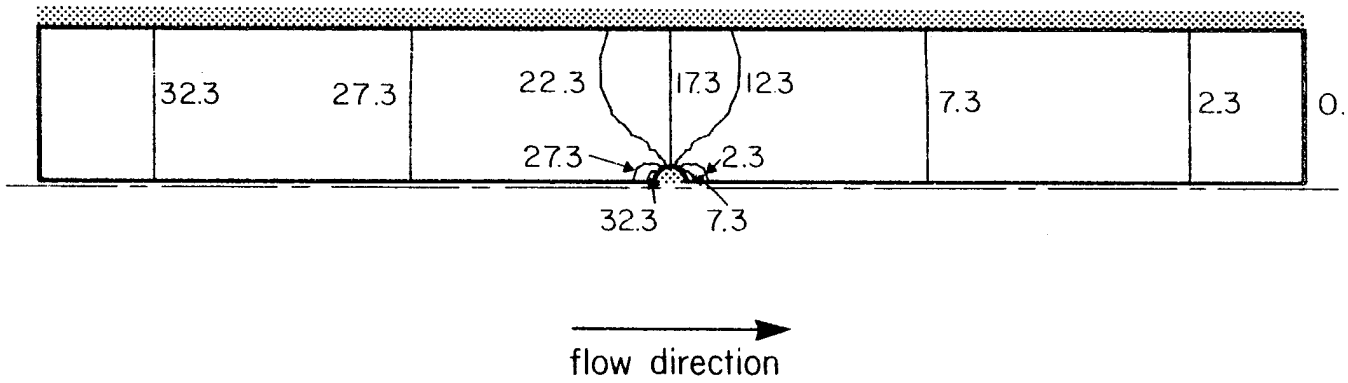

Figure 3.21 Pressure contours for Newtonian flow around a circular inclusion in a finite width channel

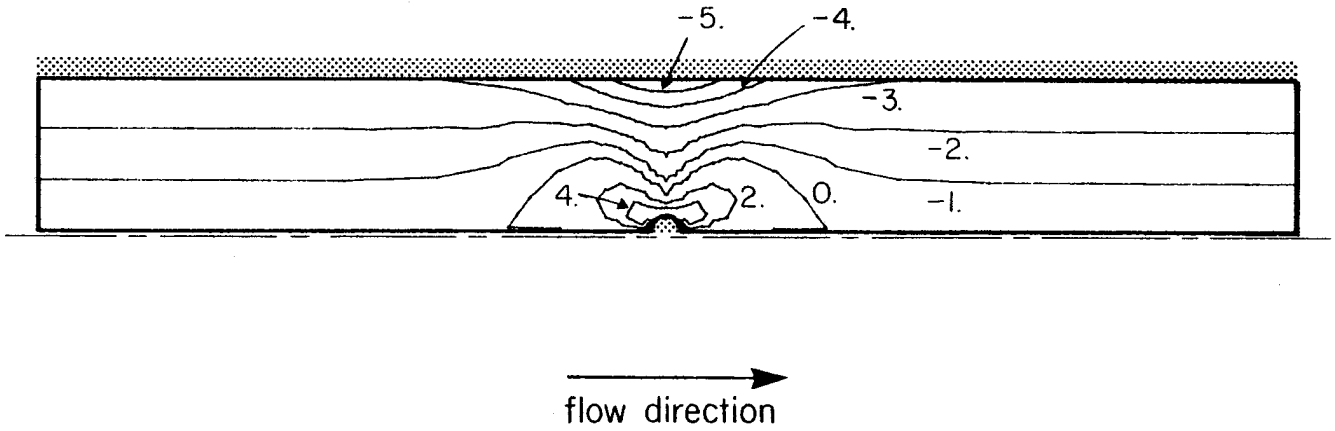

Figure 3.22 Shear stress contours for Newtonian flow around a circular inclusion in a finite width channel

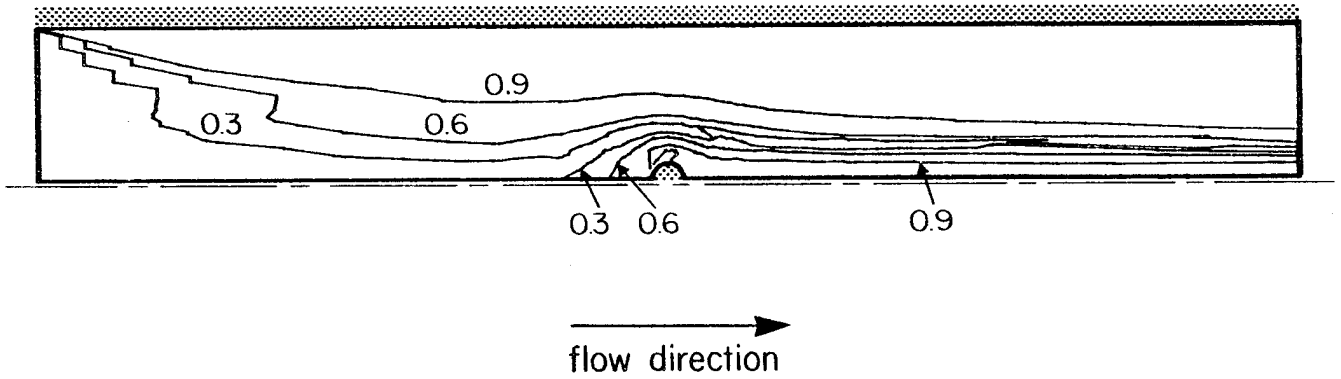

Figure 3.23 Contours of f_p resulting from Newtonian flow around a circular inclusion in a finite width channel

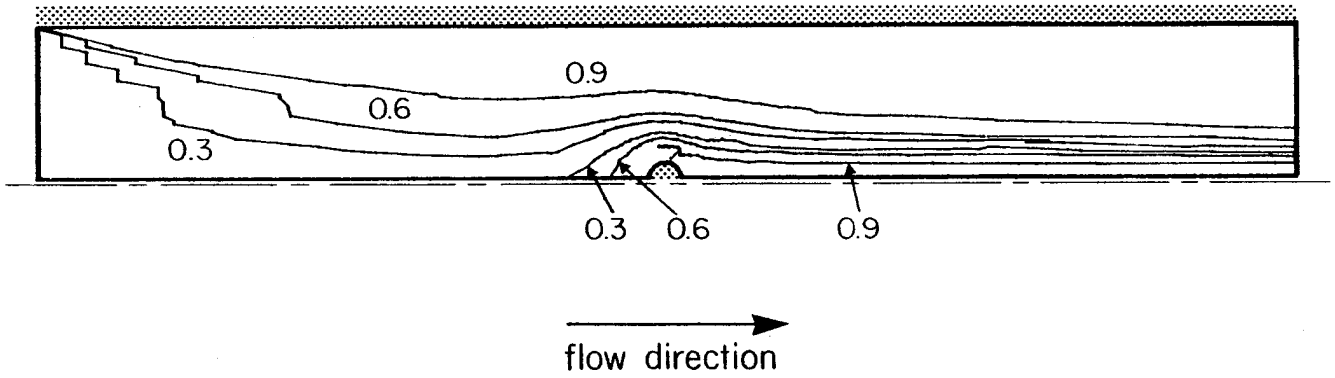

Figure 3.24 Contours of g_p resulting from Newtonian flow around a circular inclusion in a finite width channel

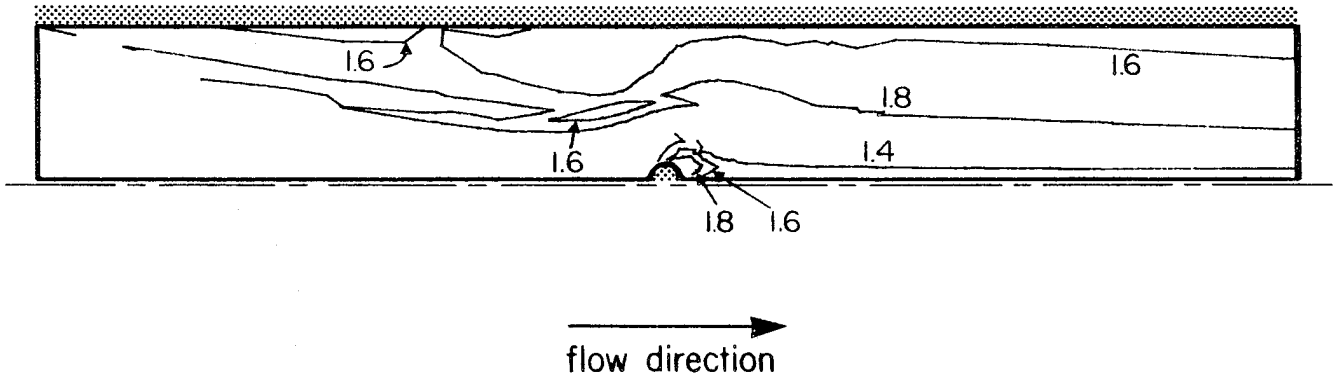

ϕ_1° is measured in radians

Figure 3.25 Mode angle contours resulting from Newtonian flow around a circular inclusion in a finite width channel. ϕ_1° is measured clockwise with respect to the perpendicular to the flow direction.

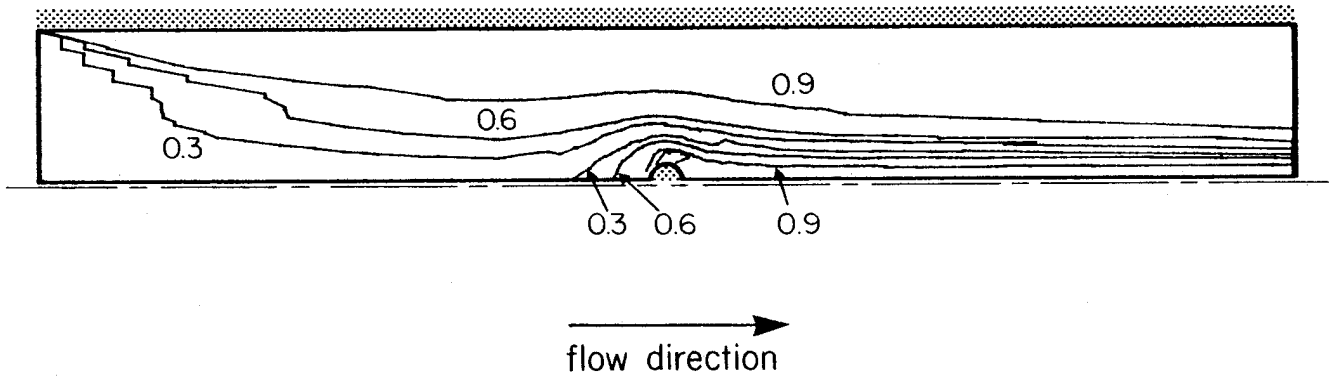

Figure 3.26 Contours of f_p resulting from flow of a power law fluid (index=0.8) around a circular inclusion in a finite width channel

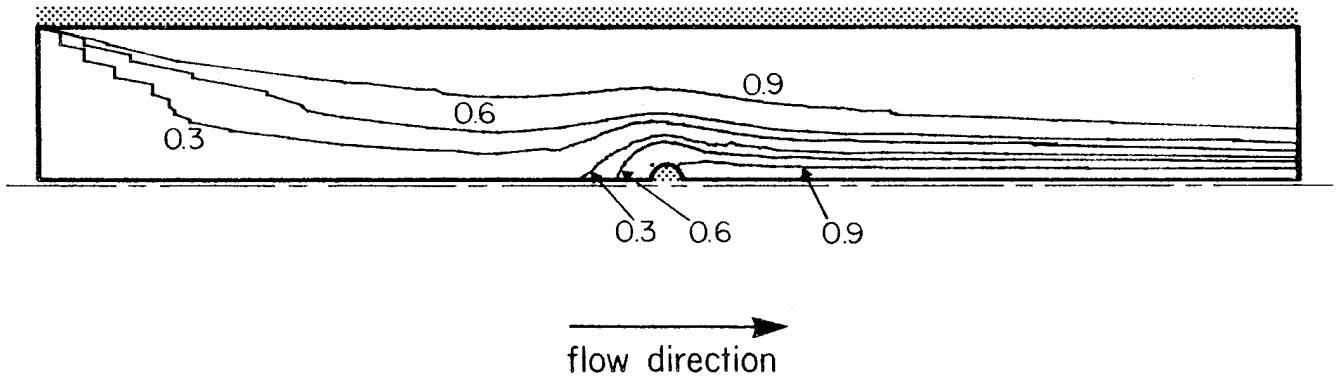

Figure 3.27 Contours of g_p resulting from flow of a power law fluid (index=0.8) around a circular inclusion in a finite width channel

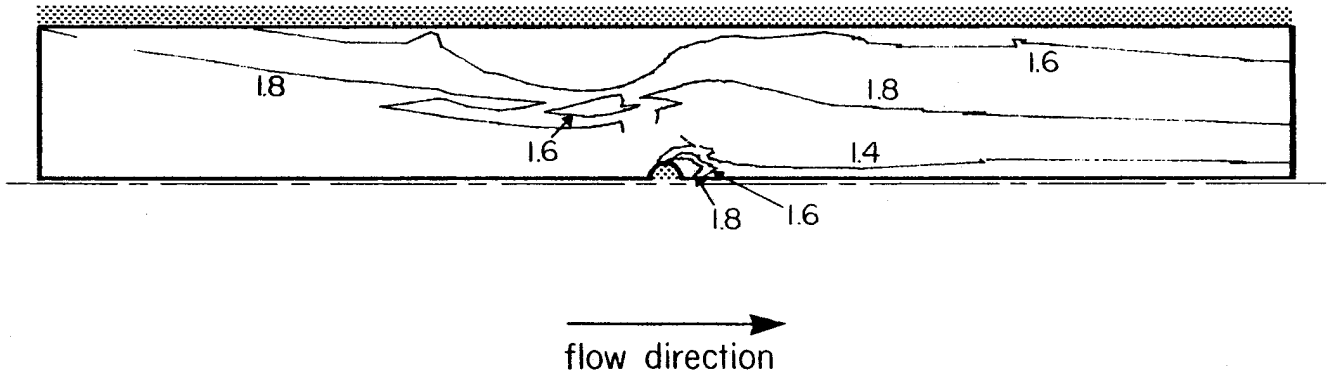

ϕ_1° is measured in radians

Figure 3.28 Mode angle contours resulting from flow of a power law fluid (index=0.8) around a circular inclusion in a finite width channel

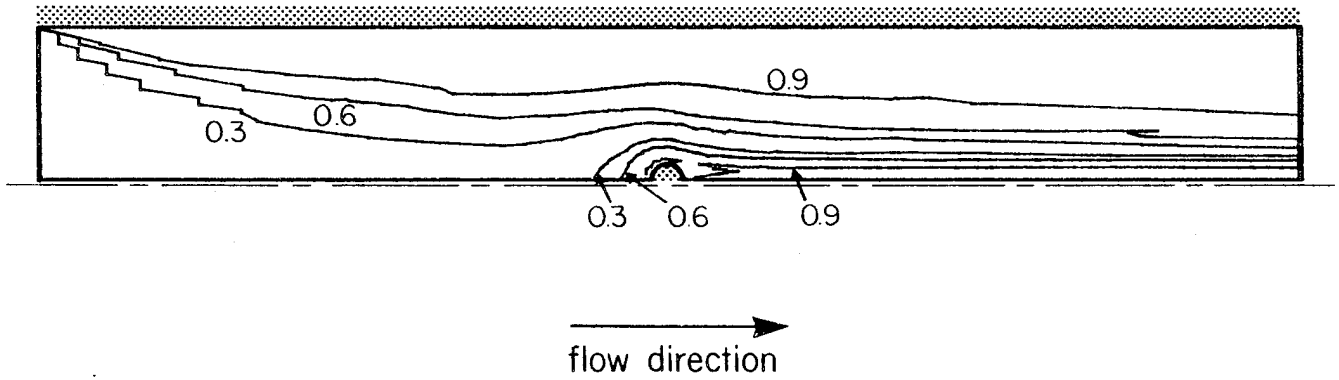

Figure 3.29 Contours of f_p resulting from flow of a power law fluid (index=0.5) around a circular inclusion in a finite width channel

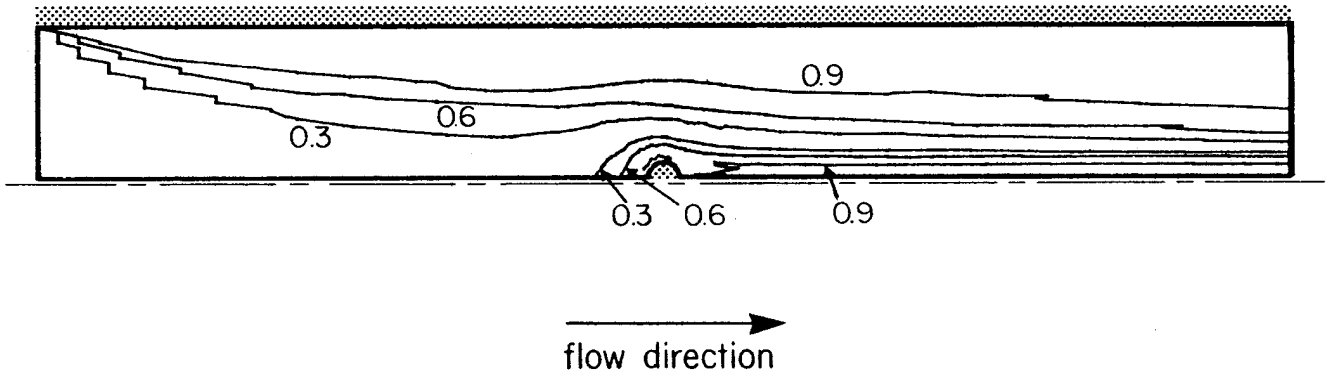

Figure 3.30 Contours of g_p resulting from flow of a power law fluid (index=0.5) around a circular inclusion in a finite width channel

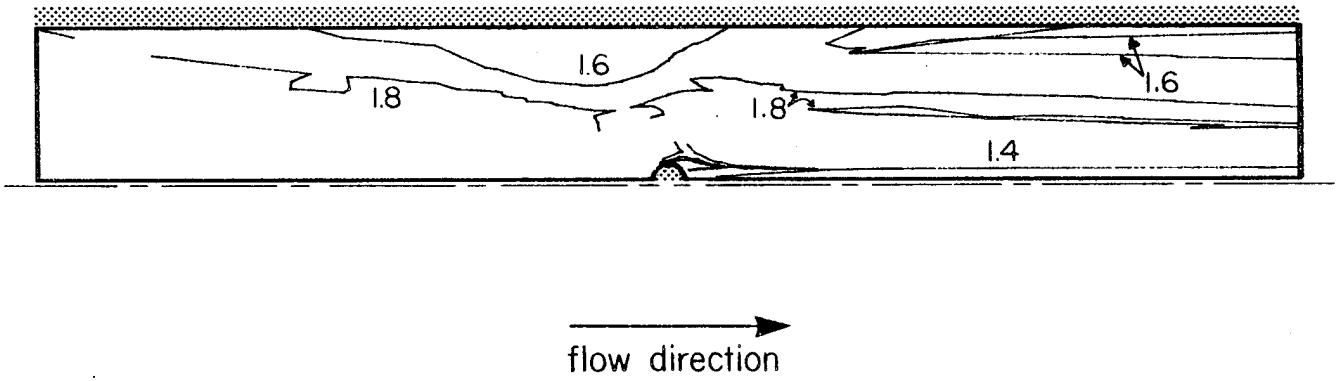

ϕ_1° is measured in radians

Figure 3.31 Mode angle contours resulting from flow of a power law fluid (index=0.5) around a circular inclusion in a finite width channel

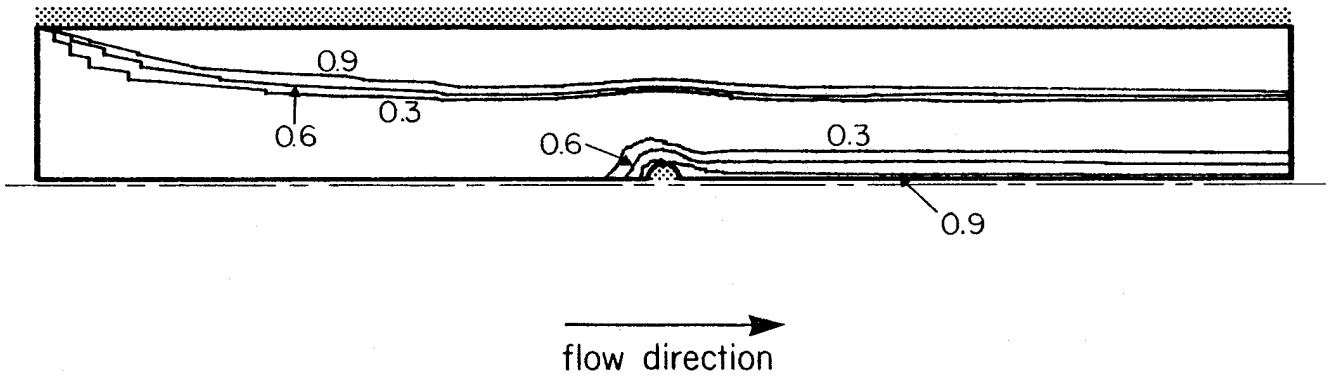

Figure 3.32 Contours of f_p resulting from flow of a power law fluid (index=0.2) around a circular inclusion in a finite width channel

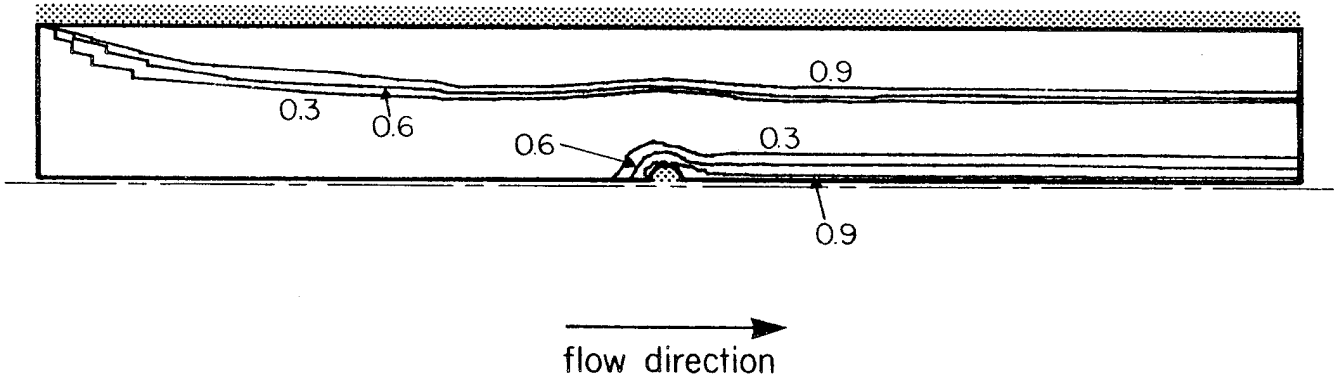

Figure 3.33 Contours of g_p resulting from flow of a power law fluid (index=0.2) around a circular inclusion in a finite width channel

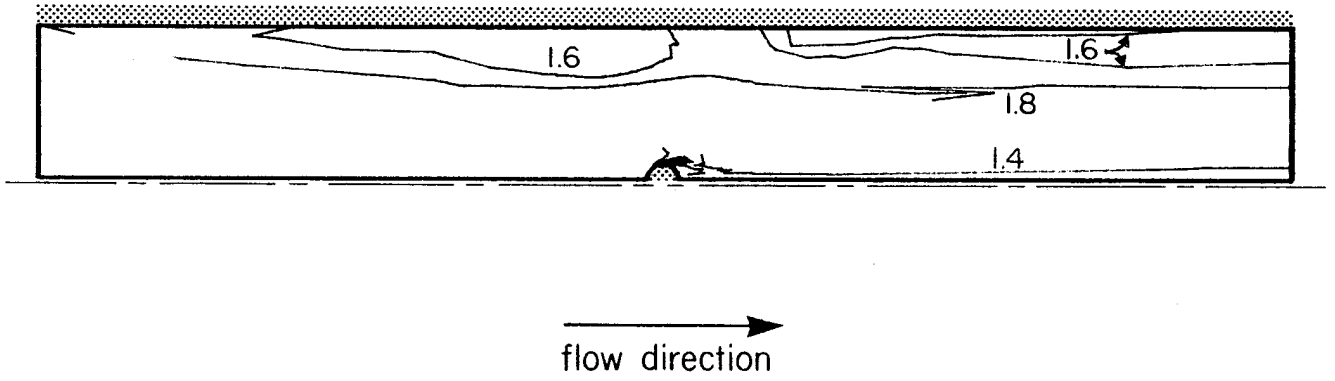

ϕ_1° is measured in radians

Figure 3.34 Mode angle contours resulting from flow of a power law fluid (index=0.2) around a circular inclusion in a finite width channel

One may wish to investigate the fiber orientation in a channel of infinite width, thus isolating the inclusion as the sole mechanism for orienting the fibers.

The finite element mesh and associated boundary conditions to determine the flow field are presented in Figure 3.35. Newtonian behavior is assumed. This example presupposes a constant unit far-field velocity profile. The left, right, and top wall boundaries are placed far enough away from the insert that the far-field velocity profile exists at these outer boundaries. The resulting stream function, pressure, and shear stress contours are depicted in Figures 3.36 through 3.38.

Having ascertained the flow solution, the fiber orientation is determined. Orientation parameter and mode angle contours are presented in Figures 3.39 through 3.41. These figures show clearly the expected presence of a boundary layer of aligned fibers resulting from flow over the inclusion.

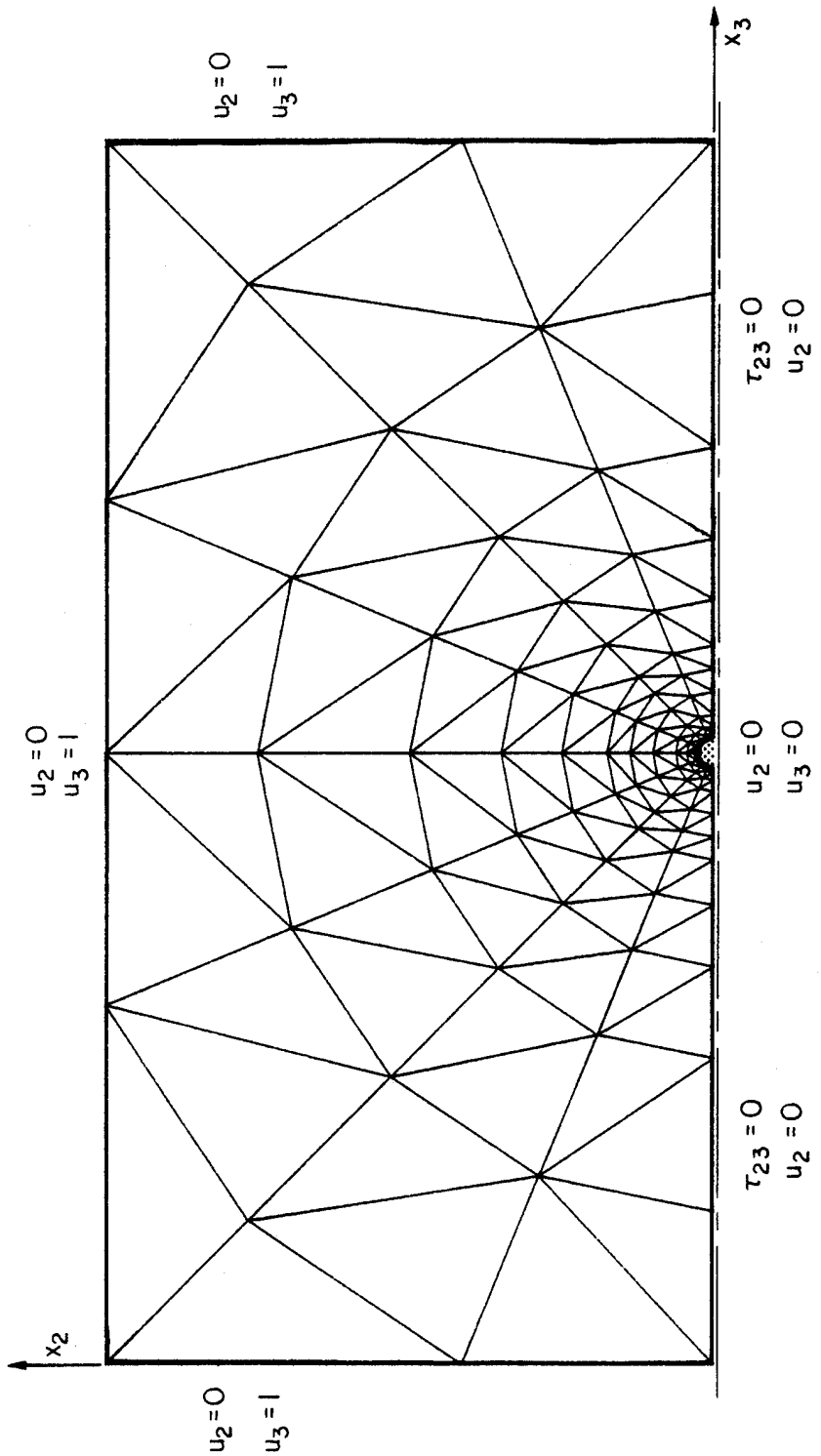

Figure 3.35 Finite element mesh and boundary conditions for determining Newtonian flow around a circular inclusion in an infinite width channel

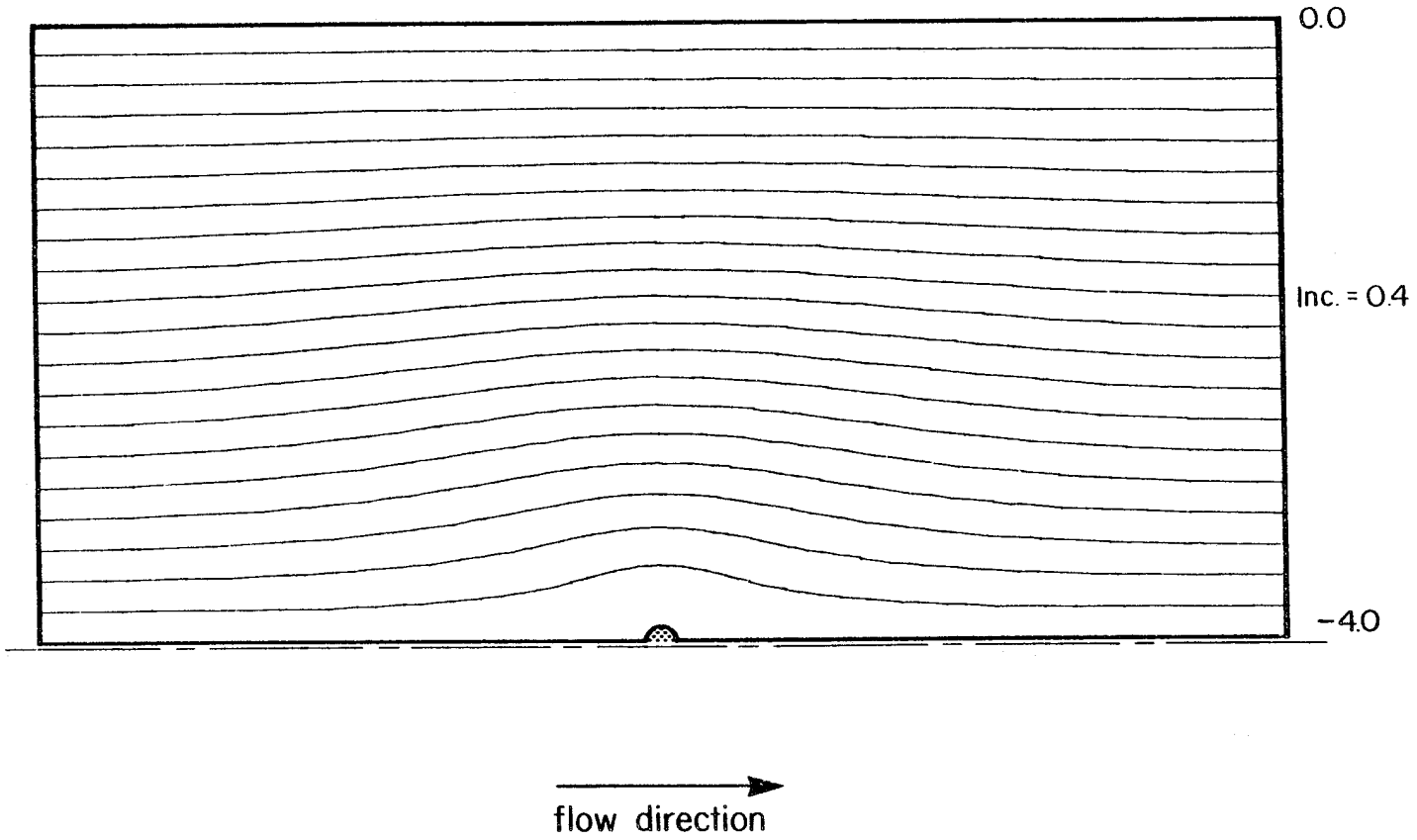

Figure 3.36 Stream function contours (streamlines) for Newtonian flow around a circular inclusion in an infinite width channel

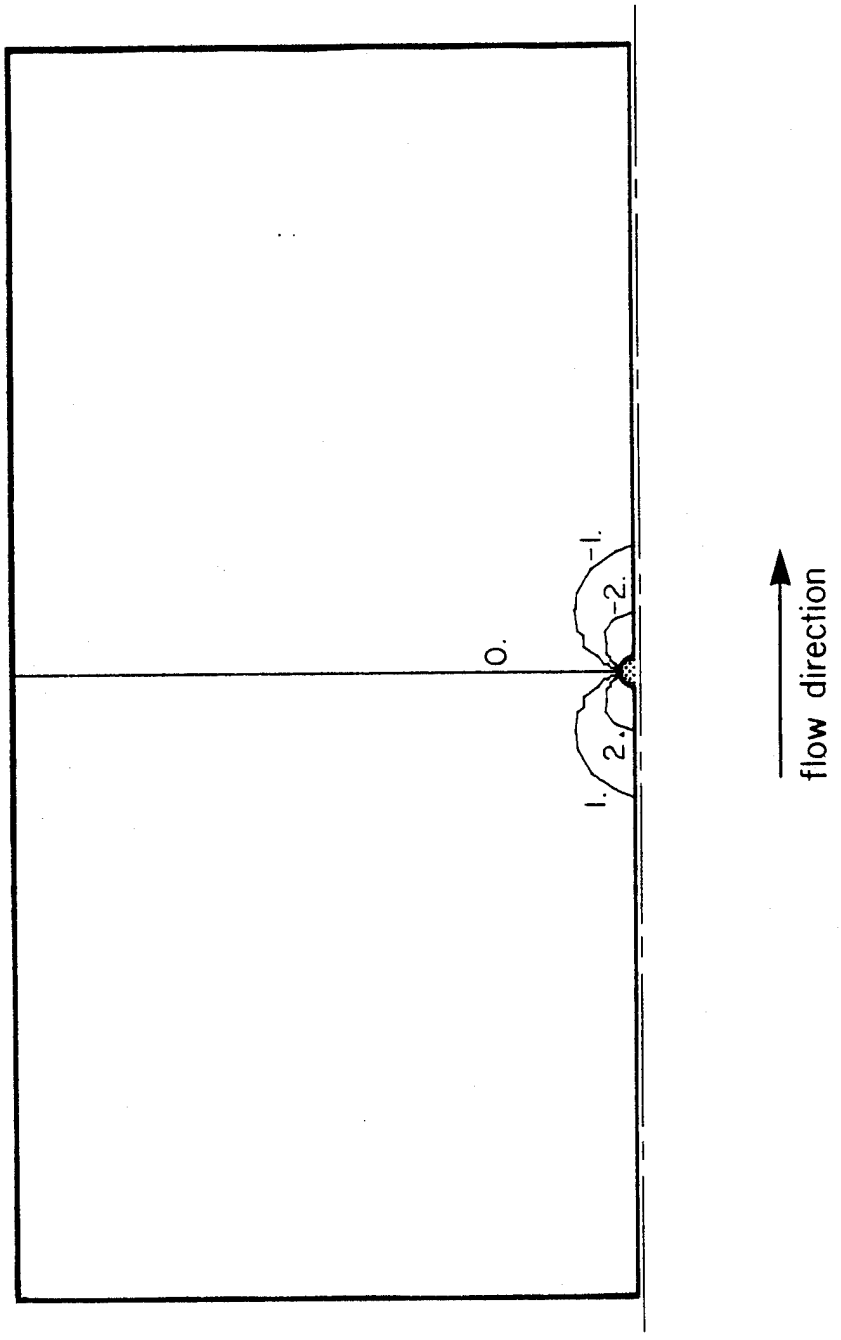

Figure 3.37 Pressure contours for Newtonian flow around a circular inclusion in an infinite width channel

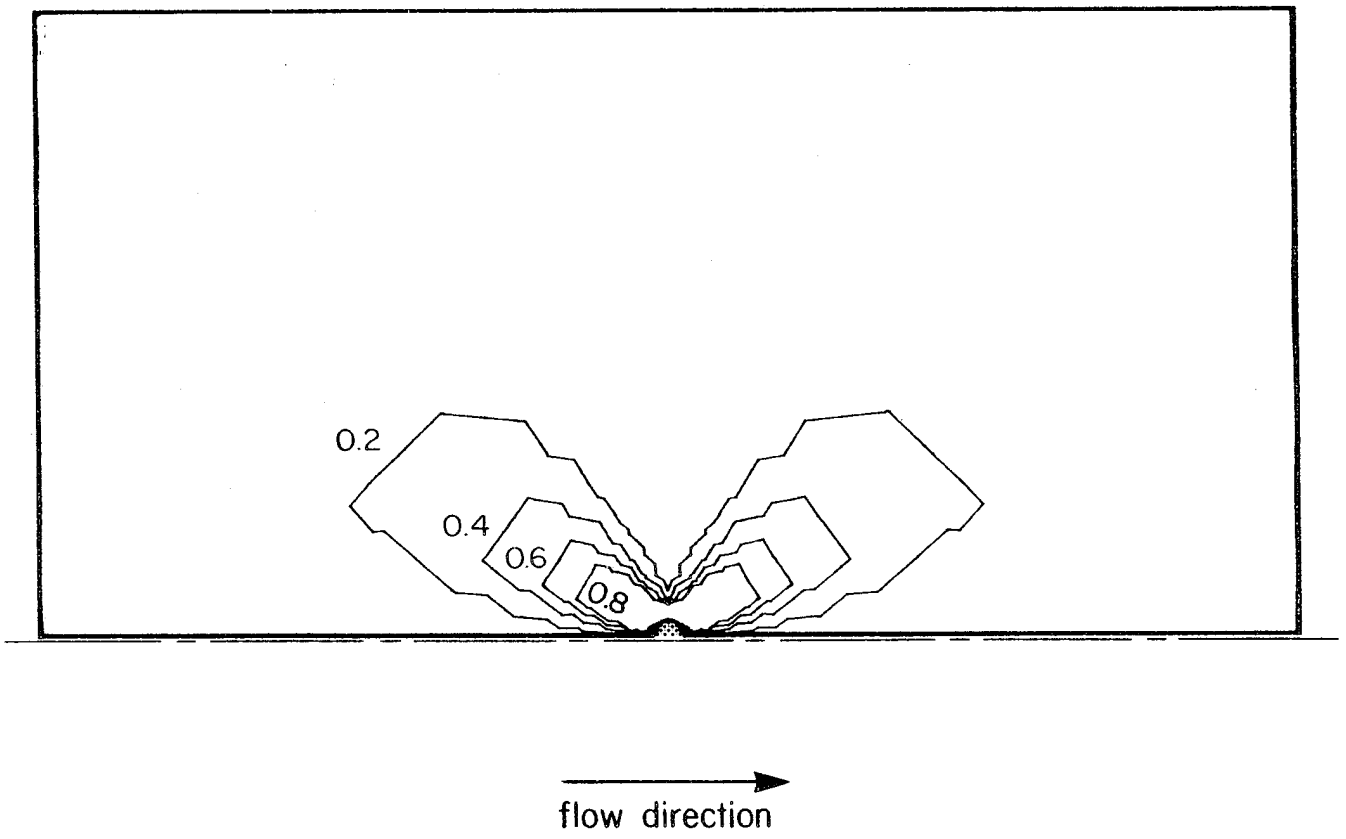

Figure 3.38 Shear stress contours for Newtonian flow around a circular inclusion in an infinite width channel

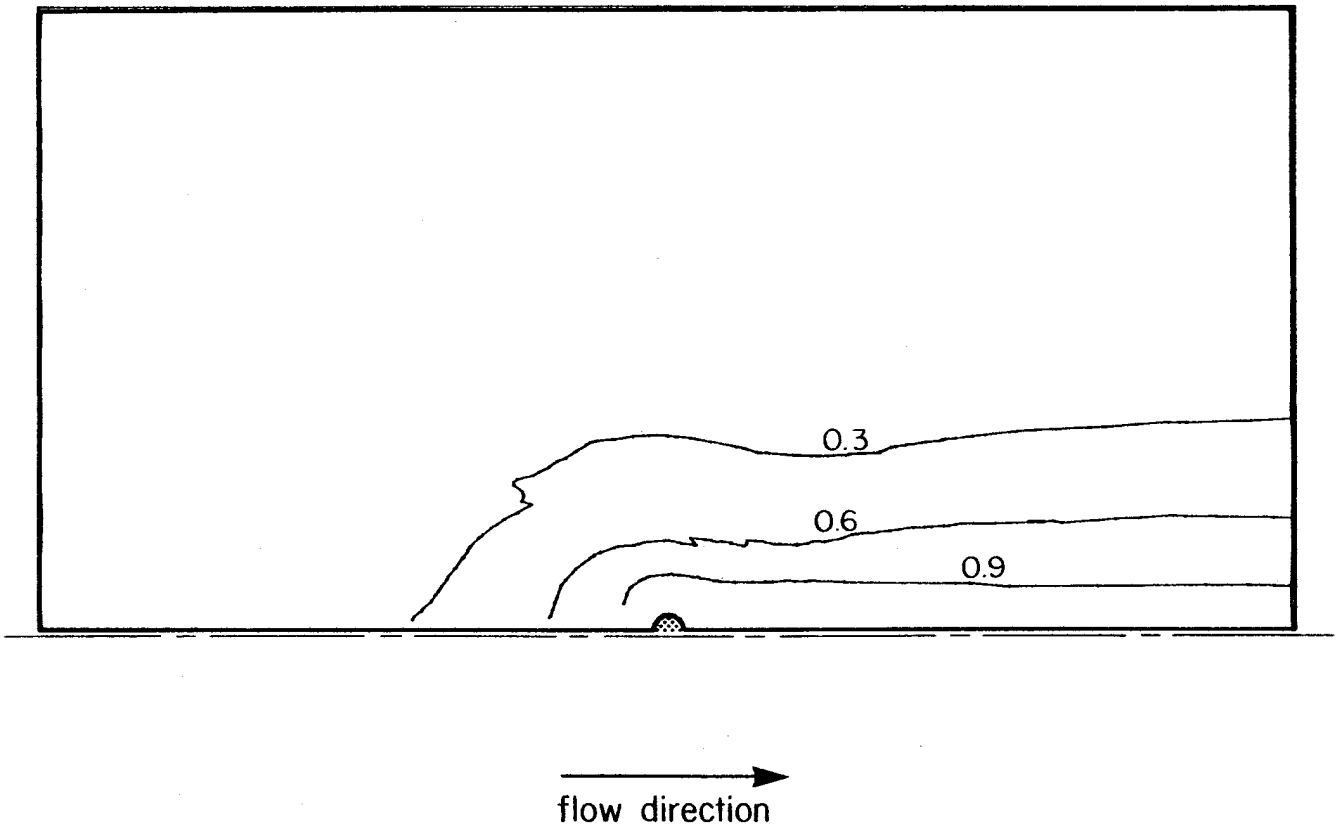

Figure 3.39 Contours of f_p resulting from Newtonian flow around a circular inclusion in an infinite width channel

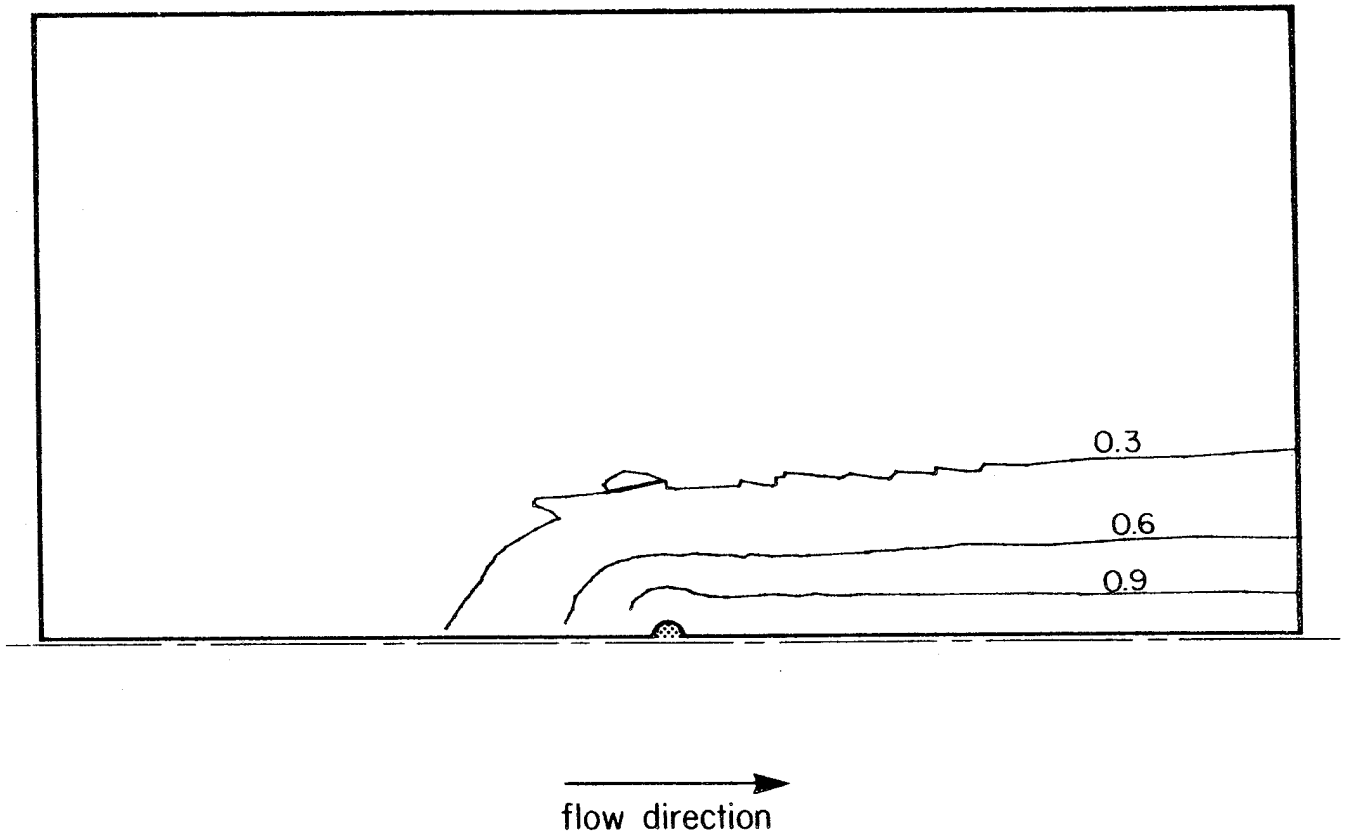

Figuree 3.40 Contours of g_p resulting from Newtonian flow around a circular inclusion in an infinite width channel

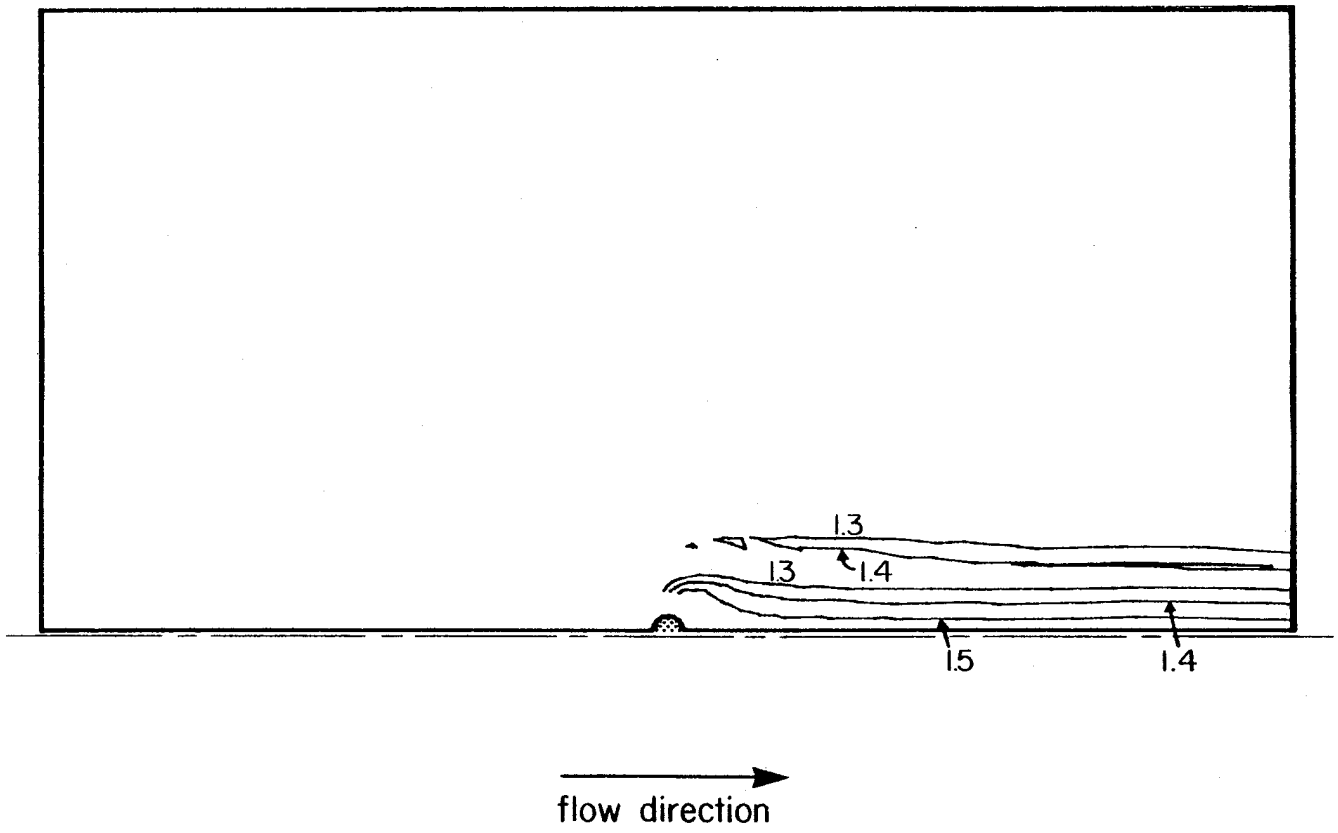

ϕ_1° is measured in radians

Figure 3.41 Mode angle contours resulting from Newtonian flow around a circular inclusion in an infinite width channel. ϕ_1° is measured clockwise with respect to the perpendicular to the flow direction.

CHAPTER 4. AXISYMMETRIC FLOW

Having developed and demonstrated the numerical method for determining fiber orientation in plane flow, attention is now turned to the determination of fiber orientation in axisymmetric flow. Defining a cylindrical coordinate system as shown in Figure 4.1, it is known from the assumption of axisymmetry that the θ direction velocity as well as the variation of the r and z direction velocities in the θ direction of the fluid are identically equal to zero. Consequently, the axisymmetric flow case represents a two-dimensional flow regime, and the method developed to predict fiber orientation in plane flow is applicable to axisymmetric flow. However, the fiber orientation equations have to be developed under the axisymmetric simplifications. This is accomplished in Section 4.1. Furthermore, in this chapter, the assumption of planar fibers is lifted, necessitating the development of a new set of orientation parameters. This topic will be discussed in Section 4.3. The analytical solution for fiber orientation in Poiseuille flow is determined in Section 4.2 and is compared with the numerical solution

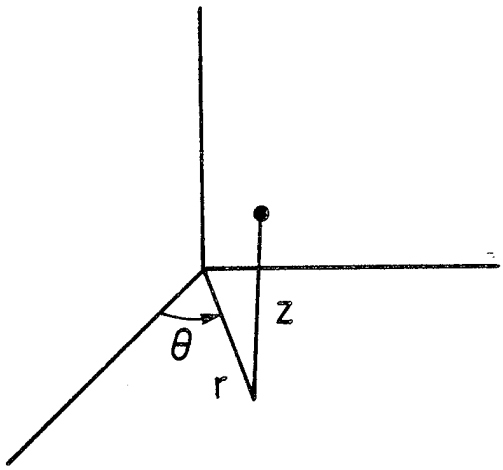

Figure 4.1. Cylindrical coordinate system

in Section 4.4. One final example, the fiber orientation in a simulated disk molding operation, provides a practical illustration of the numerical solution technique.

4.1 Fiber Orientation Equations in Axisymmetric Flow

To take full advantage of the simplifications induced by axisymmetry, modifications must be introduced into the fiber orientation equations. One can make use of the axisymmetric simplifications if the fiber orientation is described relative to a cylindrical reference frame as opposed to the Cartesian reference frame in

Figure 2.1. The most judicious choice of a cylindrical reference frame appears to be the one shown in Figure 4.2. With this choice, the angle θ_1 is preserved; it becomes

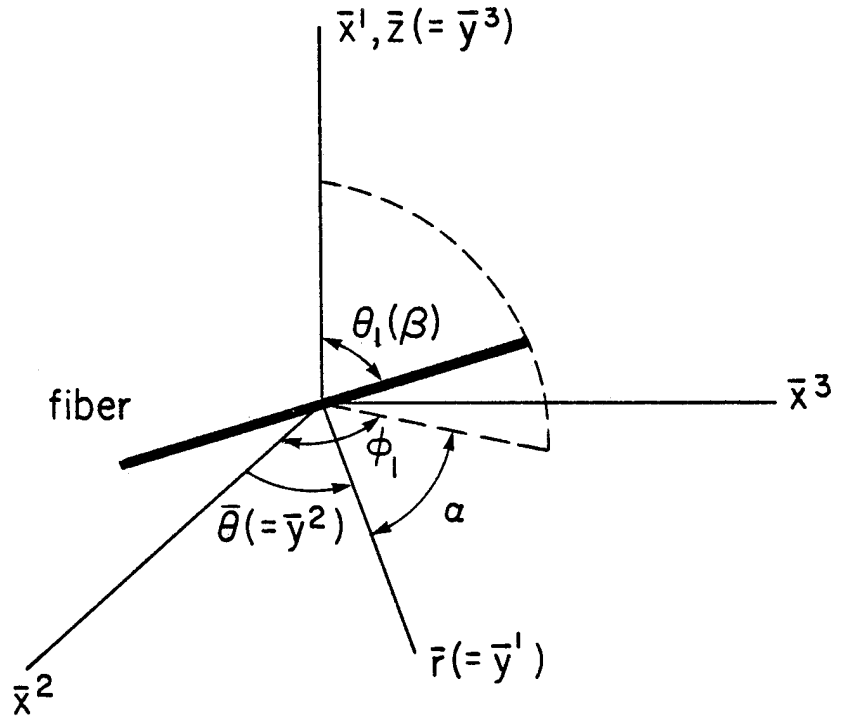

Figure 4.2. Cylindrical reference frame and orientation angles for describing fiber orientation in axisymmetric flow

the angle between the fiber and the $\bar{y}^3$ (or $\bar{z}$) axis. To avoid confusion, it is renamed as β. A new angle α is defined as the angle between the $\bar{r}$ axis and the projection of the fiber on the $\bar{x}^2$-$\bar{x}^3$ plane in a plane containing the fiber and the $\bar{z}$ axis. Reference to Figure 4.1 reveals that

$$\alpha = \phi_1 - \bar{\theta} \tag{4.1}$$

where $\bar{\theta}$ is the cylindrical coordinate angle. For the analysis that follows, the cylindrical coordinates are defined as $\bar{y}^1$, $\bar{y}^2$, and $\bar{y}^3$ where

$$\bar{y}^1 = \bar{r}$$
$$\bar{y}^2 = \bar{\theta}$$
$$\bar{y}^3 = \bar{z}$$

Referring to Figure 4.2, it is seen that the cylindrical coordinates ($\bar{y}^i$) are related to the Cartesian coordinates ($\bar{x}^i$) by

$$\bar{x}^1 = \bar{y}^3$$
$$\bar{x}^2 = \bar{r}\cos\bar{\theta} = \bar{y}^1\cos\bar{y}^2$$
$$\bar{x}^3 = \bar{r}\sin\bar{\theta} = \bar{y}^1\sin\bar{y}^2$$

From the above relations, the following partial derivatives are easily evaluated:

$$\frac{\delta\bar{x}^1}{\delta\bar{y}^1} = 0 \qquad \frac{\delta\bar{x}^1}{\delta\bar{y}^2} = 0 \qquad \frac{\delta\bar{x}^1}{\delta\bar{y}^3} = 1$$

$$\frac{\delta\bar{x}^2}{\delta\bar{y}^1} = \cos\bar{y}^2 \qquad \frac{\delta\bar{x}^2}{\delta\bar{y}^2} = -\bar{y}^1\sin\bar{y}^2 \qquad \frac{\delta\bar{x}^2}{\delta\bar{y}^3} = 0 \qquad (4.2)$$

$$\frac{\delta\bar{x}^3}{\delta\bar{y}^1} = \sin\bar{y}^2 \qquad \frac{\delta\bar{x}^3}{\delta\bar{y}^2} = \bar{y}^1\cos\bar{y}^2 \qquad \frac{\delta\bar{x}^3}{\delta\bar{y}^3} = 0$$

The partial derivative terms above are needed for tensor tranformations which will be performed later in the analysis.

To obtain the necessary equations to solve the fiber orientation in axisymmetric flow, it is necessary to transform all the vorticity and rate of deformation components in Jeffery's equations (2.1) and (2.2) to their respective components in cylindrical coordinates. To do this, one must determine the tensor character of the vorticity and rate of deformation components and then transform these quantities according to the usual rules of tensor transformation. Having transformed the tensor quantities, they are then converted into physical components.

Dealing first with vorticity components, it is known by definition that

$$\bar{z}_i = \frac{1}{2} e_{ijk} \bar{\omega}_{kj}$$

where e_{ijk} is called the permutation symbol and defined by

$$e_{ijk} = \begin{cases} 0 & \text{if any two indices are equal} \\ 1 & \text{if i,j,k are distinct and in cyclic order (i.e., 123 or 231 or 312)} \\ -1 & \text{if i,j,k are distinct but not in cyclic order (i.e., 132 or 213 or 321)} \end{cases}$$

Thus,

$$\begin{aligned} \bar{z}_1 &= \tfrac{1}{2}(\bar{\omega}_{32} - \bar{\omega}_{23}) \\ \bar{z}_2 &= \tfrac{1}{2}(\bar{\omega}_{13} - \bar{\omega}_{31}) \\ \bar{z}_3 &= \tfrac{1}{2}(\bar{\omega}_{21} - \bar{\omega}_{12}) \end{aligned} \qquad (4.3)$$

where $\underset{\sim}{\bar{\omega}}$ is the second order vorticity tensor defined by

$$\bar{\omega}_{ij} = \tfrac{1}{2}(\bar{v}_{i,j} - \bar{v}_{j,i})$$

From this definition it is obvious that $\bar{\omega}_{ij} = -\bar{\omega}_{ji}$ and,

hence, Equations (4.3) simplify to

$$\begin{aligned} \bar{z}_1 &= -\bar{\omega}_{23} \\ \bar{z}_2 &= \bar{\omega}_{13} \\ \bar{z}_3 &= -\bar{\omega}_{12} \end{aligned} \tag{4.4}$$

Now, the vorticity terms in (2.1) and (2.2) are Cartesian components and thus can represent covariant, contravariant or physical components since no distinction is made in the Cartesian system. Since the partial derivatives (4.2) are known, the vorticity terms are chosen to transform as contravariant components via

$$\bar{\omega}^{\alpha\beta}(\bar{x}) = \frac{\delta\bar{x}^{\alpha}}{\delta\bar{y}^{i}} \frac{\delta\bar{x}^{\beta}}{\delta\bar{y}^{j}} \bar{\omega}^{ij}(\bar{y}) \tag{4.5}$$

Using (4.2), (4.4), and (4.5) one can compute $\bar{z}_1(\bar{x})$:

$$\begin{aligned} \bar{z}_1(\bar{x}) &= \bar{z}^1(\bar{x}) \\ &= -\bar{\omega}^{23}(\bar{x}) \\ &= -\frac{\delta\bar{x}^2}{\delta\bar{y}^{i}} \frac{\delta\bar{x}^3}{\delta\bar{y}^{j}} \bar{\omega}^{ij}(\bar{y}) \end{aligned}$$

$$= -\frac{\delta\bar{x}^2}{\delta\bar{y}^1}\frac{\delta\bar{x}^3}{\delta\bar{y}^j}\bar{\omega}^{1j}(\bar{y}) - \frac{\delta\bar{x}^2}{\delta\bar{y}^2}\frac{\delta\bar{x}^3}{\delta\bar{y}^j}\bar{\omega}^{2j}(\bar{y})$$

$$= -\cos\bar{\theta}\left[\frac{\delta\bar{x}^3}{\delta\bar{y}^2}\bar{\omega}^{12}(\bar{y})\right] + \bar{r}\sin\bar{\theta}\left[\frac{\delta\bar{x}^3}{\delta\bar{y}^1}\bar{\omega}^{21}(\bar{y})\right]$$

$$= -\bar{r}\cos^2\bar{\theta}\,\bar{\omega}^{12}(\bar{y}) + \bar{r}\sin^2\bar{\theta}\,\bar{\omega}^{21}(\bar{y})$$

$$= -\bar{r}\,\bar{\omega}^{12}(\bar{y})$$

It is desirable to switch to physical components, which is easily accomplished as follows:

$$\bar{z}_1(x) = -\bar{r}\sqrt{g_{11}}\sqrt{g_{22}}\bar{\omega}\langle 12\rangle(\bar{y})$$

$$= -\bar{\omega}\langle 12\rangle(\bar{y})$$

$$= -\bar{\omega}_{r\theta}$$

where $\underset{\sim}{g}$ is the metric tensor.

Here, the usual bracketed notation for physcial components is eliminated and, instead, the indices are subscripted and given in terms of the coordinate labels. The same procedure is employed to determine $\bar{z}_2(\bar{x})$ and $\bar{z}_3(\bar{x})$ as a function of $\bar{\omega}\langle ij\rangle(\bar{y})$, and the results are presented in Table 4.1.

The Cartesian components of the rate of deformation tensor are computed in terms of the cylindrical components following the same procedure. First, one notes that the rate of deformation tensor is second order and defined by

$$\bar{d}_{ij} = \tfrac{1}{2}(\bar{v}_{i,j}+\bar{v}_{j,i})$$

Table 4.1

Cartesian Components of Vorticity Tensor Expressed in Terms of Cylindrical Components

$$\bar{z}_1(\bar{x}) = -\bar{\omega}_{r\theta}$$

$$\bar{z}_2(\bar{x}) = -\sin\bar{\theta}\ \bar{\omega}_{rz} - \cos\bar{\theta}\ \bar{\omega}_{\theta z}$$

$$\bar{z}_3(\bar{x}) = \cos\bar{\theta}\ \bar{\omega}_{rz} - \sin\bar{\theta}\ \bar{\omega}_{\theta z}$$

As before, the Cartesian components can represent either covariant, contravariant or physical components and, hence, the contravariant transformation is valid:

$$\bar{d}_{ij}(\bar{x}) = \bar{d}^{ij}(\bar{x})$$

$$= \frac{\delta\bar{x}^i}{\delta\bar{y}^\alpha}\frac{\delta\bar{x}^j}{\delta\bar{y}^\beta}\,\bar{d}^{\alpha\beta}(\bar{y}) \qquad (4.6)$$

Utilizing (4.2) and (4.6), the following expression may be determined for $\bar{d}_{22}(\bar{x})$:

$$\bar{d}_{22}(\bar{x}) = \bar{d}^{22}(\bar{x})$$

$$= \frac{\delta^2 \bar{x}^2}{\delta \bar{y}^i \delta \bar{y}^j}$$

$$= \frac{\delta^2 \bar{x}^2}{\delta \bar{y}^1 \delta \bar{y}^j} \bar{d}^{1j}(\bar{y}) + \frac{\delta^2 \bar{x}^2}{\delta \bar{y}^2 \delta \bar{y}^j} \bar{d}^{2j}(\bar{y})$$

$$= \cos\bar{\theta}\left[\frac{\delta \bar{x}^2}{\delta \bar{y}^1}\bar{d}^{11}(\bar{y}) + \frac{\delta \bar{x}^2}{\delta \bar{y}^2}\bar{d}^{12}(\bar{y})\right] - \bar{r}\sin\bar{\theta}\left[\frac{\delta \bar{x}^2}{\delta \bar{y}^1}\bar{d}^{21}(\bar{y}) + \frac{\delta \bar{x}^2}{\delta \bar{y}^2}\bar{d}^{22}(\bar{y})\right]$$

$$= \cos^2\bar{\theta}\ \bar{d}^{11}(\bar{y}) - \bar{r}\sin\bar{\theta}\cos\bar{\theta}\ \bar{d}^{12}(\bar{y}) - \bar{r}\sin\bar{\theta}\cos\bar{\theta}\ \bar{d}^{12}(\bar{y}) + \bar{r}^2\sin^2\bar{\theta}\ \bar{d}^{22}(\bar{y})$$

Again converting to physical components via

$$\bar{d}\langle ij\rangle = \sqrt{g_{ii}}\ \sqrt{g_{jj}}\ \bar{d}^{ij} \qquad \text{(no sum on i or j)}$$

one can determine

$$\bar{d}_{22}(\bar{x}) = \cos^2\bar{\theta}\ \bar{d}_{rr} - \sin 2\bar{\theta}\ \bar{d}_{r\theta} + \sin^2\bar{\theta}\ \bar{d}_{\theta\theta}$$

The transformation of the remaining rate of deformation components follows an identical procedure and the results are summarized in Table 4.2.

The component transformations contained in Tables 4.1 and 4.2, as well as, the angle changes can be substituted into (2.1) and (2.2) to obtain

$$\frac{\delta\alpha}{\delta t} = -\bar{\omega}_{r\theta}+(\sin\bar{\theta}\ \bar{\omega}_{rz}+\cos\bar{\theta}\ \bar{\omega}_{\theta z})\cos(\alpha+\bar{\theta})\cot\beta+(\sin\bar{\theta}\ \bar{\omega}_{\theta z} -\cos\bar{\theta}\ \bar{\omega}_{rz})\sin(\alpha+\bar{\theta})\cot\beta+B[(\sin\bar{\theta}\ \bar{d}_{\theta z}-\cos\bar{\theta}\ \bar{d}_{rz})\sin(\alpha +\bar{\theta})\cot\beta+\{\tfrac{1}{2}\sin2\bar{\theta}(\bar{d}_{rr}-\bar{d}_{\theta\theta})+\cos2\bar{\theta}\ \bar{d}_{r\theta}\}\cos2(\alpha+\bar{\theta})+(\sin\bar{\theta}\ \bar{d}_{rz} +\cos\bar{\theta}\ \bar{d}_{\theta z})\cos(\alpha+\bar{\theta})\cot\beta+\tfrac{1}{2}\{(\bar{d}_{\theta\theta}-\bar{d}_{rr}) +2\sin2\bar{\theta}\ \bar{d}_{r\theta}\}\sin2(\alpha+\bar{\theta})] \qquad (4.7)$$

Table 4.2

Cartesian Components of Rate of Deformation Tensor Expressed in Terms of Cylindrical Components

$$\bar{d}_{11}(\bar{x}) = \bar{d}_{zz}$$

$$\bar{d}_{22}(\bar{x}) = \cos^2\bar{\theta}\ \bar{d}_{rr}-\sin2\bar{\theta}\ \bar{d}_{r\theta}+\sin^2\bar{\theta}\ \bar{d}_{\theta\theta}$$

$$\bar{d}_{33}(\bar{x}) = \sin^2\bar{\theta}\ \bar{d}_{rr}+\sin2\bar{\theta}\ \bar{d}_{r\theta}+\cos^2\bar{\theta}\ \bar{d}_{\theta\theta}$$

$$\bar{d}_{12}(\bar{x}) = \cos\bar{\theta}\ \bar{d}_{rz}-\sin\bar{\theta}\ \bar{d}_{\theta z}$$

$$\bar{d}_{13}(\bar{x}) = \sin\bar{\theta}\ \bar{d}_{rz}+\cos\bar{\theta}\ \bar{d}_{\theta z}$$

$$\bar{d}_{23}(\bar{x}) = \tfrac{1}{2}\sin2\bar{\theta}(\bar{d}_{rr}-\bar{d}_{\theta\theta})+\cos2\bar{\theta}\ \bar{d}_{r\theta}$$

$$\frac{\delta\beta}{\delta t} = (\sin\bar{\theta}\ \bar{\omega}_{rz}+\cos\bar{\theta}\ \bar{\omega}_{\theta z})\sin(\alpha+\bar{\theta})+(-\sin\bar{\theta}\ \bar{\omega}_{\theta z}$$

$$+\cos\bar{\theta}\ \bar{\omega}_{rz})\cos(\alpha+\bar{\theta})+B[(\cos\bar{\theta}\ \bar{d}_{rz}-\sin\bar{\theta}\ \bar{d}_{\theta z})\cos(\alpha+\bar{\theta})\cos2\beta$$

$$+\tfrac{1}{2}\{\tfrac{1}{2}\sin2\bar{\theta}(\bar{d}_{rr}-\bar{d}_{\theta\theta})+\cos2\bar{\theta}\ \bar{d}_{r\theta}\}\sin2(\alpha+\bar{\theta})\sin2\beta$$

$$+(\sin\bar{\theta}\ \bar{d}_{rz}+\cos\bar{\theta}\ \bar{d}_{\theta z})\sin(\alpha+\bar{\theta})\cos2\beta+\tfrac{1}{4}\{(\bar{d}_{rr}-\bar{d}_{\theta\theta})\cos2\bar{\theta}$$

$$-2\sin2\bar{\theta}\ \bar{d}_{r\theta}\}\cos2(\alpha+\bar{\theta})\sin2\beta+\frac{3}{4}(\bar{d}_{rr}+\bar{d}_{\theta\theta})\sin2\beta] \qquad (4.8)$$

Since axisymmetry is assumed, (4.7) and (4.8) are independent of $\bar{\theta}$, and can be simplified by inserting any discrete value of $\bar{\theta}$, which results in the following:

$$\frac{\delta\alpha}{\delta t} = -\bar{\omega}_{r\theta}+\bar{\omega}_{\theta z}\cos\alpha\cot\beta-\bar{\omega}_{rz}\sin\alpha\cot\beta+B[-\bar{d}_{rz}\sin\alpha\cot\beta$$

$$+\bar{d}_{r\theta}\cos2\alpha+\bar{d}_{\theta z}\cos\alpha\cot\beta+\tfrac{1}{2}(\bar{d}_{\theta\theta}-\bar{d}_{rr})\sin2\alpha] \qquad (4.9)$$

$$\frac{\delta\beta}{\delta t} = \bar{\omega}_{\theta z}\sin\alpha+\bar{\omega}_{rz}\cos\alpha+B[\bar{d}_{rz}\cos\alpha\cos2\beta+\tfrac{1}{4}(\bar{d}_{rr}-\bar{d}_{\theta\theta})\cos2\alpha\sin2\beta$$

$$+\frac{3}{4}(\bar{d}_{rr}+\bar{d}_{\theta\theta})\sin2\beta] \qquad (4.10)$$

These equations can be further simplified by noting that several vorticity and rate of deformation components are identically equal to zero due to axisymmetry. For example,

$$\bar{\omega}_{r\theta} = \tfrac{1}{2}\left(\frac{1}{\bar{r}}\frac{\delta \bar{v}_r}{\delta \bar{\theta}}^{\circ} - \frac{\delta \bar{v}_\theta}{\delta \bar{r}}^{\circ} - \frac{\bar{v}_\theta}{\bar{r}}^{\circ}\right)$$

$$= 0$$

Likewise, it can be shown that $\bar{\omega}_{\theta z}$, $\bar{d}_{r\theta}$, and $\bar{d}_{\theta z}$ are also equal to zero. Table 4.3 contains a complete description of the physical components of $\underset{\sim}{\bar{\omega}}$ and $\underset{\sim}{\bar{d}}$ in terms of the velocities. Cancelling out all of the terms which are identically zero in equations (4.9) and (4.10),

$$\frac{\delta \alpha}{\delta t} = -\bar{\omega}_{rz}\sin\alpha\cot\beta + B[-\bar{d}_{rz}\sin\alpha\cot\beta + \tfrac{1}{2}(\bar{d}_{\theta\theta} - \bar{d}_{rr})\sin 2\alpha] \qquad (4.11)$$

$$\frac{\delta \beta}{\delta t} = \bar{\omega}_{rz}\cos\alpha + B[\bar{d}_{rz}\cos\alpha\cos 2\beta + \tfrac{1}{4}(\bar{d}_{rr} - \bar{d}_{\theta\theta})\cos 2\alpha\sin 2\beta$$

$$+\frac{3}{4}(\bar{d}_{rr} - \bar{d}_{\theta\theta})\sin 2\beta] \qquad (4.12)$$

These are the resulting equations describing fiber orientation relative to cylindrical coordinate reference axes in axisymmetric flow.

To this point, a coordinate system which

translates with the fiber center and whose axes remain fixed in direction has been adopted. As before, one may wish to describe fiber orientation relative to an inertial reference frame. A prudent choice of an inertial reference frame is one whose axes lie in the directions of the $\bar{y}^i$ axes. Thus, the cylindrical frame y^1, y^2, y^3 is incorporated where each y^i axis of this system lies in the same direction as the corresponding $\bar{y}^i$ axis of the $\bar{y}^1$, $\bar{y}^2$, $\bar{y}^3$ system. In this inertial reference frame, (4.11) and (4.12) transform to

$$\frac{D\alpha}{Dt} = -\omega_{rz}\sin\alpha\cot\beta+B[-d_{rz}\sin\alpha\cot\beta+\tfrac{1}{2}(d_{\theta\theta}-d_{rr})\sin2\alpha] \qquad (4.13)$$

$$\frac{D\beta}{Dt} = \omega_{rz}\cos\alpha+B[d_{rz}\cos\alpha\cos2\beta+\tfrac{1}{4}(d_{rr}-d_{\theta\theta})\cos2\alpha\sin2\beta$$

$$+\frac{3}{4}(d_{rr}+d_{\theta\theta})\sin2\beta] \qquad (4.14)$$

where

$$\frac{D(\ )}{Dt} = \frac{\delta(\ )}{\delta t} + v_r\frac{\delta(\ )}{\delta r} + v_z\frac{\delta(\ )}{\delta z}$$

is the substantial time derivative. The time derivative $\frac{\delta(\ )}{\delta t}$ vanishes when the boundary conditions are time independent.

With the above fiber orientation equations at hand, it is now possible to determine solutions for fiber orientation in axisymmetric flow.

Table 4.3

Physical Components of the Rate of Deformation and Vorticity Tensors in Axisymmetric Flow

$$\bar{\omega}\langle ij\rangle = \tfrac{1}{2}\begin{bmatrix} 0 & 0 & \dfrac{\delta \bar{v}_r}{\delta \bar{z}} - \dfrac{\delta \bar{v}_z}{\delta \bar{r}} \\ 0 & 0 & 0 \\ \dfrac{\delta \bar{v}_z}{\delta \bar{r}} - \dfrac{\delta \bar{v}_r}{\delta \bar{z}} & 0 & 0 \end{bmatrix}$$

$$\bar{d}\langle ij\rangle = \begin{bmatrix} \dfrac{\delta \bar{v}_r}{\delta \bar{r}} & 0 & \tfrac{1}{2}\left(\dfrac{\delta \bar{v}_r}{\delta \bar{z}} + \dfrac{\delta \bar{v}_z}{\delta \bar{r}}\right) \\ 0 & \bar{v}_r/\bar{r} & 0 \\ \tfrac{1}{2}\left(\dfrac{\delta \bar{v}_r}{\delta \bar{z}} - \dfrac{\delta \bar{v}_z}{\delta \bar{r}}\right) & 0 & \dfrac{\delta \bar{v}_z}{\delta \bar{z}} \end{bmatrix}$$

4.2 Analytical Solution for Fiber Orientation in Poiseuille Flow

The pressure driven, steady, laminar, incompressible flow of a Newtonian fluid through a long, smooth round tube provides a flow situation from which an analytical solution for fiber orientation may be determined. The geometry for this flow is depicted in Figure 4.3. For simplicity, a unit radius and unit flow are considered. The velocity

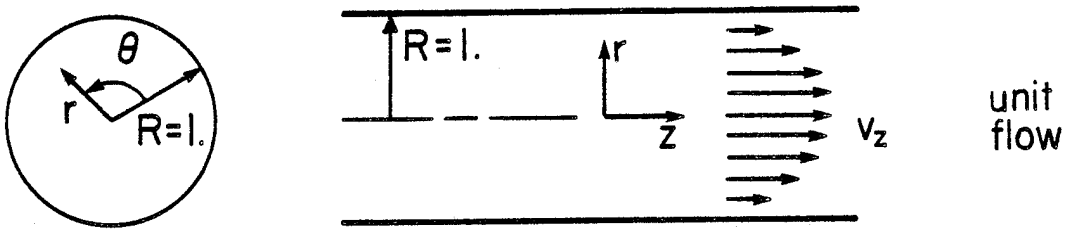

Figure 4.3 Schematic of Poiseuille flow

components are independent of θ, thus the problem is axisymmetric.

The flow solution is not difficult to determine since the flow is unidirectional:

$$v_r = v_\theta = 0$$

$$v_z = 2(1-r^2)$$

The only non-zero vorticity and rate of deformation components are

$$\omega_{rz} = -\tfrac{1}{2}\frac{dv_z}{dr} = 2r$$

$$d_{rz} = \tfrac{1}{2}\frac{dv_z}{dr} = -2r$$

Substituting into the fiber orientation equations (4.13) and (4.14), one obtains (for time independent boundary conditions):

$$\frac{\delta\alpha}{\delta z} = \frac{r\ \sin\alpha\cot\beta}{1-r^2}\ (B-1) \qquad (4.15)$$

$$\frac{\delta\beta}{\delta z} = \frac{r\ \cos\alpha}{1-r^2}\ (1-B\ \cos\ 2\beta) \qquad (4.16)$$

For large aspect ratios which exist in fibers, B is very nearly equal to unity (i.e.; for r_p=50, B=2499/2501). Consequently, one may conclude from (4.15) that

$$\frac{\delta\alpha}{\delta z} = 0$$

Hence, α is a constant and (4.16) becomes an ordinary differential equation in β. For fibers initially perpendicular to the flow streamline (i.e., $\beta=\pi/2$ at $z=0$), the solution to (4.16) is

$$\cot \beta = r_p \tan\left[\frac{-2r\ z\ \cos\ \alpha}{(1-r^2)(r_p+1/r_p)}\right] \tag{4.17}$$

The solution for in-plane fibers is plotted in Figure 4.4 for a fiber aspect ratio of 50. A comparison of Figures 3.2 and 4.4 reveals that the in-plane fibers show identical orientation behavior with in-plane fibers in plane Poiseuille flow. This is an expected result since in-plane fibers experience identical fluid deformations and rotation in both flows.

Equation (4.17) provides a known analytical solution for fiber orientation in an axisymmetric flow although it is necessarily restricted to a particular initial fiber orientation. Nevertheless, it can be used to check the validity of the results predicted by the numerical scheme.

To complete the development of the fiber orientation scheme, orientation parameters must be determined for non-planar orientation states. This is accomplished in the next section.

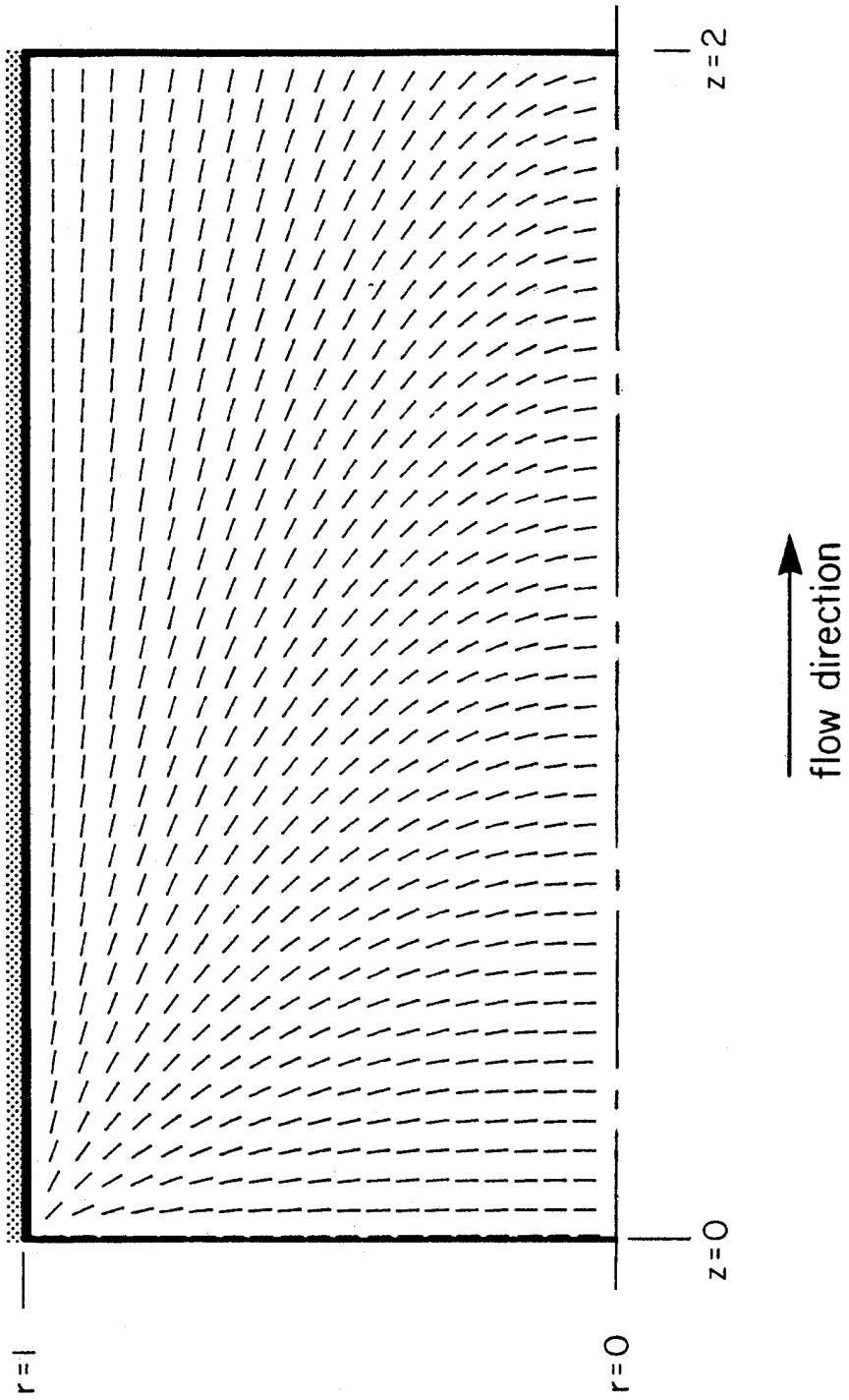

Figure 4.4 Fiber orientation in Poiseuille flow for in-plane fibers initially perpendicular to flow streamlines

4.3 Orientation Parameters for Non-Planar Fibers

In dealing with axisymmetric flows, the planar fiber orientation assumption has been lifted. Thus the orientation distribution becomes a function of two angles as shown in Figure 4.5; viz,

$$n = n(\gamma,\zeta)$$

such that

$$\int_0^{\pi}\int_0^{\pi/2} n(\gamma,\zeta)\sin\gamma \, d\gamma \, d\zeta = 1$$

The angle ζ is the planar angle defined in Section 3.4 while γ is an axial angle. Both γ and ζ are measured from principal material axes. The distributions are assumed to have the following symmetrics:

$$n(\gamma,\zeta) = n(\gamma+\pi,\zeta)$$

$$n(\gamma,\zeta) = n(-\gamma,\zeta+\pi)$$

$$n(\gamma,\zeta) = n(\gamma,-\zeta)$$

Here, the first two symmetrics reflect the fact that the orientation angles are not unique and the last symmetry

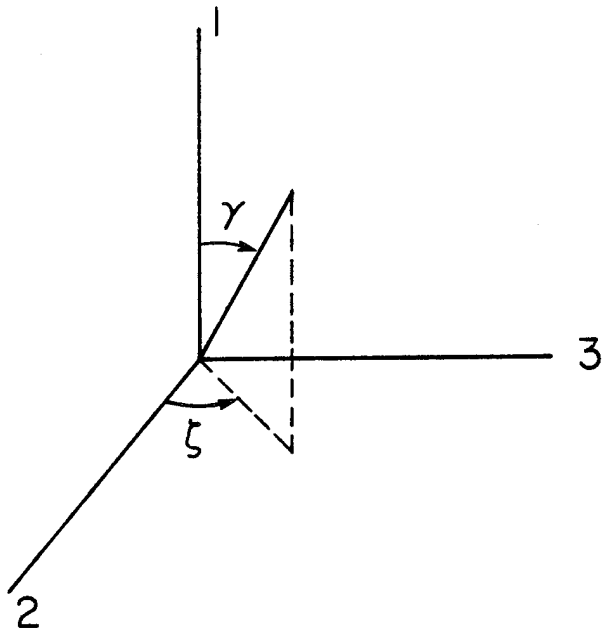

Figure 4.5 Angle descriptors for orientation density function

states that the distributions in ζ is symmetric about the 2 axis. If one further assumes that the orientation density function is separable, i.e.,

$$n(\gamma,\zeta) = n_1(\gamma)n_2(\zeta)$$

then McGee [14] has shown that the following parameters relating fiber orientation to the material properties

result:

$$f_p = 2\int_0^{\pi/2} n_2(\zeta)\cos^2\zeta \, d\zeta - 1$$

$$g_p = \frac{1}{5}\left[8\int_0^{\pi/2} n_2(\zeta)\cos^4\zeta \, d\zeta - 3\right]$$

$$f_a = \left[3\int_0^{\pi/2} \cos^2\gamma \; n_1(\gamma)\sin\gamma \, d\gamma - 1\right]/2$$

$$g_a = \left[5\int_0^{\pi/2} \cos^4\gamma \; n_1(\gamma)\sin\gamma \, d\gamma - 1\right]/4$$

Here, f_p and g_p are the same orientation parameters defined in Equations (3.8) and (3.9), while f_a and g_a represent new orientation parameters which occur in the absence of the planar distribution assumption.

The angles γ and ζ must be related to the orientation angles α and β in Figure 4.2. McGee has determined that the axial angle γ can be measured from any of the principal material axes. If the z axis is assumed to be a principal axis, then γ simply represents β. With the z axis chosen as one principal axis, the direction associates with the modal value of α, $\alpha°$, in the r-θ plane provides an estimate for a second principal axis. The

procedure for calculating ϕ_1° presented in Section 3.4, may also be utilized to determine α°. The principal axes are depicted in Figure 4.6. The angle ζ is simply related to α by

$$\zeta = \alpha - \alpha^\circ$$

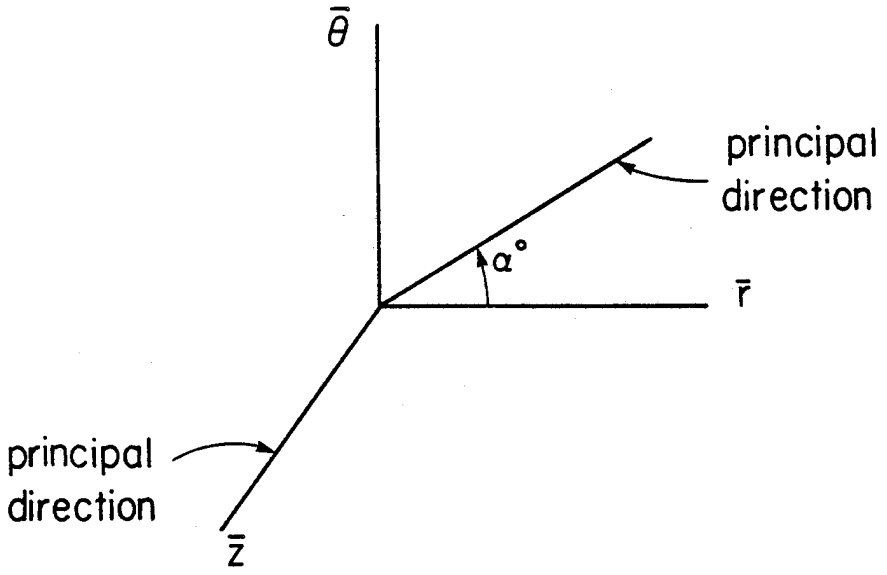

Figure 4.6 Principal axes from which orientation distribution is measured

Incorporating the above assumptions, the orientation parameters may be expressed in terms of α and β via

$$f_p = 2\int_{\alpha°}^{\alpha°+\pi/2} n_2(\alpha)\ \cos^2(\alpha-\alpha°)d\alpha - 1$$

$$g_p = \frac{1}{5}\left[8\int_{\alpha°}^{\alpha°+\pi/2} n_2(\alpha)\ \cos^4(\alpha-\alpha°)d\alpha - 3\right]$$

$$f_a = \left[3\int_{o}^{\pi/2} \cos^2\beta\ n_1(\beta)\sin\beta\ d\beta - 1\right]/2$$

$$g_a = \left[5\int_{o}^{\pi/2} \cos^4\beta\ n_1(\beta)\sin\beta\ d\beta - 1\right]/4$$

It remains to determine the orientation parameters in terms of a finite number of fibers. For f_p and g_p, the derivation follows identically that presented in Section 3.4 and the following expressions result:

$$f_p = \frac{2}{N}\sum_{i=1}^{N} \cos^2(\alpha_i-\alpha°) - 1$$

$$g_p = \frac{1}{5}\left[\frac{8}{N}\sum_{i=1}^{N} \cos^4(\alpha_i-\alpha°)-3\right]$$

where α_i is the α-angle associated with the i^{th} fiber and N is the total number of fibers.

To derive an expression for f_a , one starts with the following approximation for the integral expression:

$$f_a \cong \left[3 \sum_{i=1}^{k} n_1(\beta_i)\cos^2\beta_i \sin\beta_i \Delta\beta - 1 \right]/2 \qquad (4.18)$$

where the integral has been divided into k distinct intervals and β_i represents some value of β in the i^{th} interval. Now, denoting m_i as the number of fibers in the i^{th} interval, it is possible to determine

$$\frac{m_i}{N} = n_1(\beta_i)\sin\beta_i \Delta\beta$$

Inserting into (4.18), one obtains

$$f_a = \left[\frac{3}{N} \sum_{i=1}^{k} m_i \cos^2\beta_i - 1 \right]/2$$

or equivalently,

$$f_a = \left[\frac{3}{N} \sum_{i=1}^{N} \cos^2\beta_i - 1 \right]/2$$

Following the same procedure, the following expression for g_a may be derived:

$$g_a = \left[\frac{5}{N}\sum_{i=1}^{N} \cos^4\beta_i - 1\right]/4$$

The expressions relating the orientation parameters to the orientation of individual fibers are summarized in Table 4.4.

Table 4.4

Orientation Parameters for Non-Planar Fiber Distributions

$$f_p = \frac{2}{N}\sum_{i=1}^{N} \cos^2(\alpha_i - \alpha°) - 1$$

$$g_p = \frac{1}{5}\left[\frac{8}{N}\sum_{i=1}^{N} \cos^4(\alpha_i - \alpha°) - 3\right]$$

$$f_a = \left[\frac{3}{N}\sum_{i=1}^{N} \cos^2\beta_i - 1\right]/2$$

$$g_a = \left[\frac{5}{N}\sum_{i=1}^{N} \cos^4\beta_i - 1\right]/4$$

4.3.1 Random Fiber Orientation

A random fiber orientation state occurs when the orientation parameters are all equal to zero. Table 4.5 lists the orientation angles for ten fibers which lead to a random orientation distribution. These orientation angles are used in the subsequent examples to simulate initially random fiber distributions.

Table 4.5

Orientation Angles for Ten Randomly Oriented Fibers

β, rad	α, rad
0.314	0.942
-0.565	2.199
-0.723	0.314
0.880	1.571
-0.942	2.827
1.100	0.628
1.225	1.885
-1.257	2.513
1.382	0.0
-1.414	1.257

4.4 Numerical Solutions

In this section numerical solutions for fiber orientation in axisymmetric flows are presented. The first example involves the determination of the fiber orientation in Poiseuille flow, and the results are compared with the analytical solution developed in Section 4.2. In a second example, the fiber orientation in a simulated disk molding operation is determined.

4.4.1 Poiseuille Flow

To check the numerical scheme, the numerical solution for fiber orientation in Poiseuille flow (see Figure 4.3) is determined. The finite element mesh with associated boundary conditions to solve for the flow is presented in Figure 4.7. The stream function, pressure and shear stress contours for the fluid mechanics solution are shown in Figures 4.8 through 4.10.

Having ascertained the flow solution, the fiber orientation is determined. A comparison of analytically and numerically predicted orientation is presented in Table 4.6 along the $\psi = 9/16$ streamline. This streamline corresponds to the path r=0.5. The agreement between the numerical and analytical values is excellent.

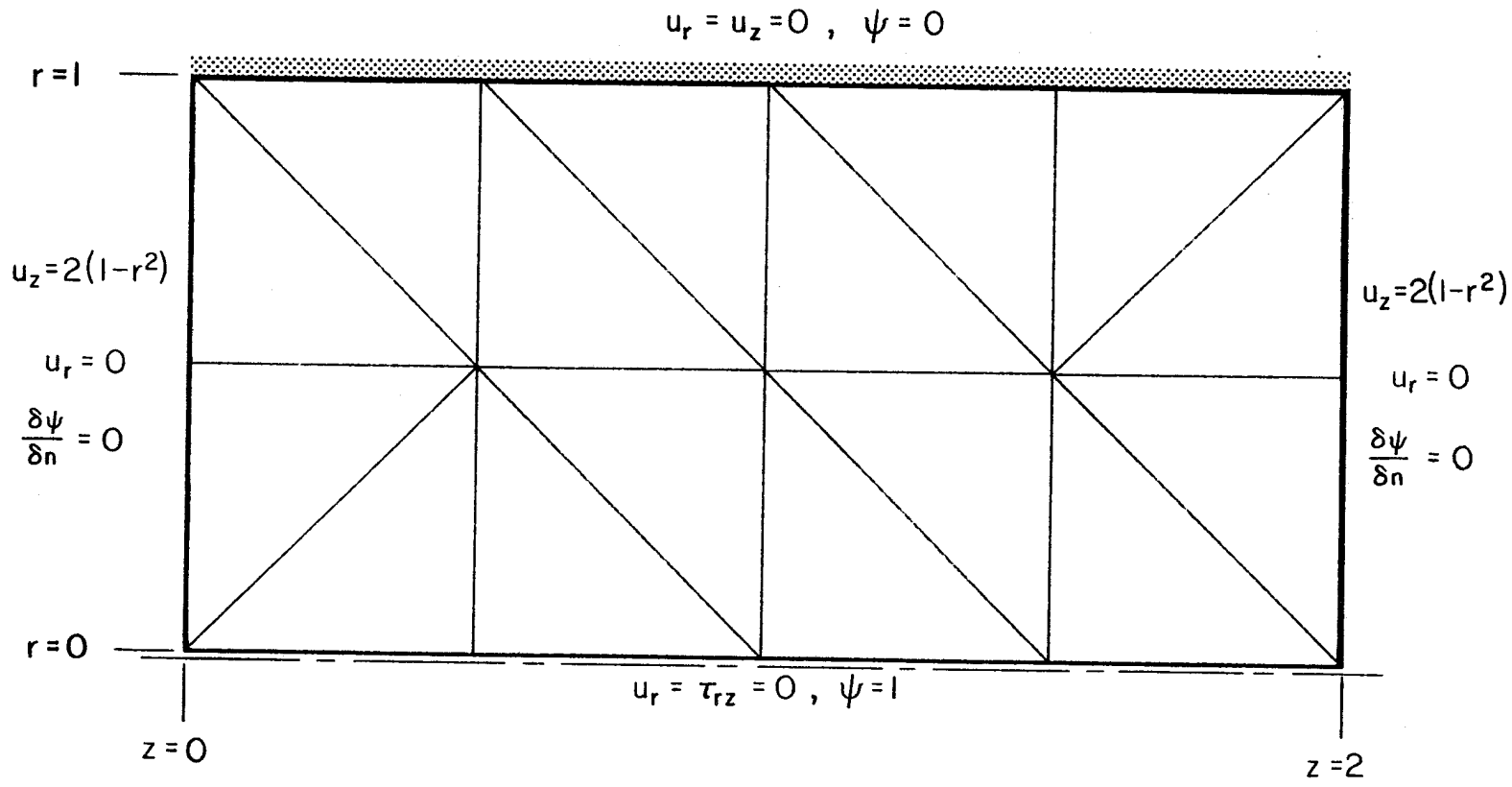

Figure 4.7 Finite element mesh and boundary conditions for solution of Poiseuille flow

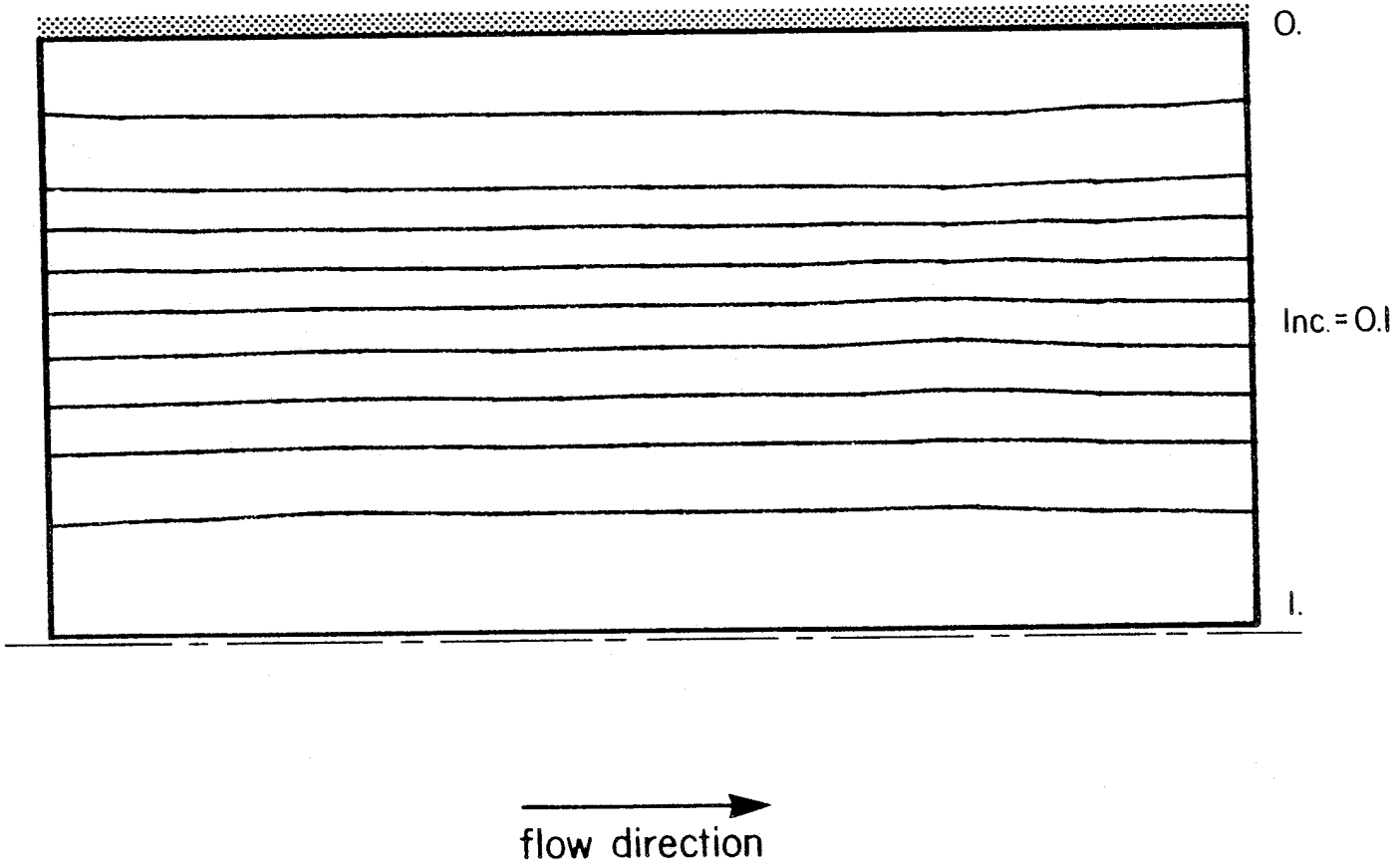

Figure 4.8 Stream function contours (streamlines) in Poiseuille flow

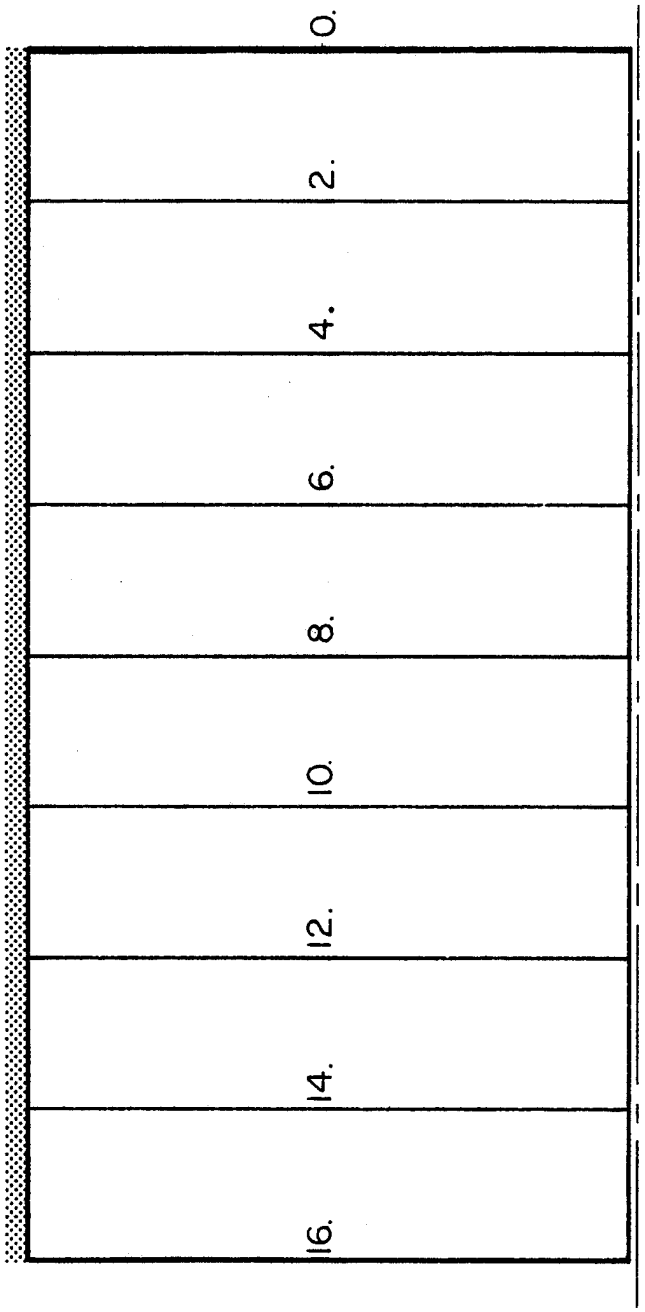

Figure 4.9 Pressure contours in Poiseuille flow

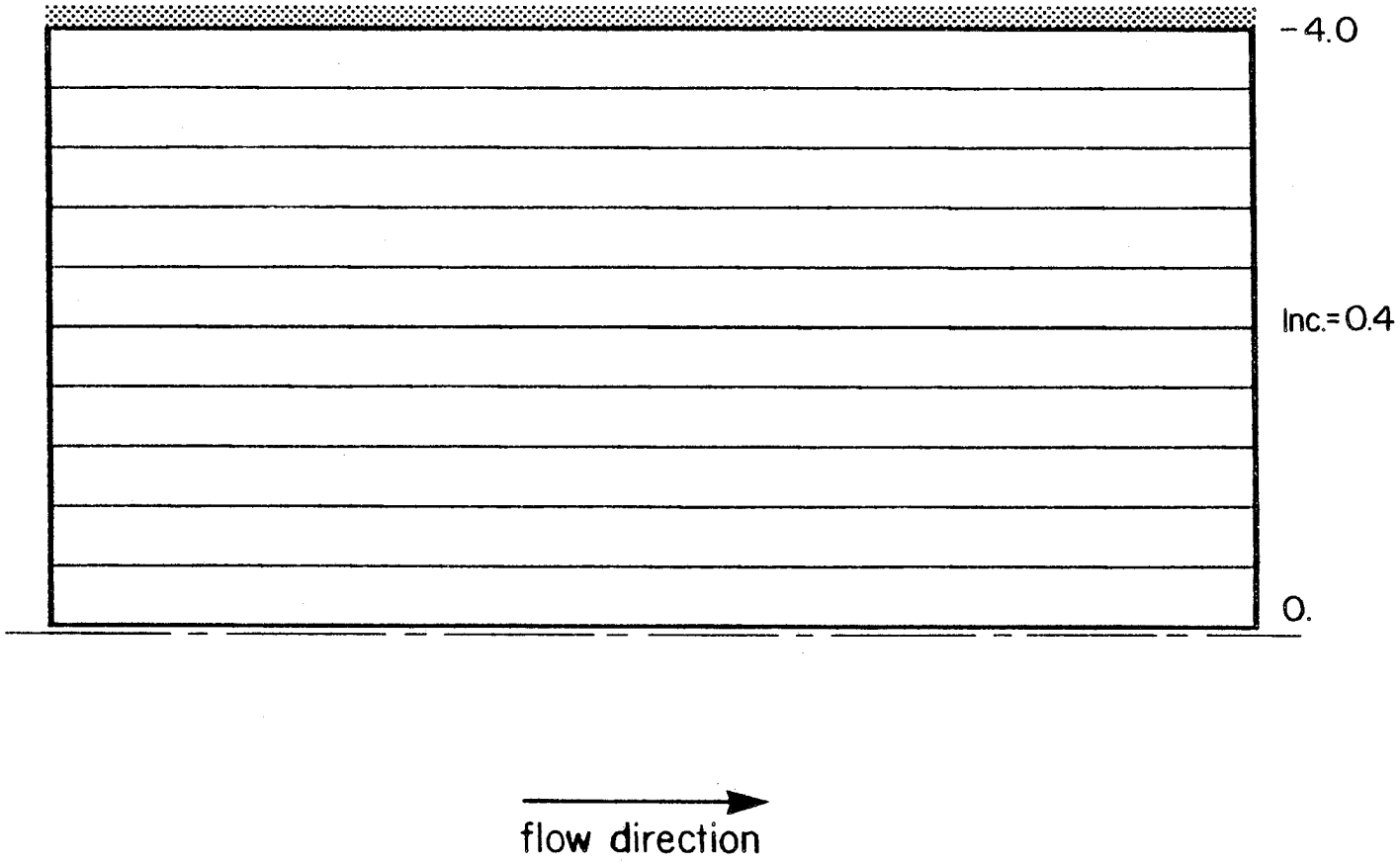

Figure 4.10 Shear stress contours in Poiseuille flow

It is also of interest to plot the orientation parameter contours for an initially random orientation distribution. Reference to Section 4.2 reveals that the α orientations remain constant; hence, one need not plot contours of $\alpha°$, f_p , and g_p. Plots of f_a and g_a are presented in Figures 4.11 and 4.12, respectively. From these plots, one detects the presence of the boundary layer of aligned fibers parallel to the wall boundary.

Table 4.6

Comparison of Numerical and Analytical Solutions for Fiber Orientation in Poiseuille Flow along the Streamline $\psi = 9/16$

x	Initial Orientations β, rad	α, rad	Numerical Solutions β, rad	α, rad	Analytical Solutions β, rad	α, rad
0.5	1.571	0.0	2.16	0.0	2.16	0.0
1.0	1.571	0.0	2.50	0.0	2.50	0.0
1.5	1.571	0.0	2.69	0.0	2.68	0.0
0.5	1.571	0.785	2.02	0.785	2.01	0.785
1.0	1.571	0.785	2.33	0.785	2.33	0.785
1.5	1.571	0.785	2.54	0.785	2.53	0.785

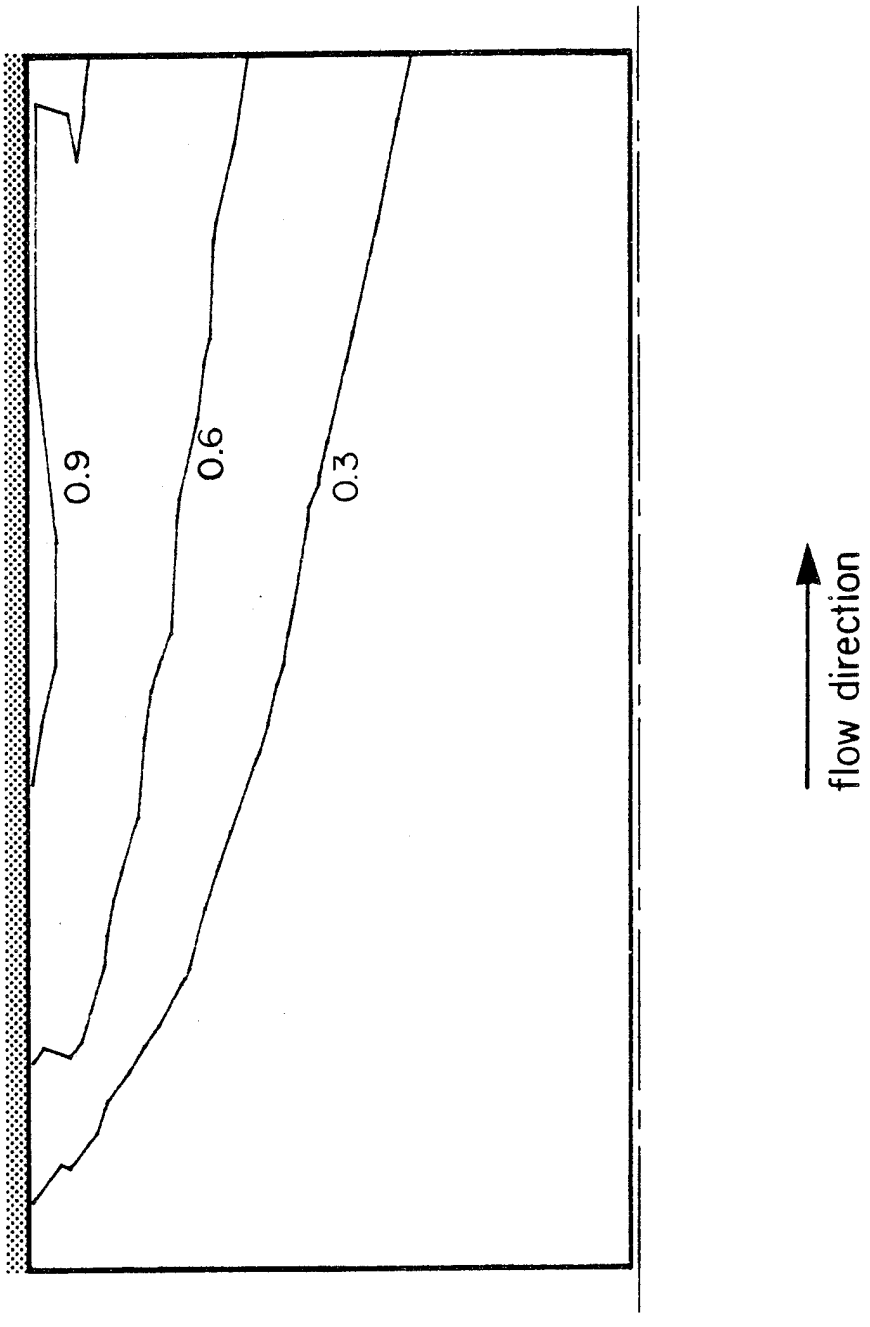

Figure 4.11 Contours of f_a in Poiseuille Flow. γ is measured with respect to the flow direction.

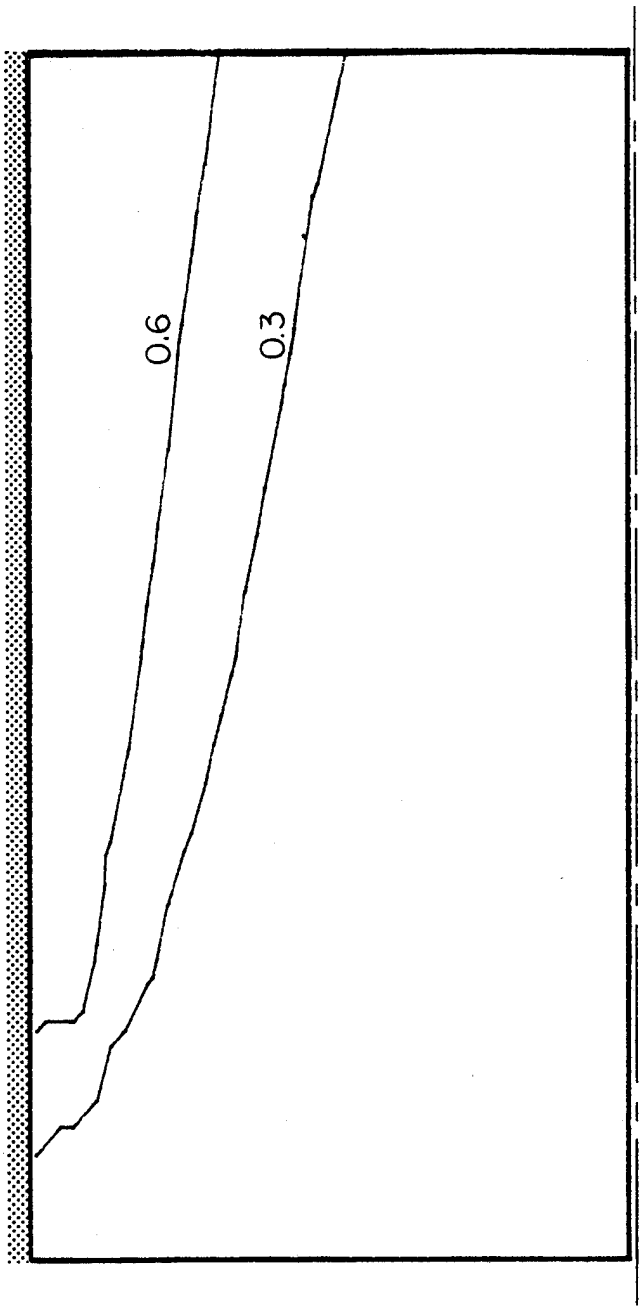

Figure 4.12 Contours of g_a in Poiseuille flow

4.4.2 Simulated Disk Molding Operation

A final example involves simulating an actual axisymmetric disk molding operation. Figure 4.13 depicts the geometry for the problem. In the usual manner, the flow solution is determined first. The finite element mesh and associated boundary conditions for Newtonian flow are presented in Figure 4.14. A constant velocity profile exists along the boundary where the fluid enters the domain simulating the effect of a plunger pushing the fluid. The usual no-slip condition is employed along the wall boundaries. The normal velocity and shear stress vanish along the centerline. The boundary condition along the exit boundary is the analytically determined solution for radial flow satisfying the continuity and Navier-Stokes equations. The resulting stream function, pressure, and shear stress contours are presented in Figures 4.15 through 4.17, respectively.

With the flow solution at hand, the fiber orientation may be determined. To gain a better visual perception of the type of orientation that occurs, initially in-plane fibers ($\alpha=0$) are treated first. Examination of (4.11) reveals that in-plane fibers remain in-plane; hence, fiber plots can be drawn. Figures 4.18 through 4.20 present fiber plots along three streamlines: one near

both wall boundaries in the disk section and one which runs through the disk center. Several conclusions may be drawn from these in-plane fiber plots:

(1) Rapid alignment of in-plane fiber occurs in the sprue section of all three streamlines. This is due to the very high normal stresses which exist in the converging flow.

(2) In-plane fibers preferentially orient parallel to the flow streamlines near the wall boundaries in the disk.

(3) In-plane fibers orient perpendicular to the flow streamlines in the center of the disk.

Next, the orientation is determined for initial non-planar random orientation distributions. Figures 4.21 through 4.25 present the resulting contours of f_a. From these figures, the following conclusions may be reached:

(1) A very high degree of alignment in the z direction ($f_a \geq 0.9$) occurs throughout the converging sprue section.

(2) In the wall region in the disk, the fibers align perpendicular to the z direction ($f_a \leq -0.4$)

(3) In the center section of the disk, the distribution is moderately aligned in the z direction ($f_a \stackrel{\sim}{=} 0.6$) near the sprue, becoming

widely dispersed ($f_a \tilde{=} 0$) near the exit region of the flow.

Contours of f_p are shown in Figures 4.26 through 4.29. From these figures, one may conclude that, except for a strip in the central region of the disk, the α alignment is nearly perfect. To ascertain the direction of α alignment, contours of $\alpha°$ are plotted in Figures 4.30 and 4.31. These figures reveal an in-plane alignment of fibers ($\alpha=0$) in both the sprue section and wall regions. In the central region of the disk a moderate degree of orientation exists ($f_a \tilde{=} 0.6$) with a varying mode angle.

4.4.3 Comparison of Predicted and Actual Orientation

From micrographs, Ellery [4] has determined the fiber orientation in axisymmetric disks under slow fill rates for glass reinforced phenolics. Ellery found a high degree of fiber orientation parallel to the flow streamlines in the wall region of the disk and a high degree of orientation in the "hoop" direction in the center section of the disk. This experimentally determined orientation is depicted in Figure 4.32.

A comparison of the experimentally observed orientation with the numerical prediction reveals a very good agreement in the wall region of the disk. In the

center section, however, the numerical scheme does not predict a high degree of hoop direction reinforcement. Table 4.7 presents the orientation of ten initially randomly oriented fibers at the beginning of the disk section and at the exit location along the streamline which traverses the center section of the disk. It is seen that the fiber orientation is predominantly in-plane at the beginning of the radial section, and thus hoop direction alignment cannot occur. However, those fibers which do have a significant degree of out-of-plane tilting at the entrance to the disk do tend to orient in the hoop direction. If one introduces a fiber tilted 45° out-of-plane at the entrance to the disk, then upon reaching the exit section the fiber has achieved a hoop direction alignment. Thus the discrepancy between experimentally observed and numerically predicted orentation may be explained by postulating that fiber interactions cause a significant degree of out-of-plane tilting in the entrance region of the disk, and the orientation mechanisms are able to orient the resulting non-planar fibers in the hoop direction.

Table 4.7

Numerically Predicted Orientations of Individual Fibers along Center Streamline in an Axisymmetric Disk

(1) Initial Orientation, rad		(2) Orientation at Beginning of Radial Section, rad		(3) Final Orientation, rad	
β	α	β	α	β	α
0.314	0.942	-1.99	3.1	-2.79	2.5
-0.565	2.199	-1.92	3.14	-2.87	3.10
-0.723	0.314	2.05	0.18	2.38	1.26
0.880	1.571	-2.16	3.13	-2.87	3.03
-0.942	2.827	-2.50	3.04	-2.78	2.34
1.100	0.628	2.08	0.19	2.38	1.27
1.225	1.885	1.33	3.12	0.324	2.75
-1.257	2.513	2.18	0.01	2.87	0.04
1.382	0.000	2.18	0.000	2.87	0.000
-1.414	1.257	-1.82	3.02	-2.37	1.89
-	-	1.571	0.785	1.63	1.54

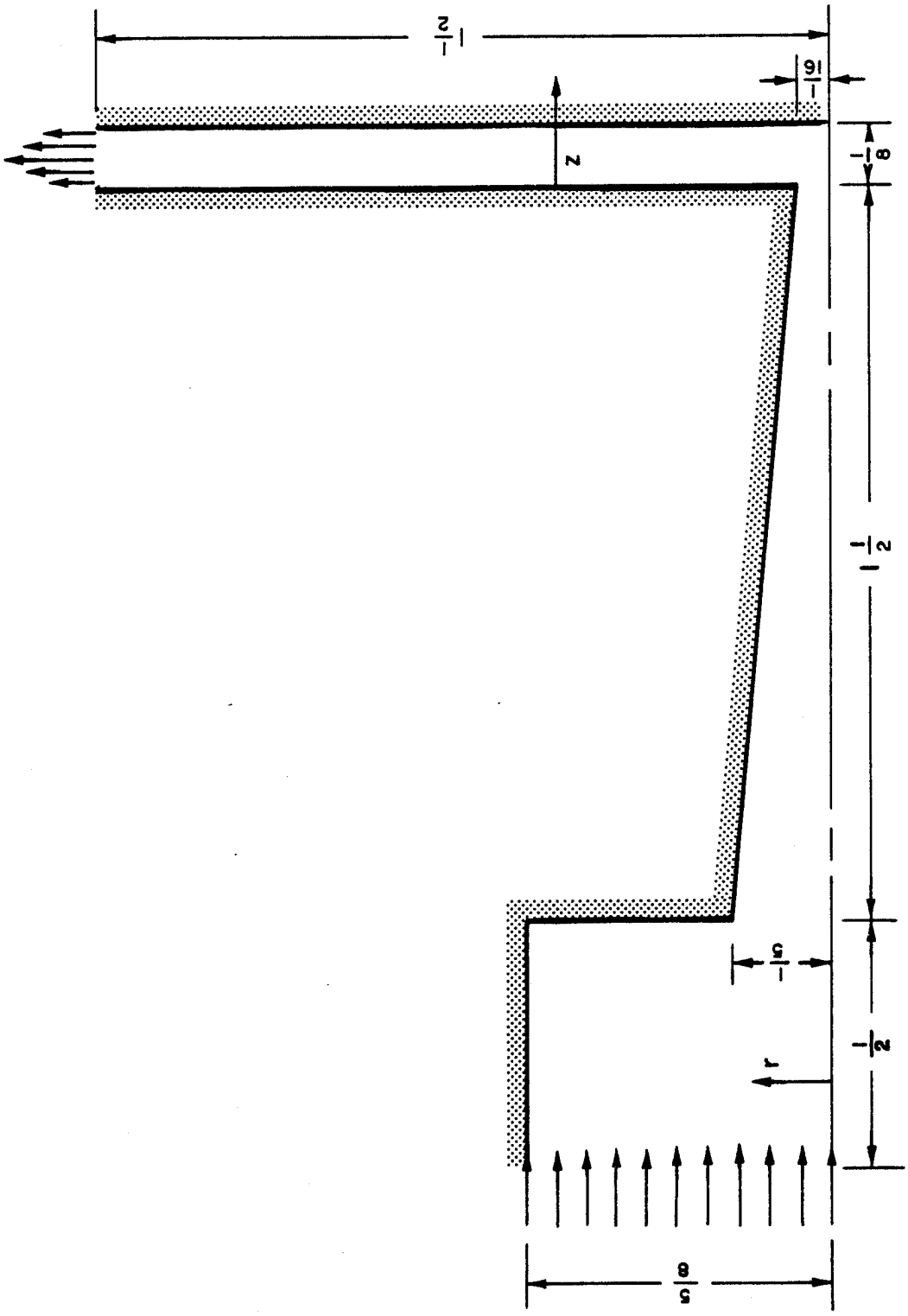

Figure 4.13 Schematic for molding an axisymmetric disk

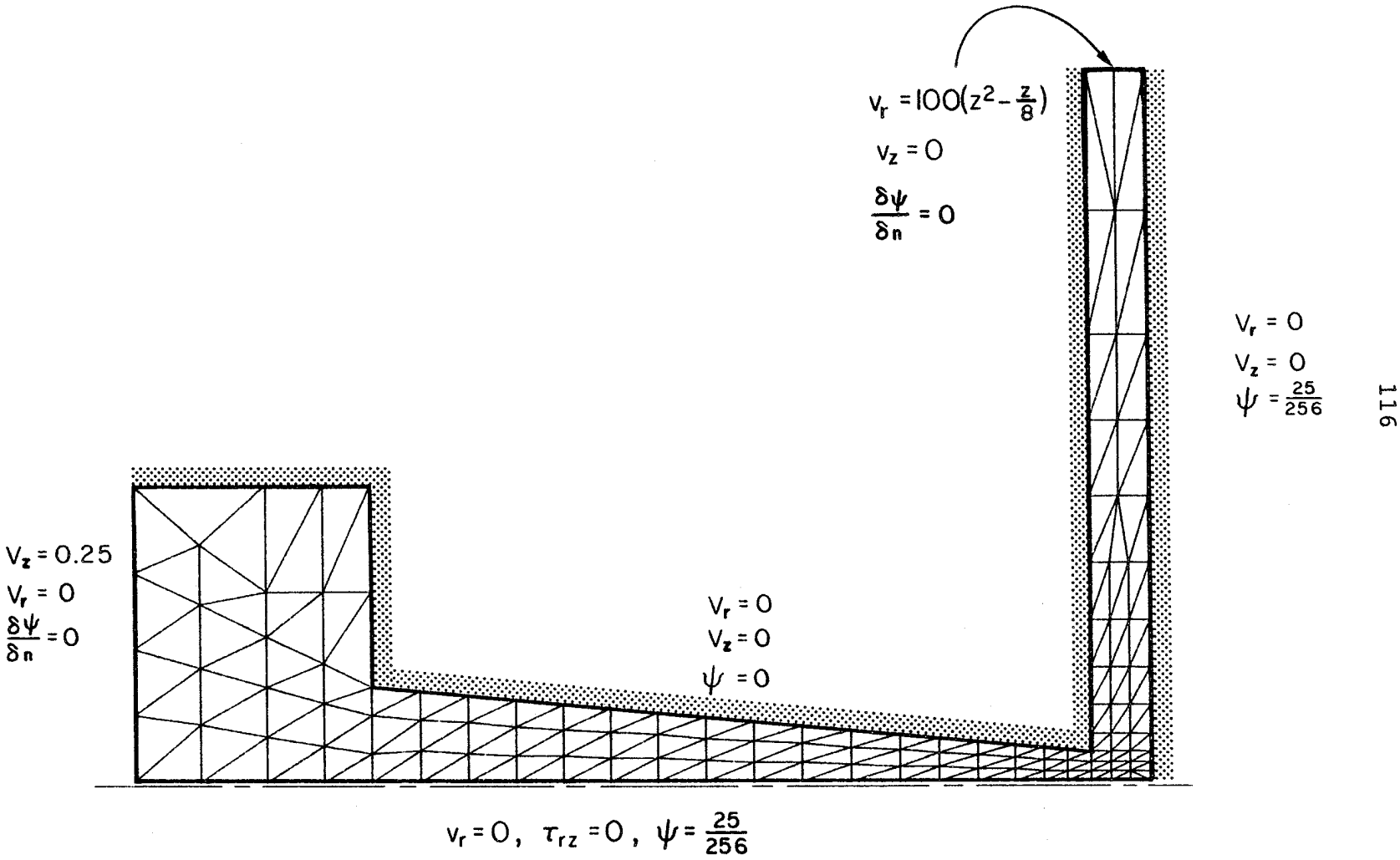

Figure 4.14 Finite element mesh for axisymmetric disk molding simulation

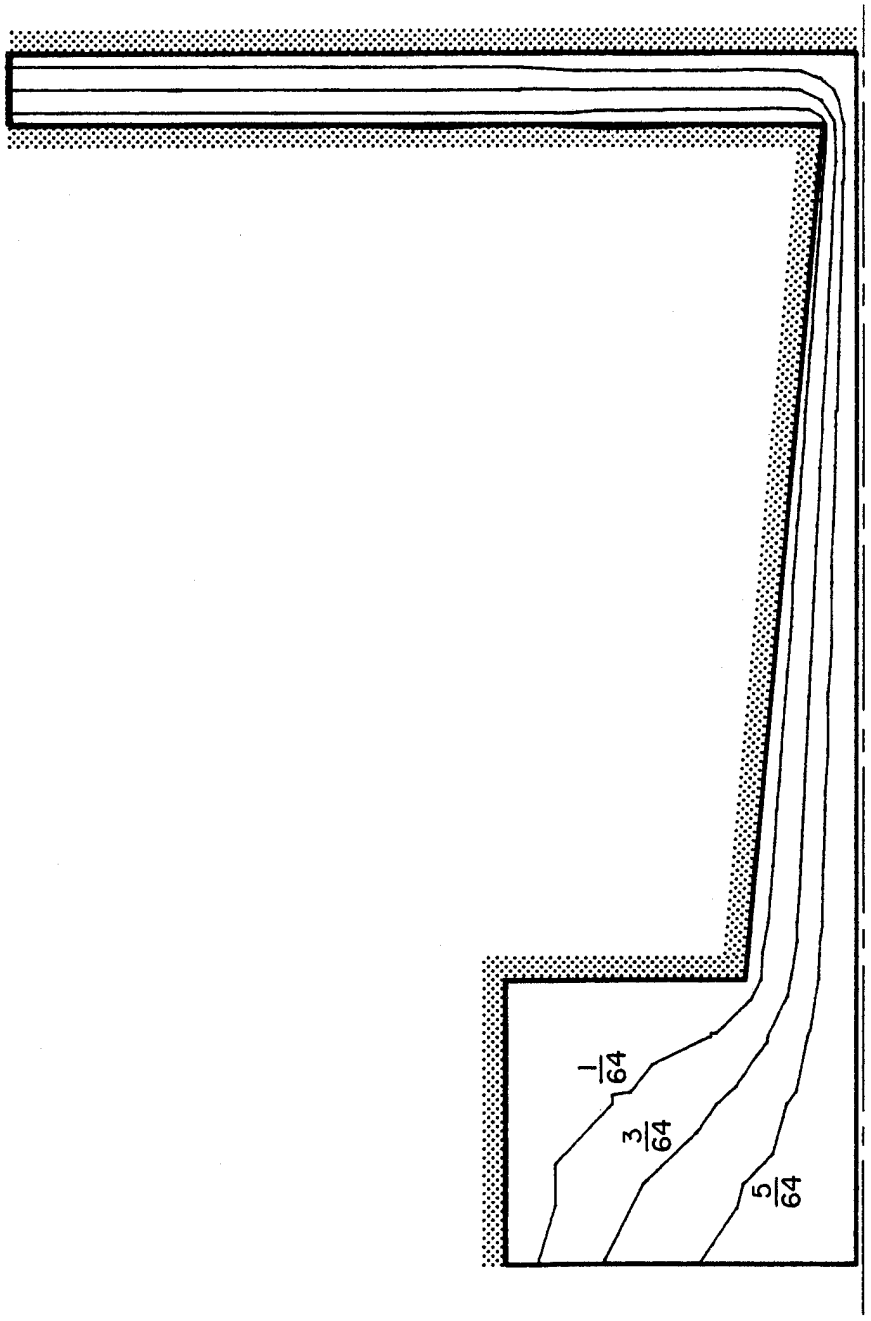

Figure 4.15 Stream function contours (streamlines) for Newtonian flow in axisymmetric disk molding simulation

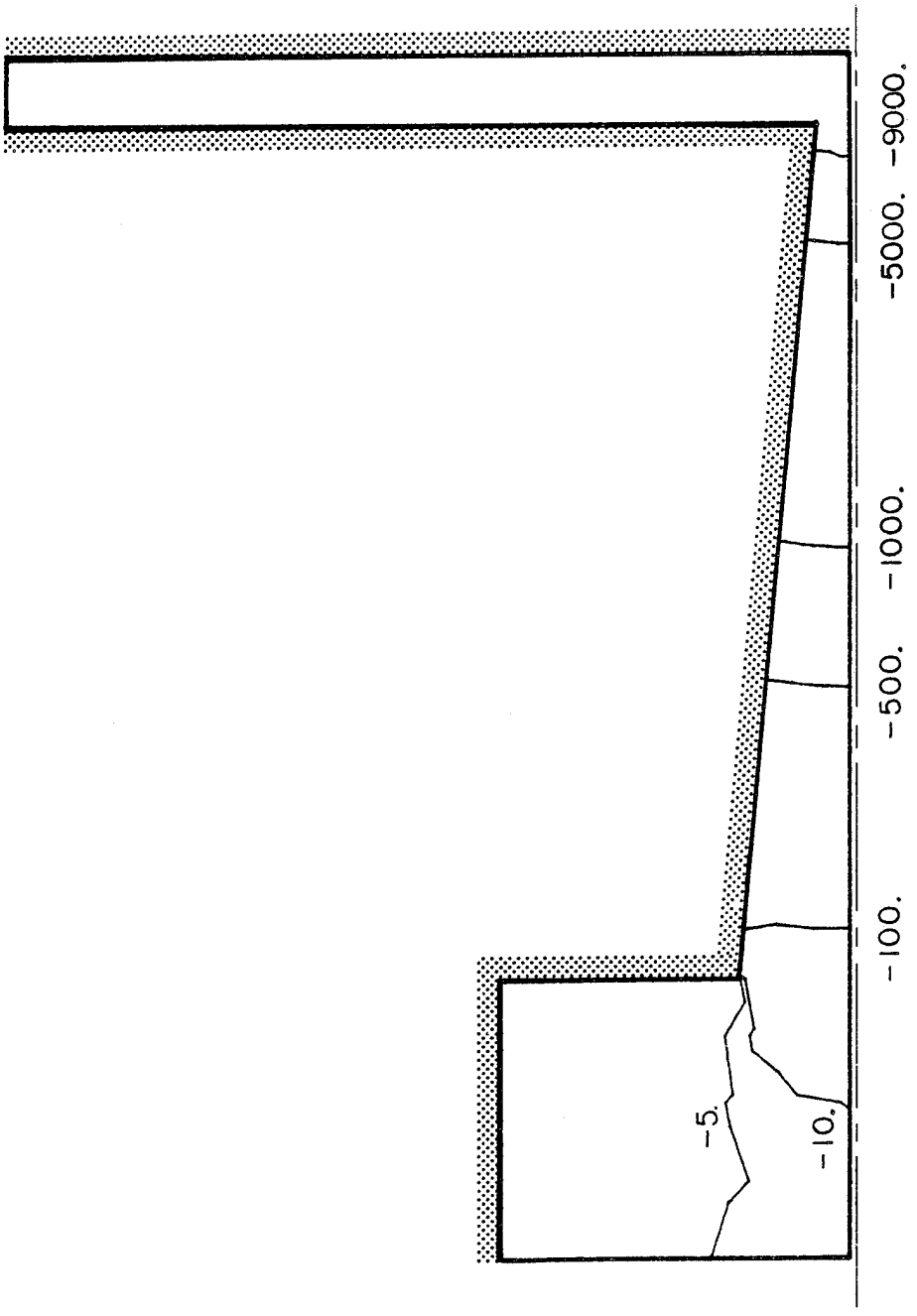

Figure 4.16 Pressure contours for Newtonian flow in axisymmetric disk molding simulation

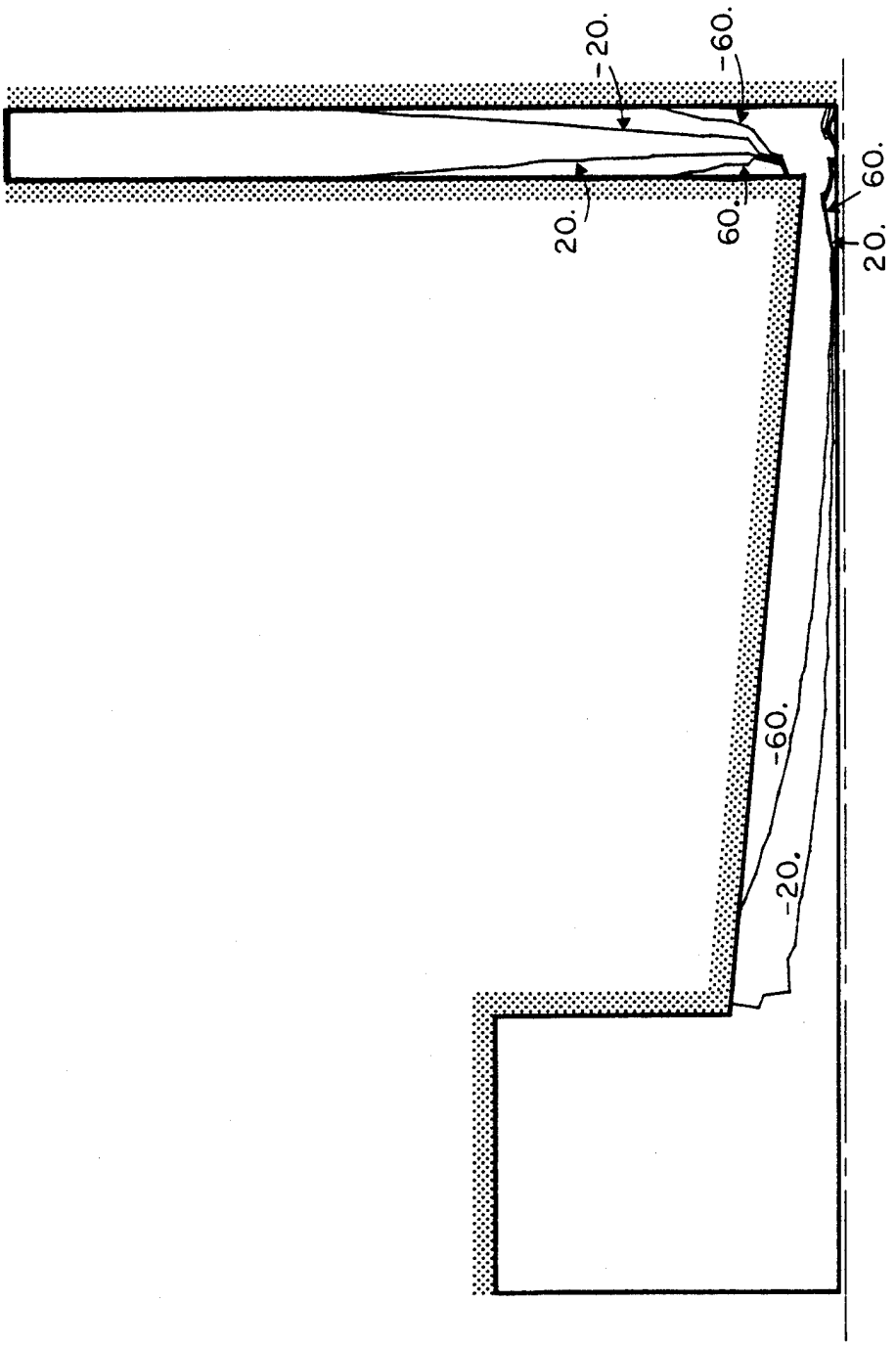

Figure 4.17 Shear stress contours for Newtonian flow in axisymmetric disk molding simulation

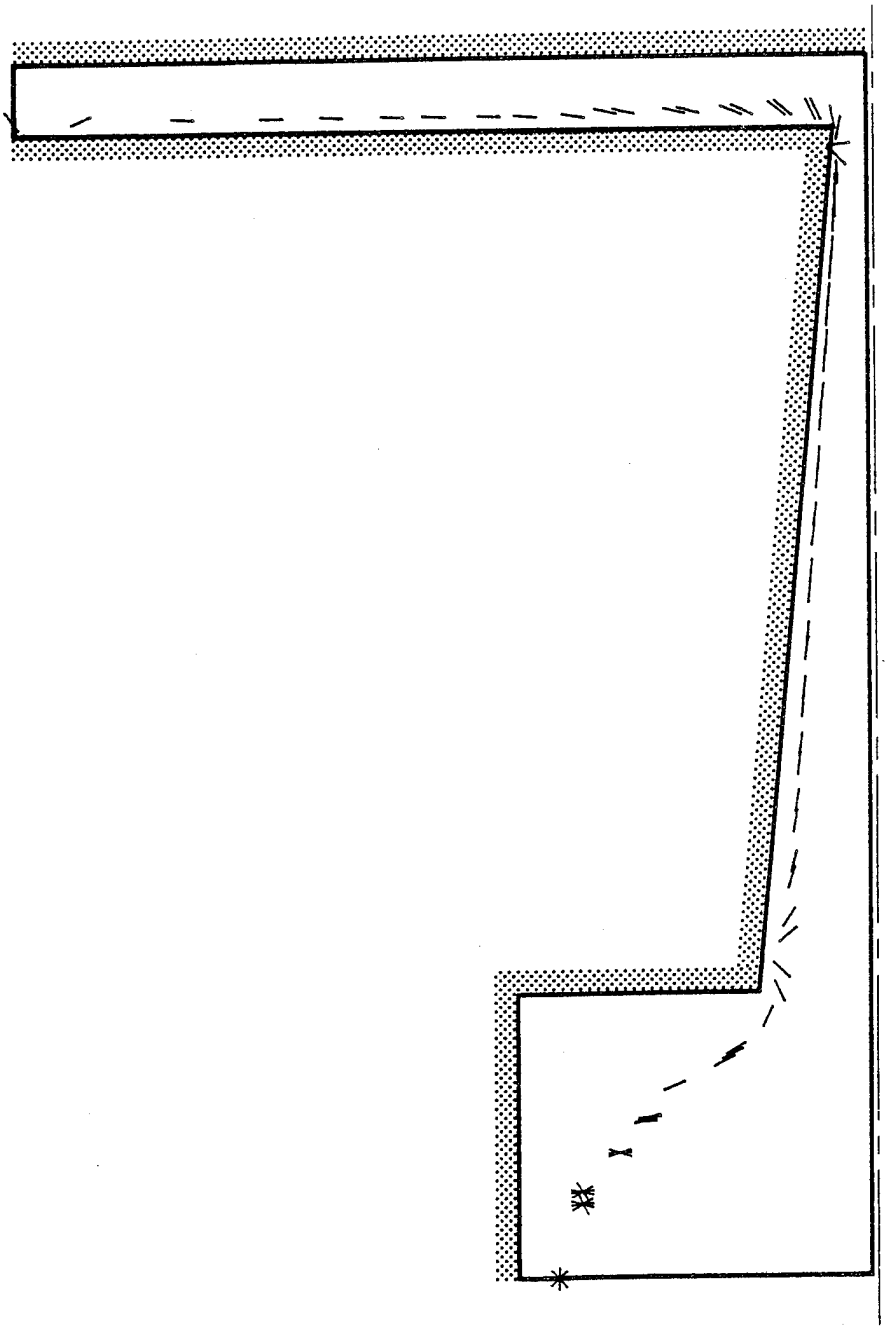

Figure 4.18 In-plane fiber orientation along a streamline near inside wall boundary

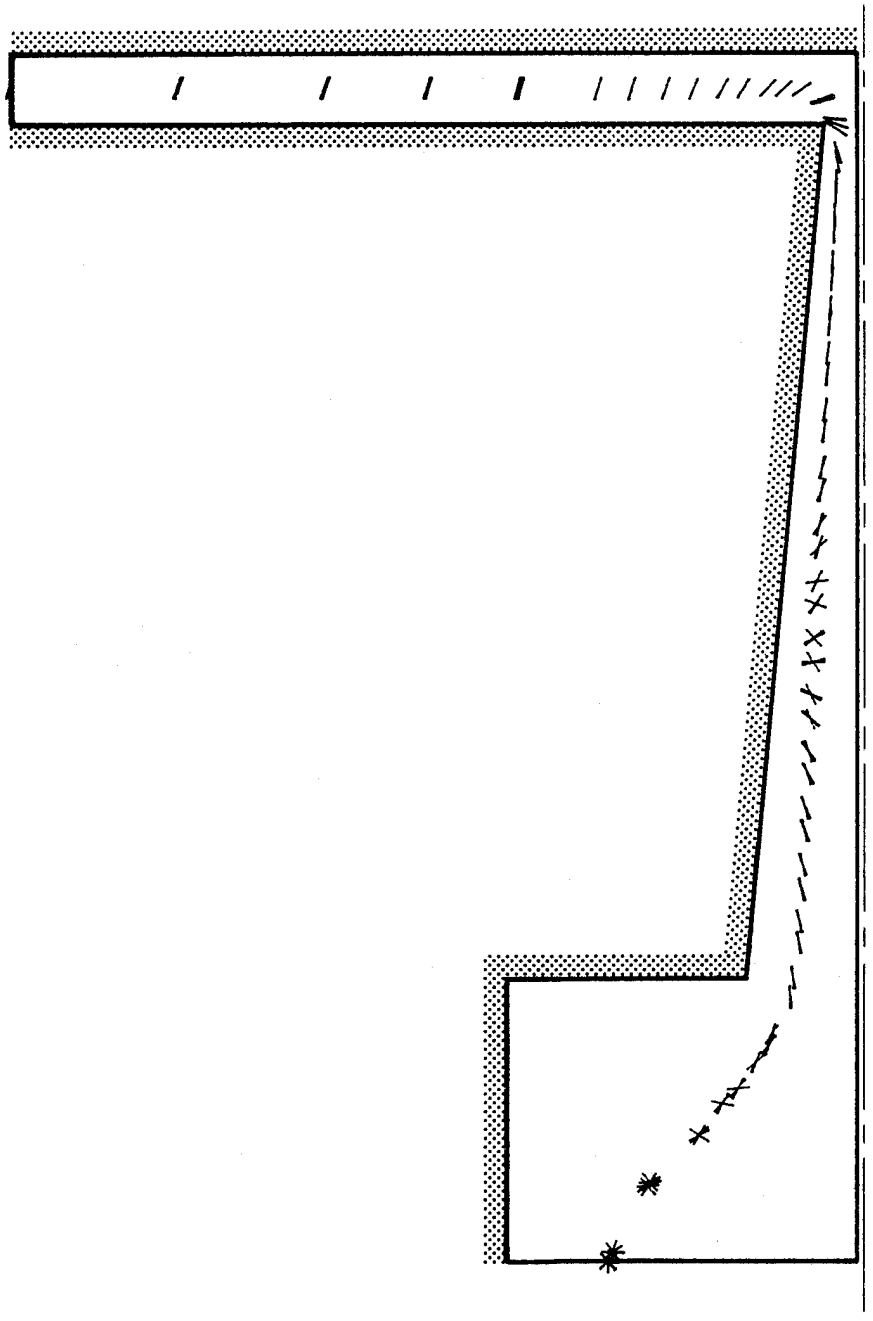

Figure 4.19 In-plane fiber orientation along a streamline in center of disk

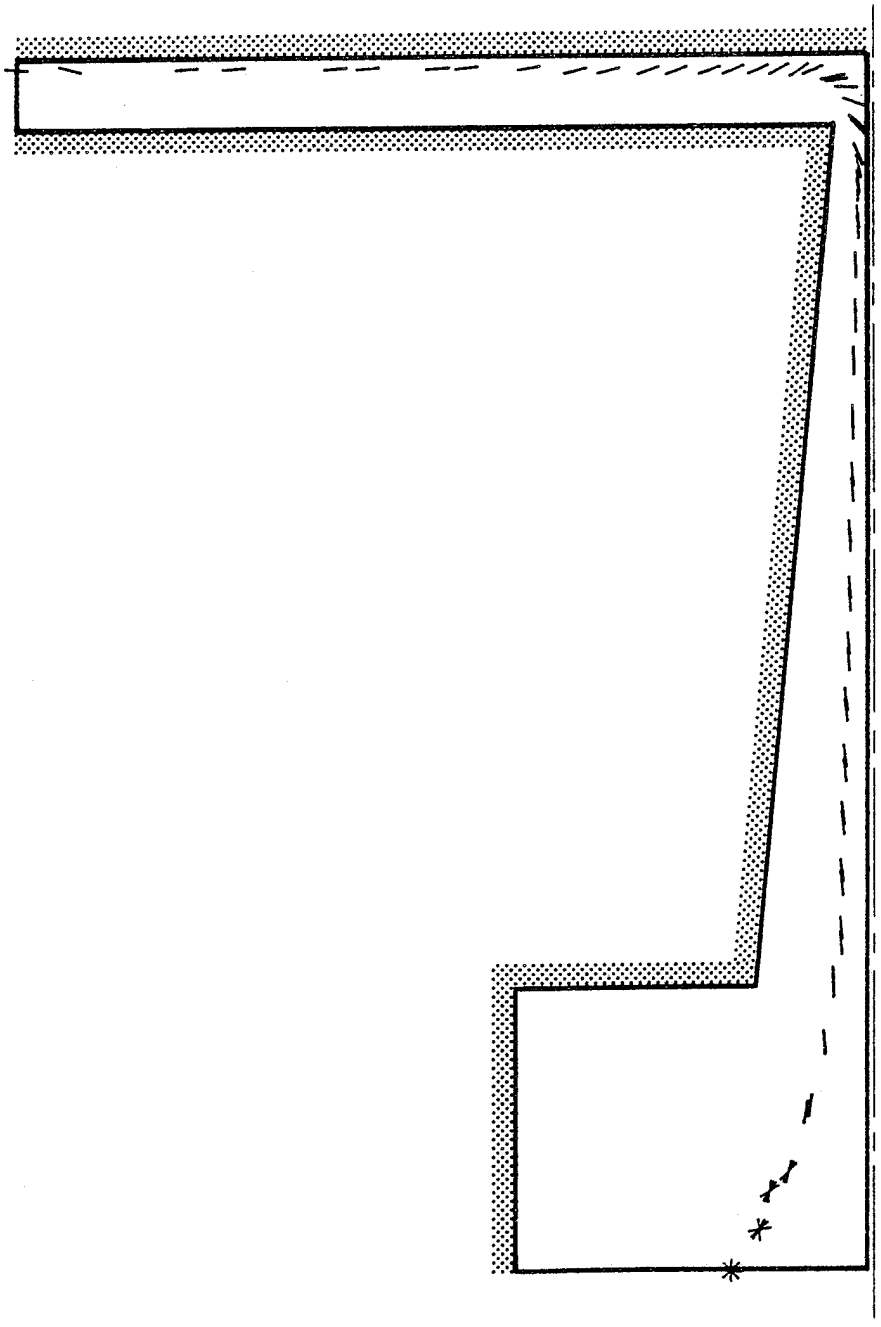

Figure 4.20 In-plane fiber orientation along a streamline near outside wall boundary

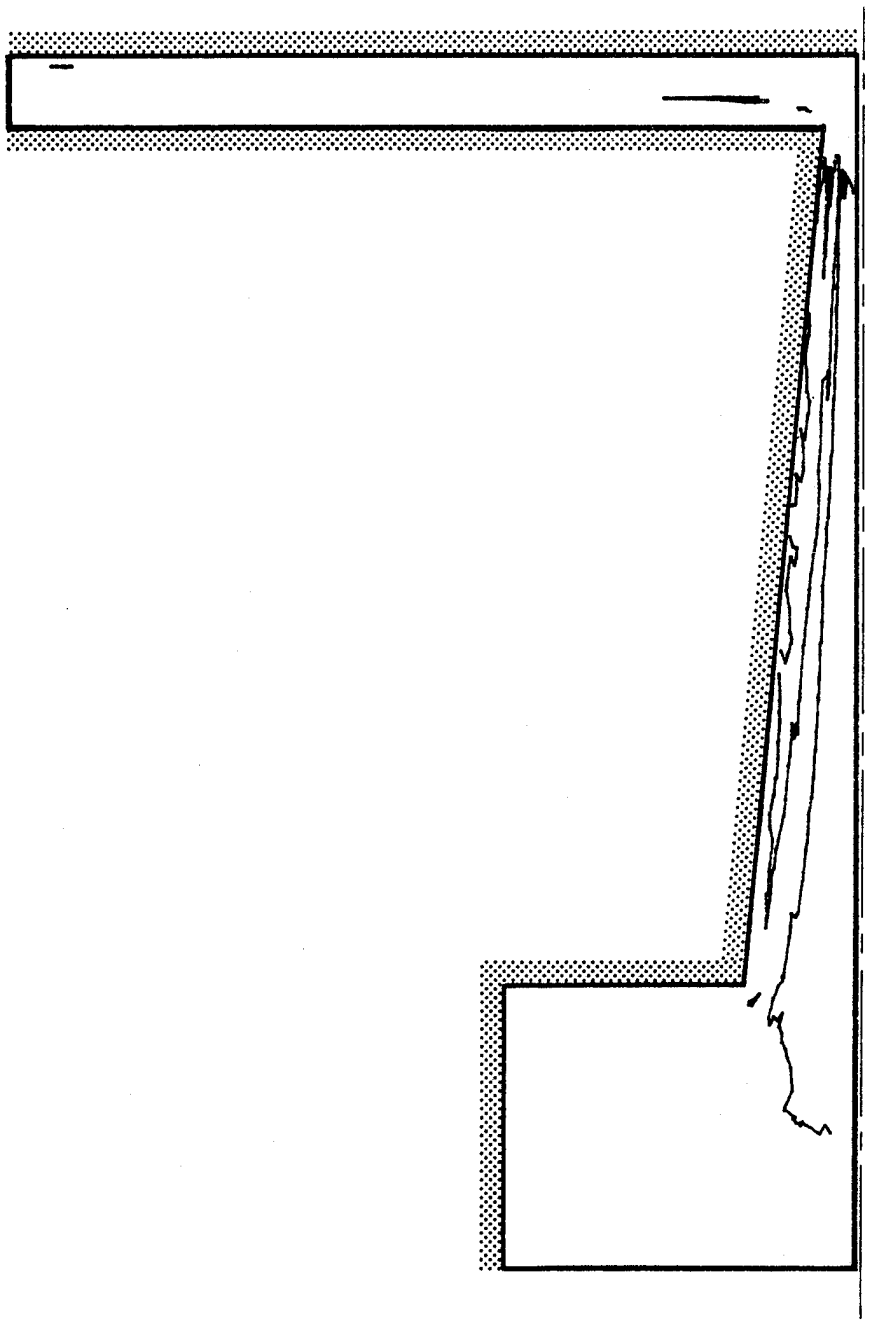

Figure 4.21 Contours of f_a=0.9 in axisymmetric disk molding simulation

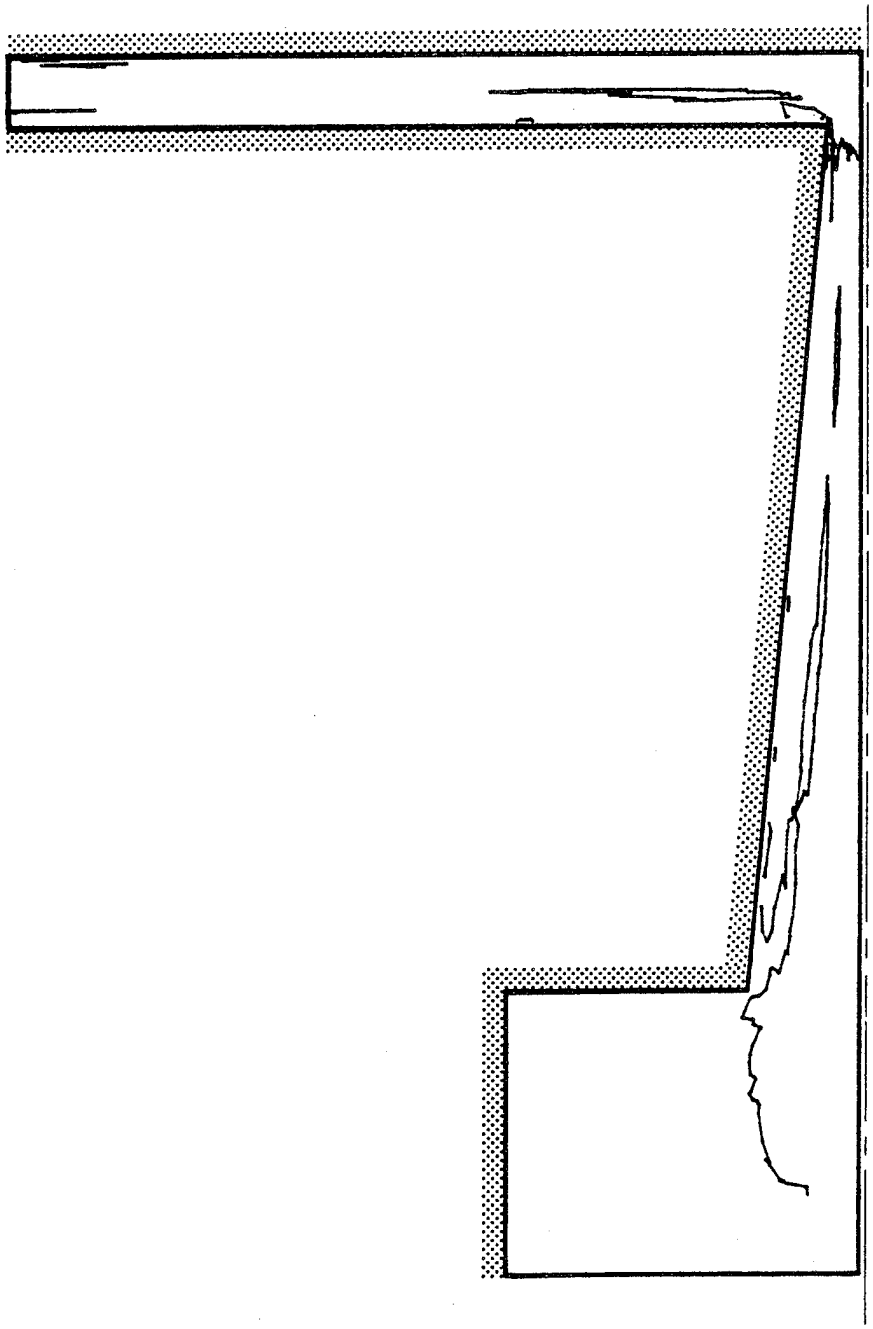

Figure 4.22 Contours of f_a=0.6 in axisymmetric disk molding simulation

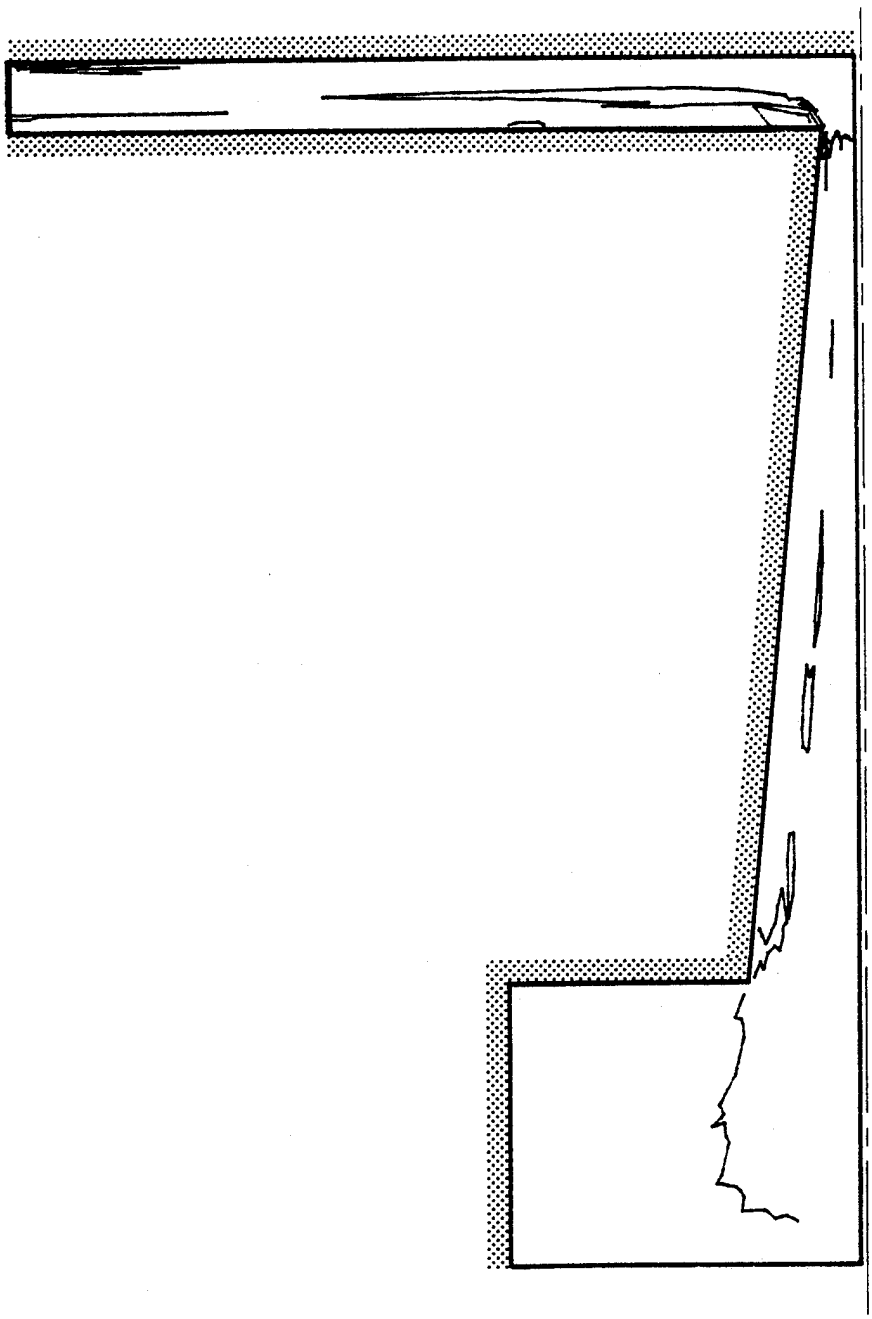

Figure 4.23 Contours of f_a=0.3 in axisymmetric disk molding simulation

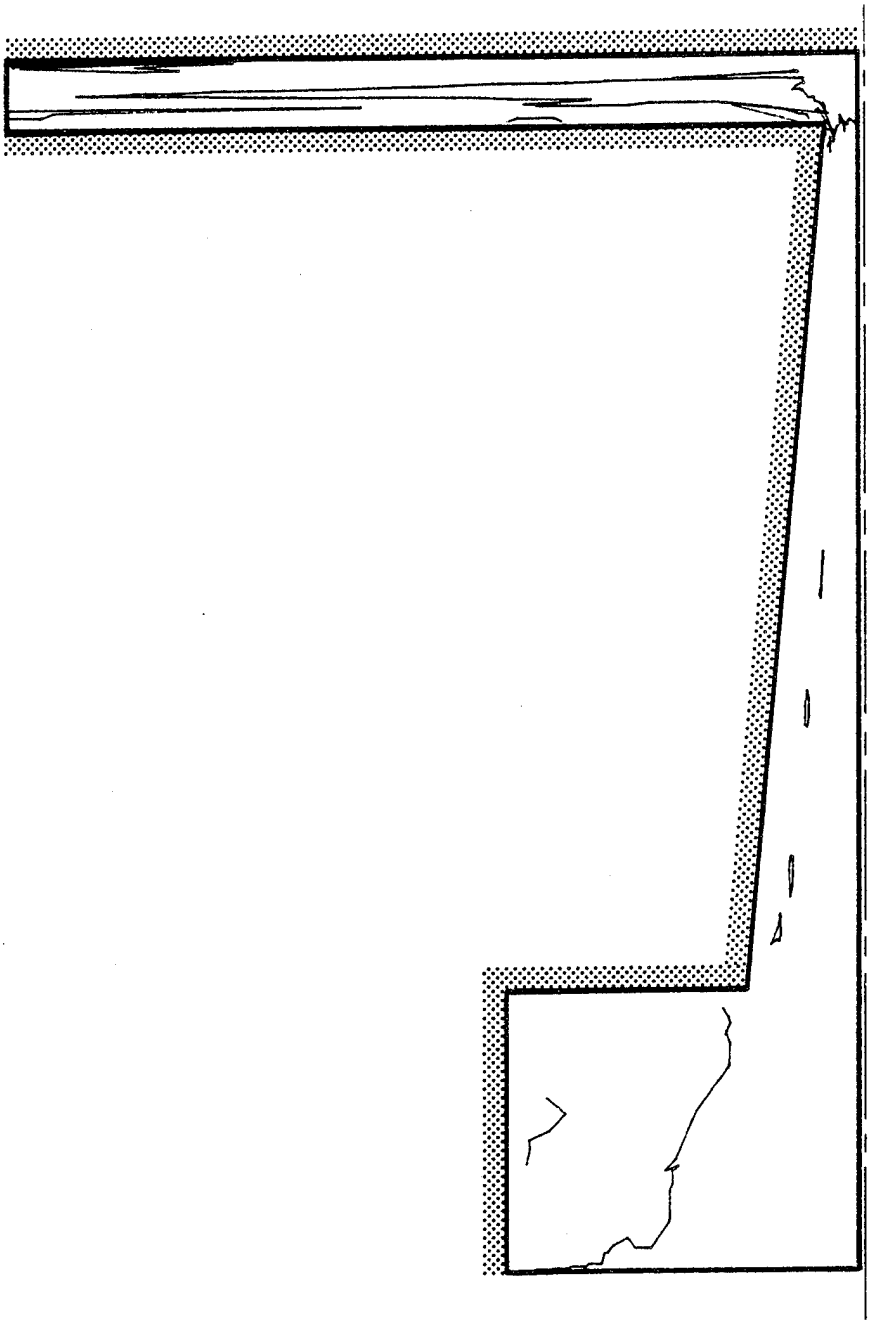

Figure 4.24 Contours of f_a=0 in axisymmetric disk molding simulation

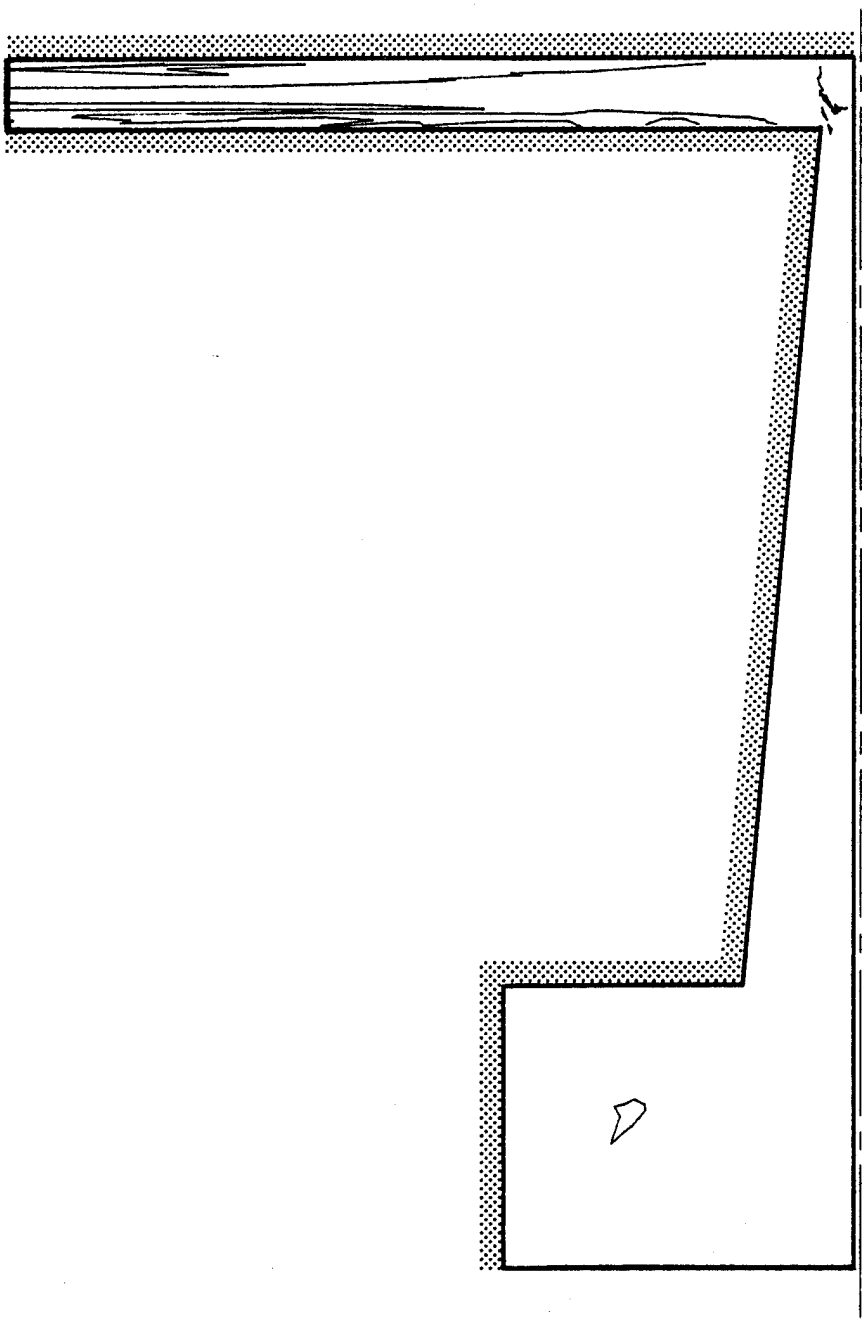

Figure 4.25 Contours of f_a=-0.4 in axisymmetric disk molding simulation

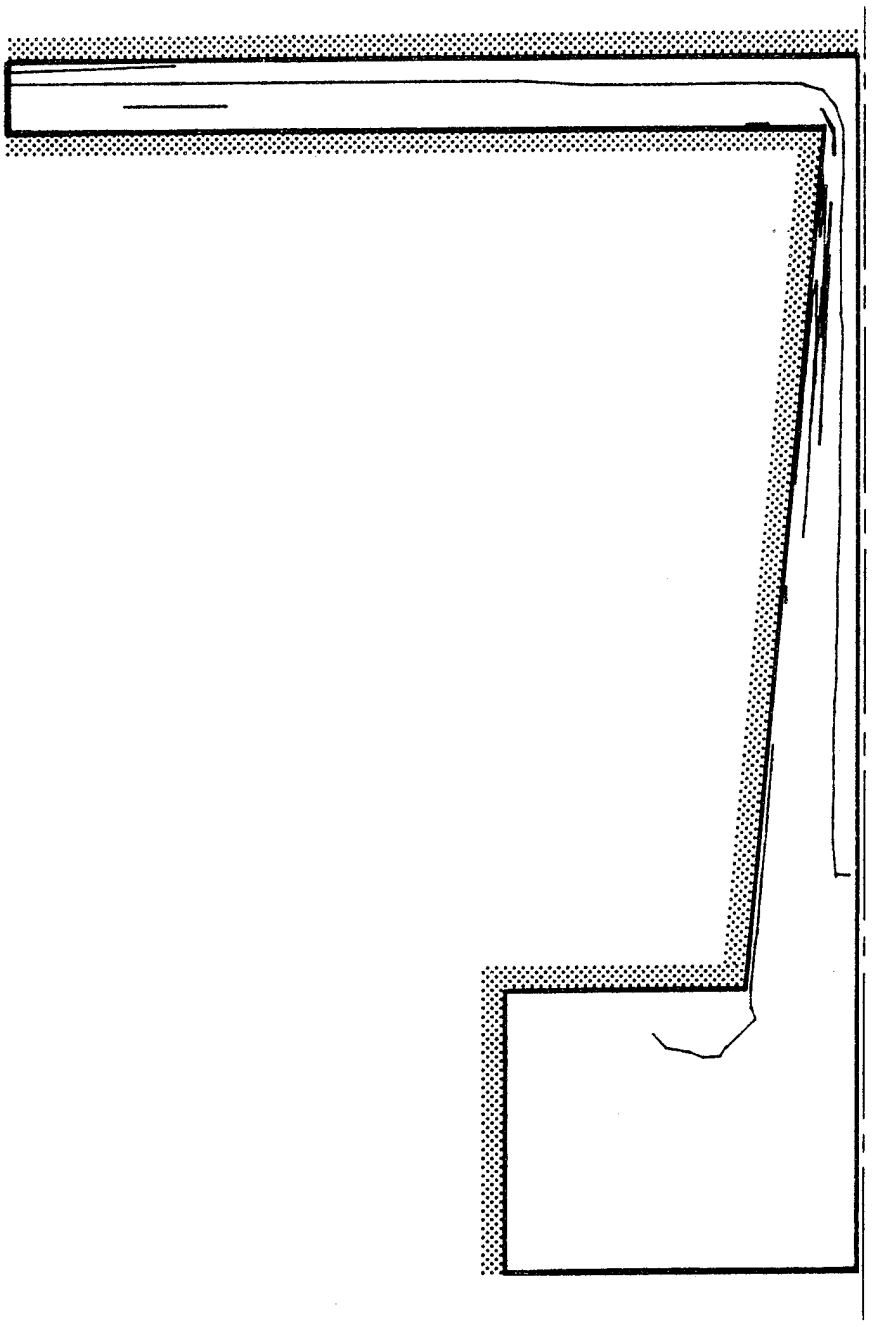

Figure 4.26 Contours of f_p=0.999 in axisymmetric disk molding simulation

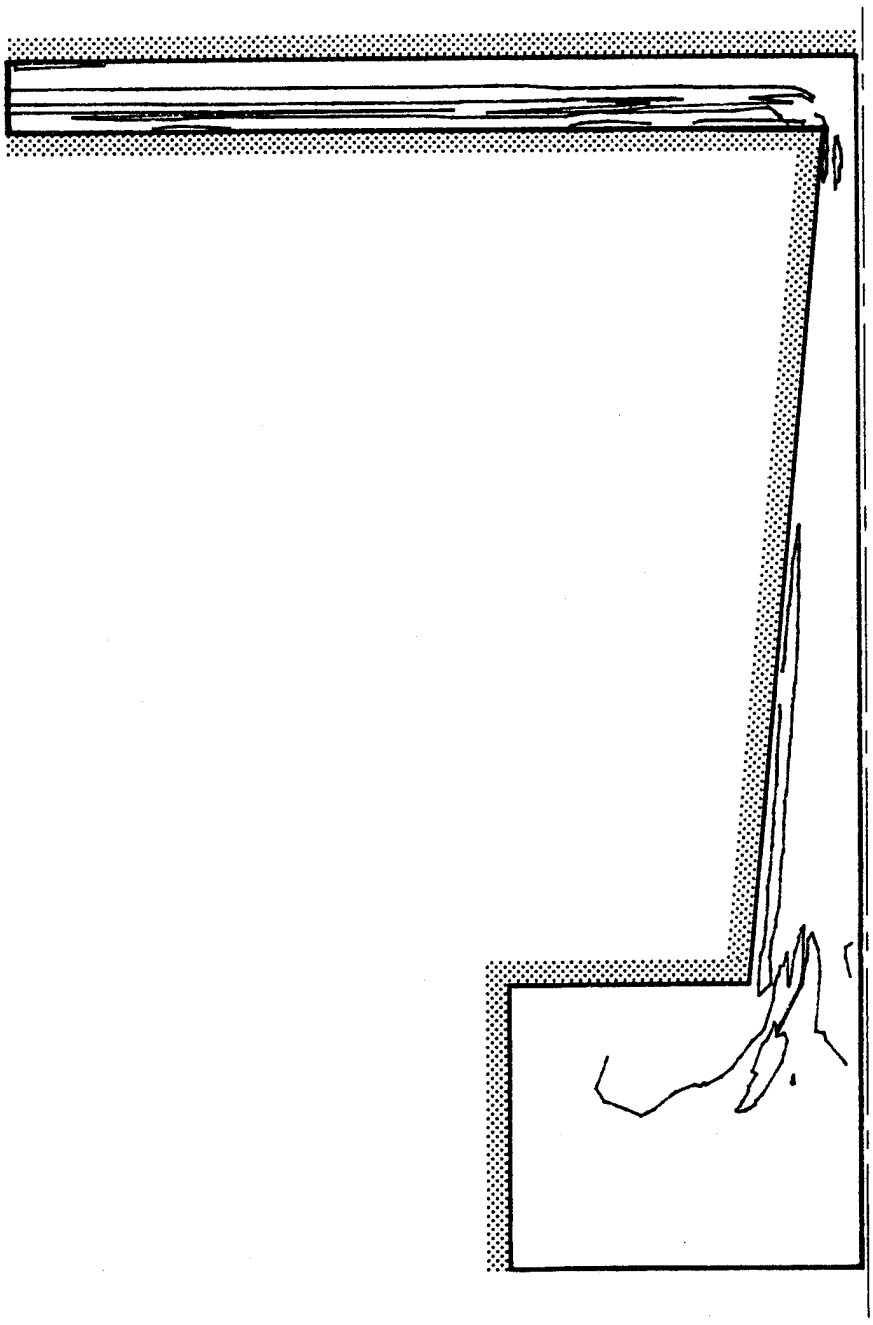

Figure 4.27 Contours of f_p=0.9 in axisymmetric disk molding simulation

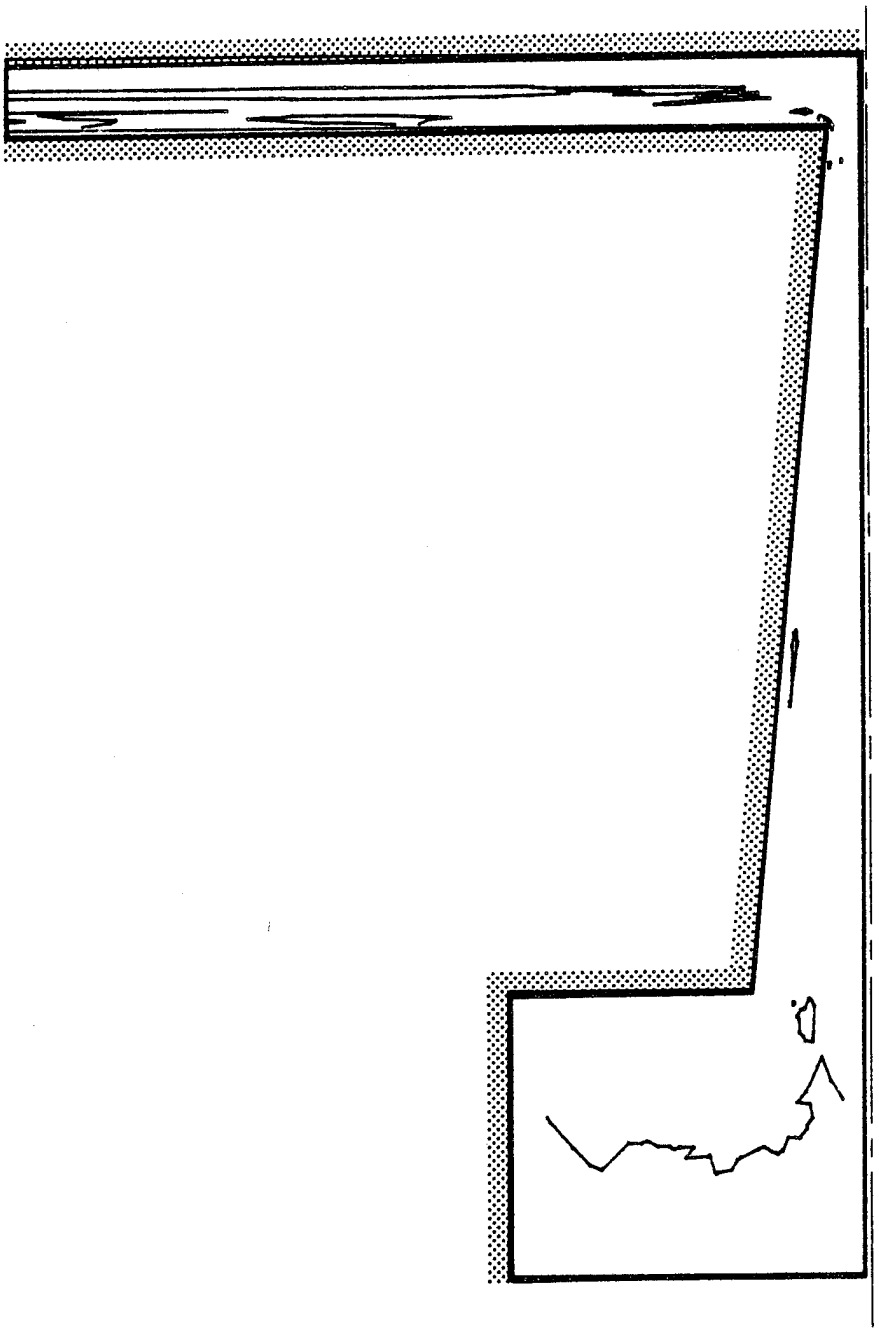

Figure 4.28 Contours of f_p=0.6 in axisymmetric disk molding simulation

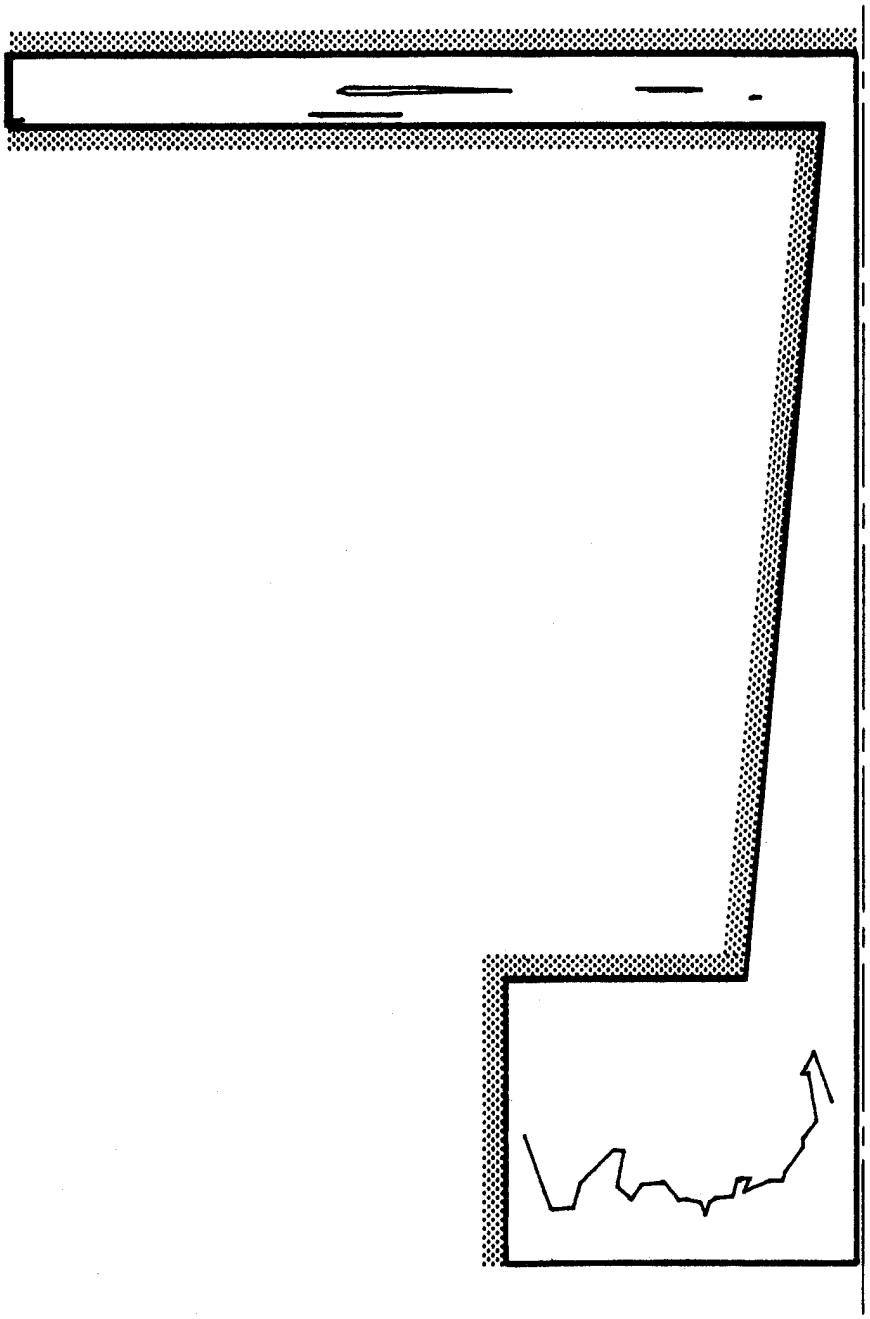

Figure 4.29 Contours of f_p=0.3 in axisymmetric disk molding simulation

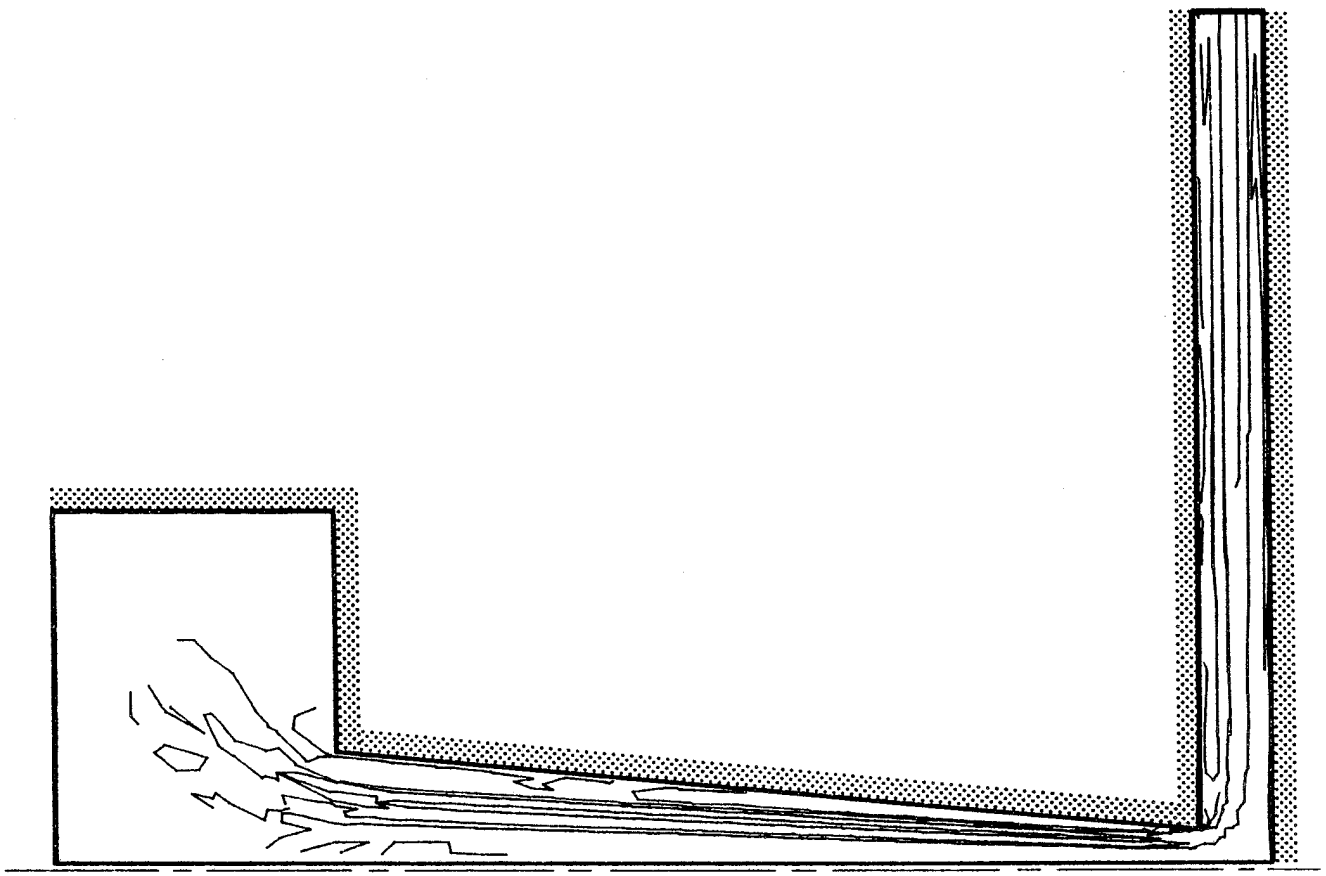

$\alpha°$ is measured in radians

Figure 4.30 Contours of $\alpha°=0$ in axisymmetric disk molding simulation

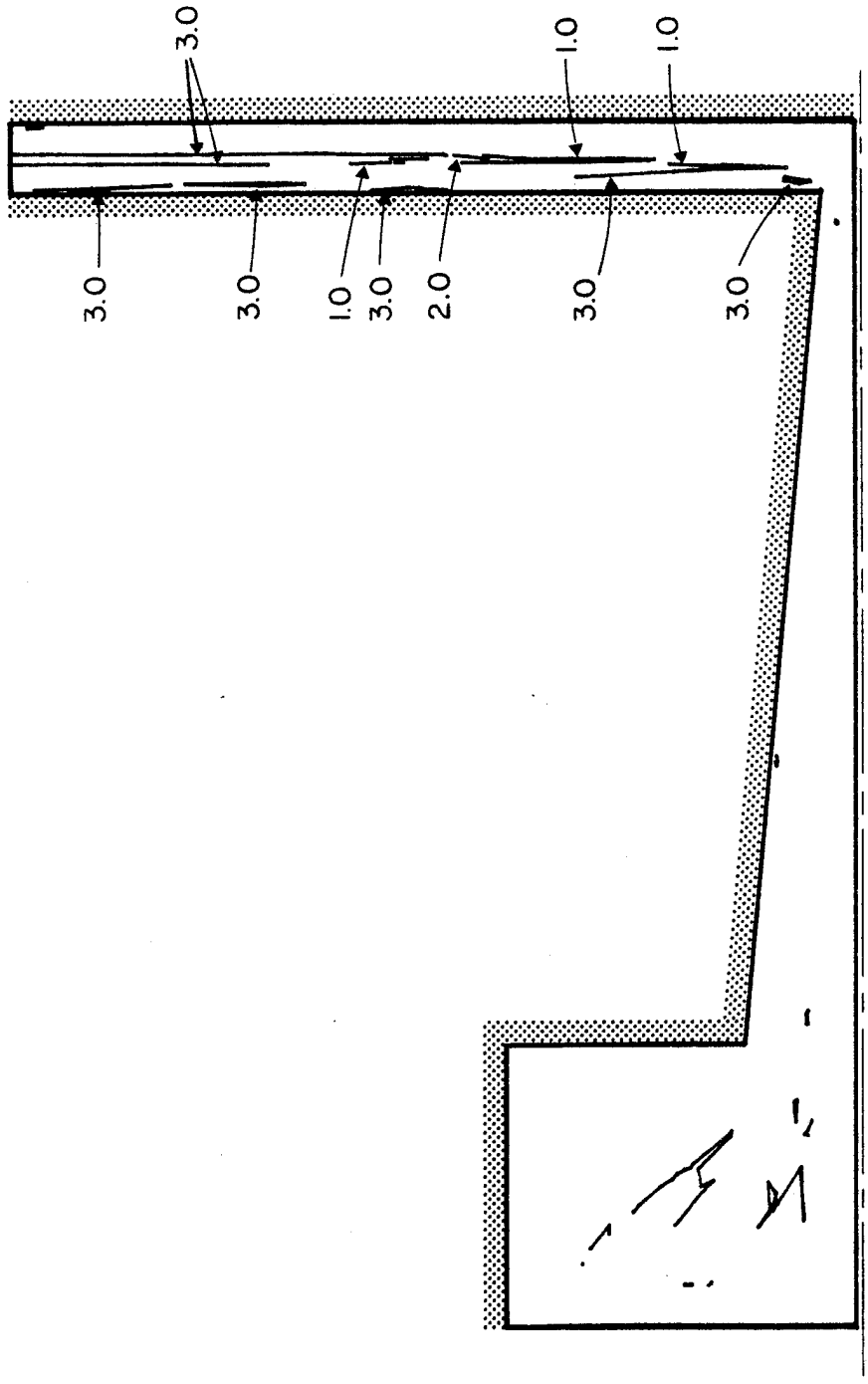

Figure 4.31 Contours of $\alpha°$=1.0, 2.0, 3.0 in axisymmetric disk molding simulation

$\alpha°$ is measured in radians

Figure 4.32 Experimentally observed fiber orientation in an axisymmetric disk

CHAPTER 5. CONCLUSIONS

A numerical method has been developed for determining the fiber orientation in arbitrary plane and axisymmetric flows. The resulting fiber dispersion is depicted by orientation parameters, which relate the degree of fiber alignment to the material properties. In axisymmetric flow, non-planar distributions are treated while only planar distributions are allowed in plane flow. The validity of the numerical method was proved by comparing numerical results with known analytical solutions.

Several examples were considered. In Poiseuille flow, a distinct boundary layer of aligned fibers parallel to the flow streamlines was shown to exist in the wall region. This prediction correlates well with experimental observations. It was determined that the presence of a circular inclusion lead to boundary layer of aligned fibers adjacent to and downstream from the insert. A prediction for the fiber orientation in an axisymmetric disk was established. The prediction correlated well with experimental observations in the wall region of the disk and the discrepancy in the central region could be explained by

the failure of the theory to account for fiber interactions.

Several extensions to the theory are possible. A more elaborate procedure to determine the principal material axes in non-planar distributions should be developed. In the axisymmetric flow examples presented in Section 4.4, it was assumed that the z axis represented a local principal material direction. Clearly, this assumption in invalid for many flows, and a procedure needs to be developed to determine the principal axes from the orientations of a finite number of fibers. One possible method of attack is to assume that the peak in the orientation density function defines one principal axis and develop a procedure to determine the peak. Having found one principal axis, the problem is no more difficult than the determination of the principal axes in a planar distribution.

A second extension involves the determination of the effect of the fiber orientation on the viscosity of the suspension. If this effect is significant, then an iterative scheme would be necessary to determine the fiber orientation, as duscussed in Section 2.1.

Givler [5] has discussed several other possible extensions to the theory, including studying three-dimensional and transient flows and determining the

orientation equations for a viscoelastic suspending medium. These extensions enable more accurate simulation of the molding processes.

REFERENCES

1. Bird, R. B., Stewart, W. E. and Lightfoot, E. N., Transport Phenomena, John Wiley and Sons, 1960.

2. Crochet, M. J., Finite Element Methods for Solids and Fluids, unpublished.

3. Denn, M. M., Process Fluid Mechanics, Prentice Hall, 1980.

4. Ellery, S. A., "Composition Induced Fiber Orientations and a Determination of the Flow Processes in Transfer and Injection Molded Thermosets," Center for Composite Materials, Internal Report, Univ. of Delaware, 1982.

5. Givler, R. C., "Numerically Predicted Fiber Orientations in Dilute Suspensions," Master's Thesis, Univ. of Delaware, 1981.

6. Goettler, L. A., Leib, R. L. and Lambright, A. J., "Short Fiber Reinforced Hose - A New Concept in Production and Performance," Rubber Chemistry and Technology, 52, no. 4, 1979.

7. Goldsmith, H. and Mason, S. G., in Rheology: Theory and Application, edited by Eirich, F. R., Academic Press, 1967.

8. Hawkins, G. A., Multilinear Analysis for Students in Engineering and Science, John Wiley and Sons, 1963.

9. Jeffery, G. B., "The Motion of Ellipsoidal Particles Immersed in a Viscous Fluid," Proc. Roy. Soc., A 102, 161, 1922.

10. Maschmeyer, R. O. and Hill, C. T., "Rheology of Concentrated Suspensions of Fibers in Tube Flow," Trans. Soc. Rheol., 21, 183, 195, 1977.

11. McCullough, R. L., "Anisotropic Behavior of Crystalline Polymers," Treatise on Materials Science and Technology, 10, part B, 453, 1977.

12. McCullough, R. L., Introduction to the Statistical Analysis of Experimental Data, unpublished.

13. McCullough, R. L., Pipes, R. B. and Whitney, J. M., Analytical Methods for Composite Materials: Thermoelastic, Transport and Strength Properties, unpublished.

14. McGee, S., "The Influence of Microstructure on the Elastic Properties of Composite Materials," Ph.D. Thesis, University of Delaware, 1982.

APPENDIX 1

INVESTIGATION OF THE SYMMETRY OF AN ORIENTATION DISTRIBUTION

In developing the orientation parameters, the orientation distribution has been assumed to be symmetric about the mode. In this appendix, the validity of this assumption is investigated for planar distributions in the plane Poiseuille flow example in Section 3.5.1. A random fiber orientation distribution is input at the beginning of the ψ=-0.29 streamline and the skewness of the distribution is studied at selected locations downstream. The degree of skewness is described by the coefficient of skewness (a_3) defined by

$$a_3 = M_3/(M_2)^{3/2}$$

where M_2 and M_3 are the second and third central moments, respectively, defined by

$$M_i = \frac{1}{N} \sum_{j=1}^{N} (\phi_{1_j} - \bar{\phi}_1)^i$$

The coefficient of skewness is determined for varying numbers of fibers.

Figures A1.1, A1.2, and A1.3 depict the orientations of 100 initially random fibers at 0.5, 1.0, and 1.5 inches downstream, respectively, from the random end. Also presented in these figures are the numerically computed mode angles. In Figure A1.4, the magnitude of a_3 is plotted as a function of the number of fibers at these same locations. It is readily observed that $|a_3|$ decreases to small values as the number of fibers is increased. Since the orientation distribution function is more accurately modelled by larger numbers of fibers, it may be concluded that the assumption of symmetric distributions is valid for this example. While the conclusions from this specific example cannot be extended to other flows, the results do lend credence to the assumption of symmetric distributions.

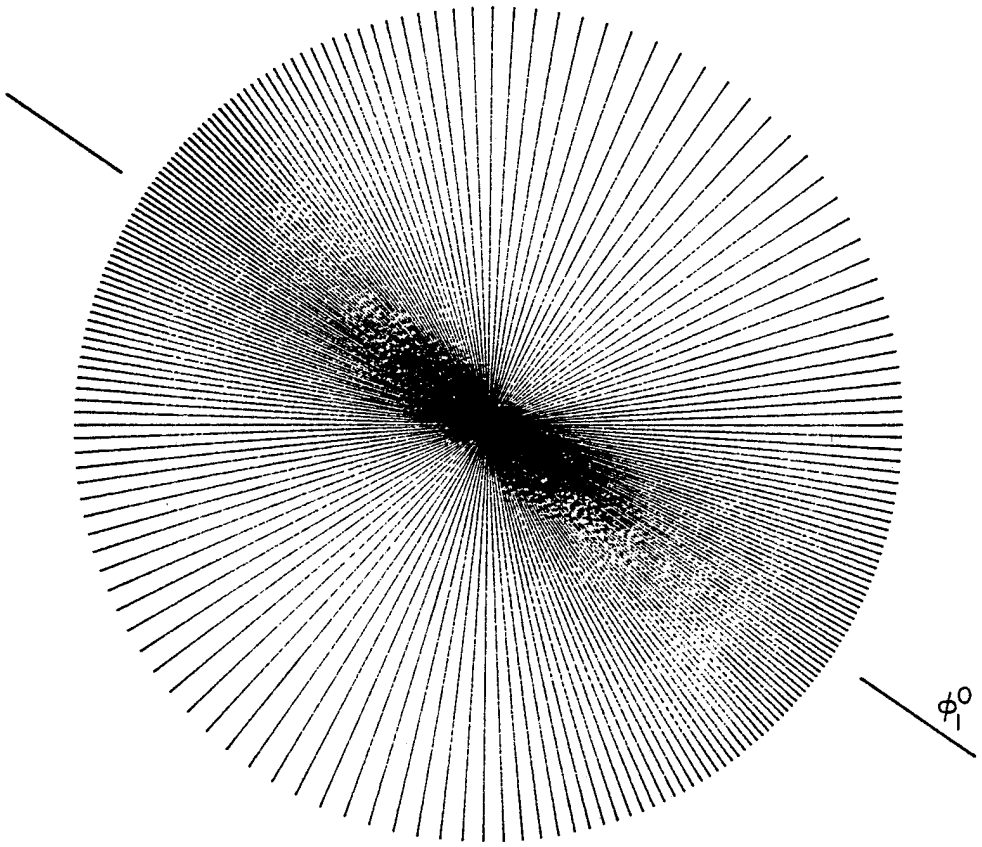

Figure A1.1 Distribution of 100 initially random fibers in plane Poiseuille flow at a location 0.5 inches downstream along the ψ=-0.29 streamline

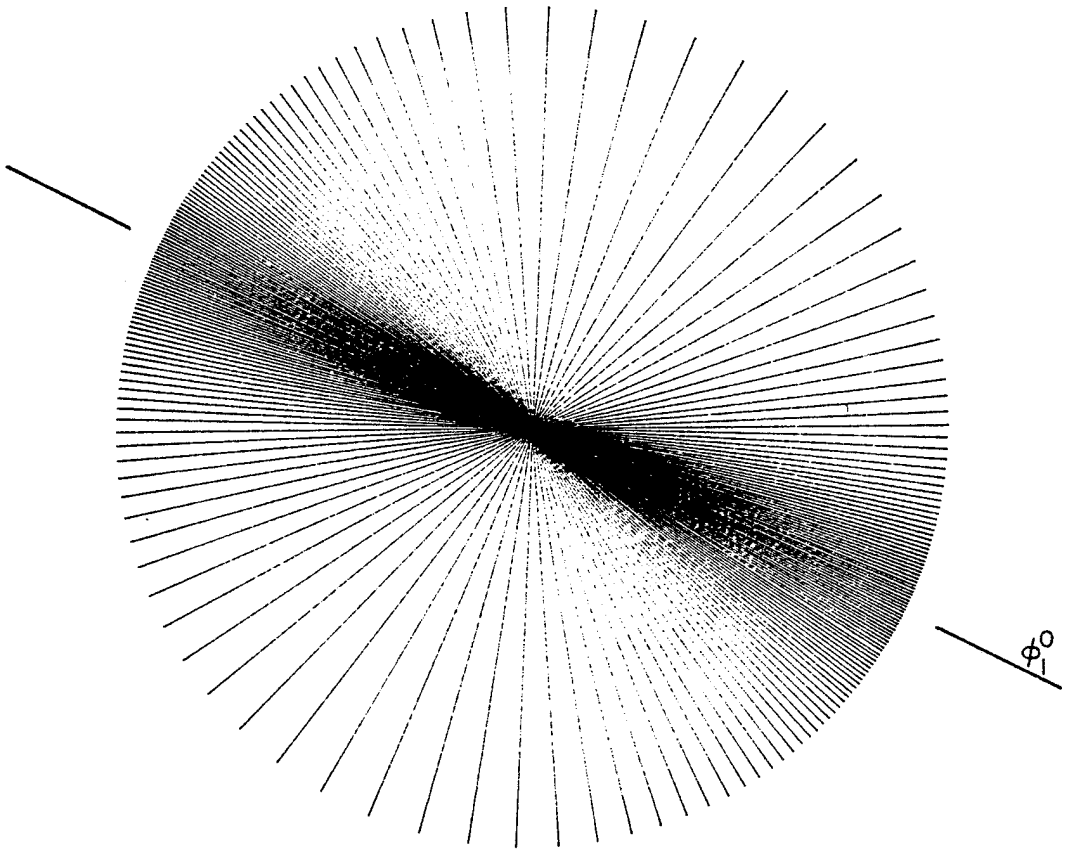

Figure A1.2 Distribution of 100 initially random fibers in plane Poiseuille flow at a location 1.0 inch downstream along the ψ=-0.29 streamline

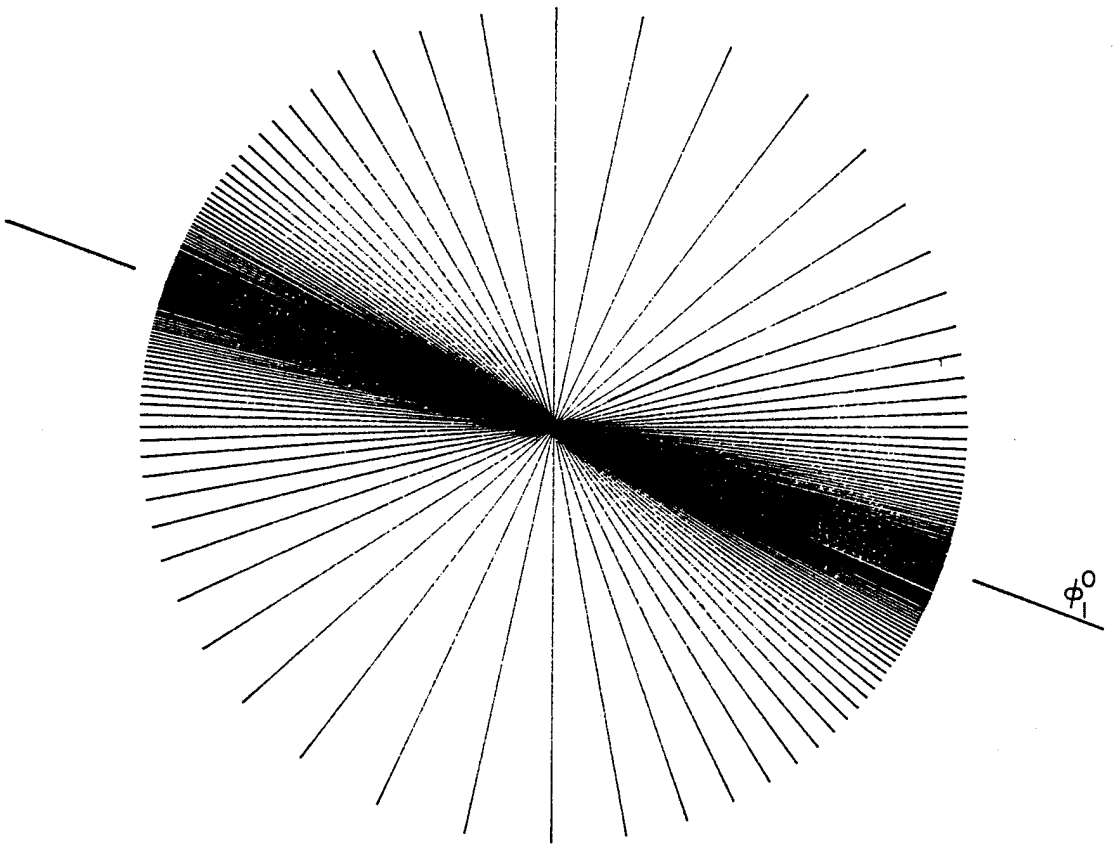

Figure A1.3 Distribution of 100 initially random fibers in plane Poiseuille flow at the location 1.5 inches downstream along the ψ=-0.29 streamline

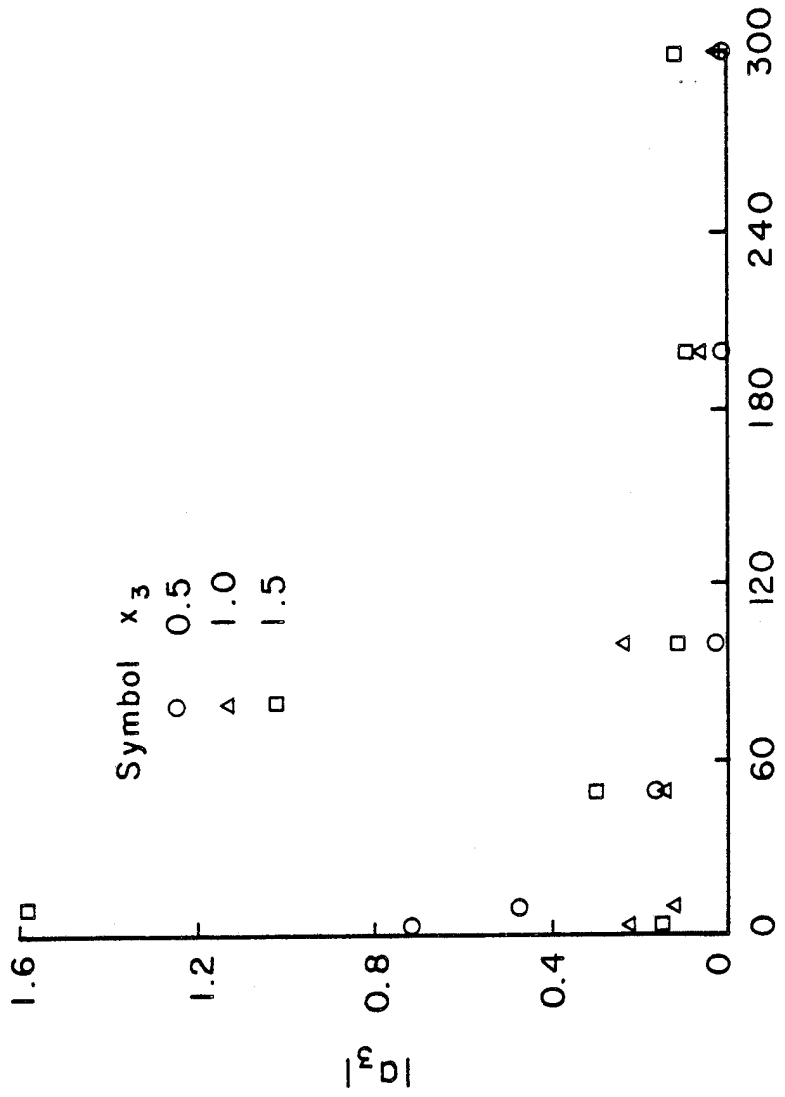

Figure A1.4 $|a_3|$ vs. number of fibers

APPENDIX 2

INVESTIGATION OF NUMBER OF FIBERS NEEDED TO ACCURATELY PREDICT ORIENTATION PARAMETERS

In using the numerical orientation model, one needs an estimate of how many fibers are needed to adequately model the distribution and thus give accurate estimates for both the mode angle and orientation parameters. Obviously, if too few fibers are used, grossly inaccurate results may be obtained. On the other hand, too many fibers leads to wasted computer time.

For this investigation, orientations were studied at selected locations along the ψ=-0.29 streamline in the plane Poiseuille flow example presented in Section 3.5.1. These locations are identical to those studied in Appendix 1. Plots of ϕ_1° , f_p , and g_p as a function of the number of fibers are presented in Figures A2.1 through A2.3, respectively, for locations 0.5, 1.0, and 1.5 inches downstream from the initial point in the streamline, where a random orientation state is input. It can be seen from the figures that all parameters attain fixed values at all locations when the number of fibers exceeds 50. To

determine the dependence on numbers of fiber for fewer than 50 fibers, magnified plots are presented in Figures A2.4 through A2.6. From these figures, one can conclude that in all cases, as few as 10 fibers provide accurate predictions for all the parameters. This result is very encouraging in light of the fact that it is desirable to work with as few fibers as possible.

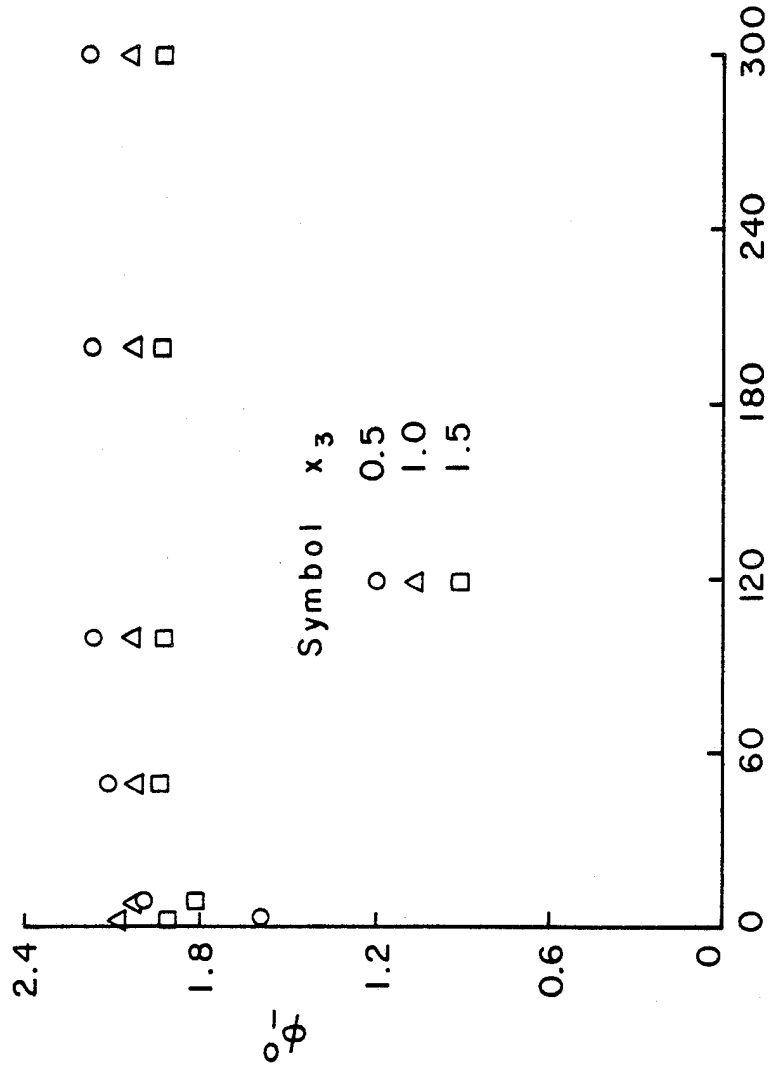

Figure A2.1 ϕ_1° vs. number of fibers

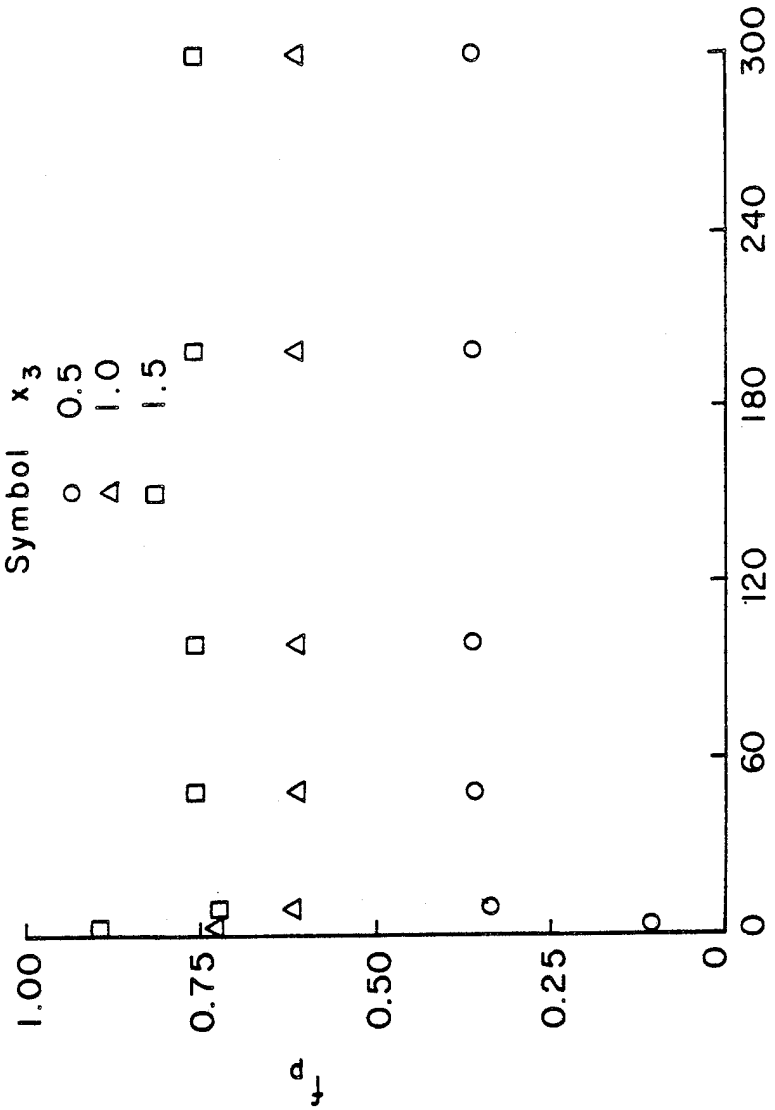

Figure A2.2 f_p vs. number of fibers

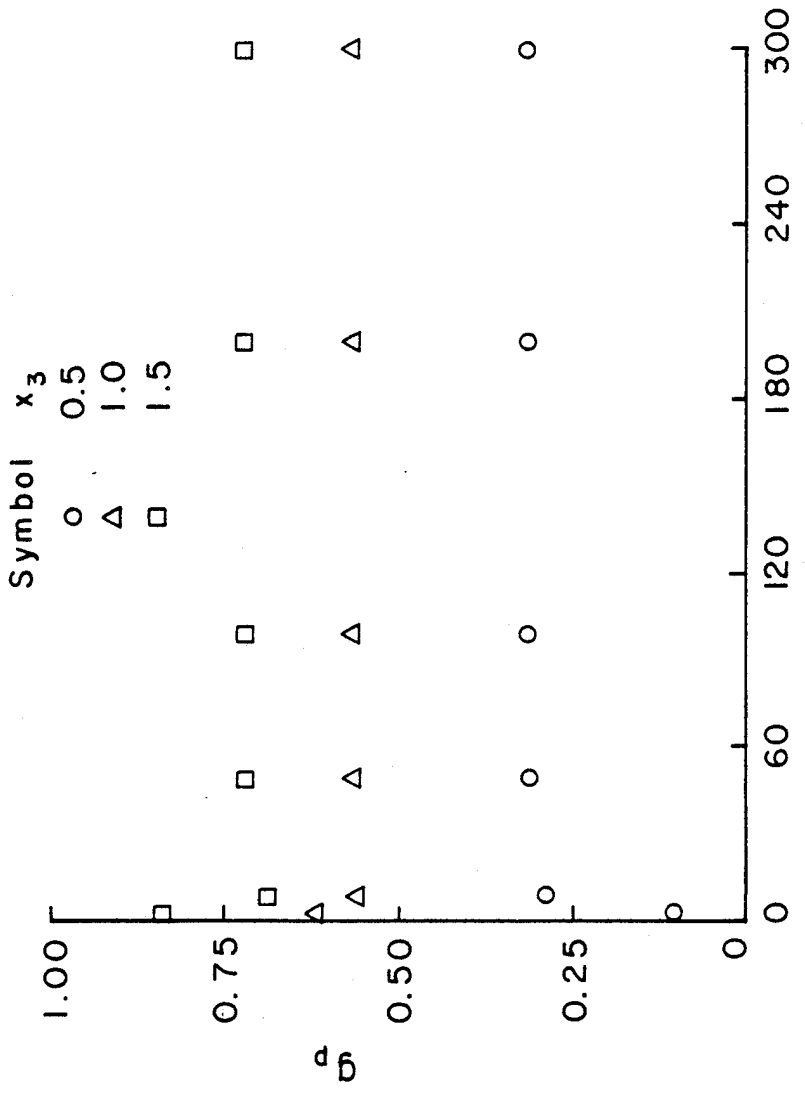

Figure A2.3 q_p vs. number of fibers

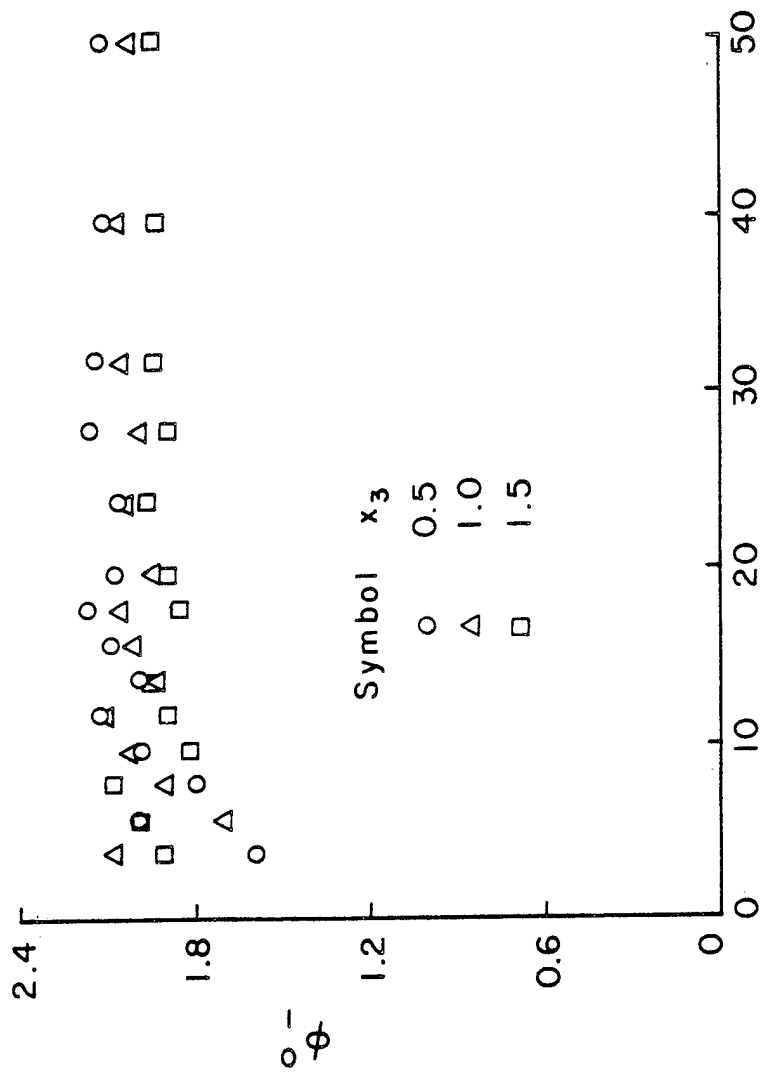

Figure A2.4 Magnified plot of ϕ_1° vs. number of fibers

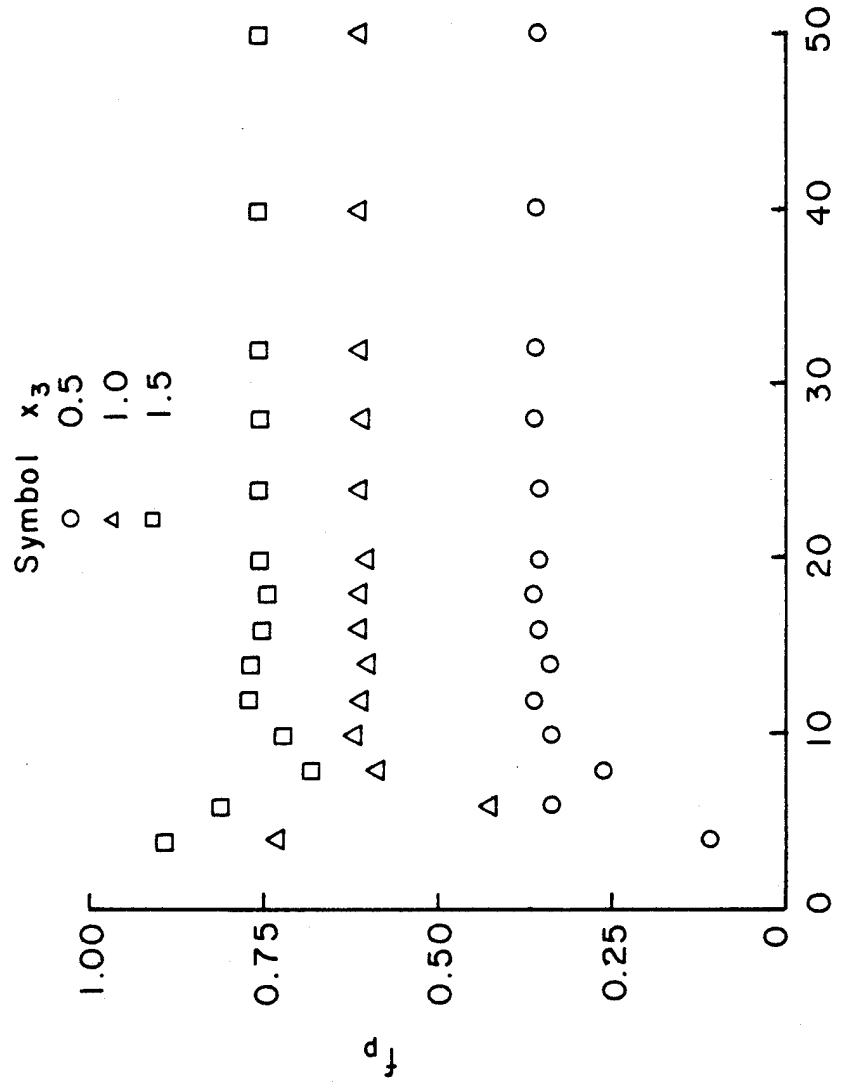

Figure A2.5 Magnified plot of f_p vs. number of fibers

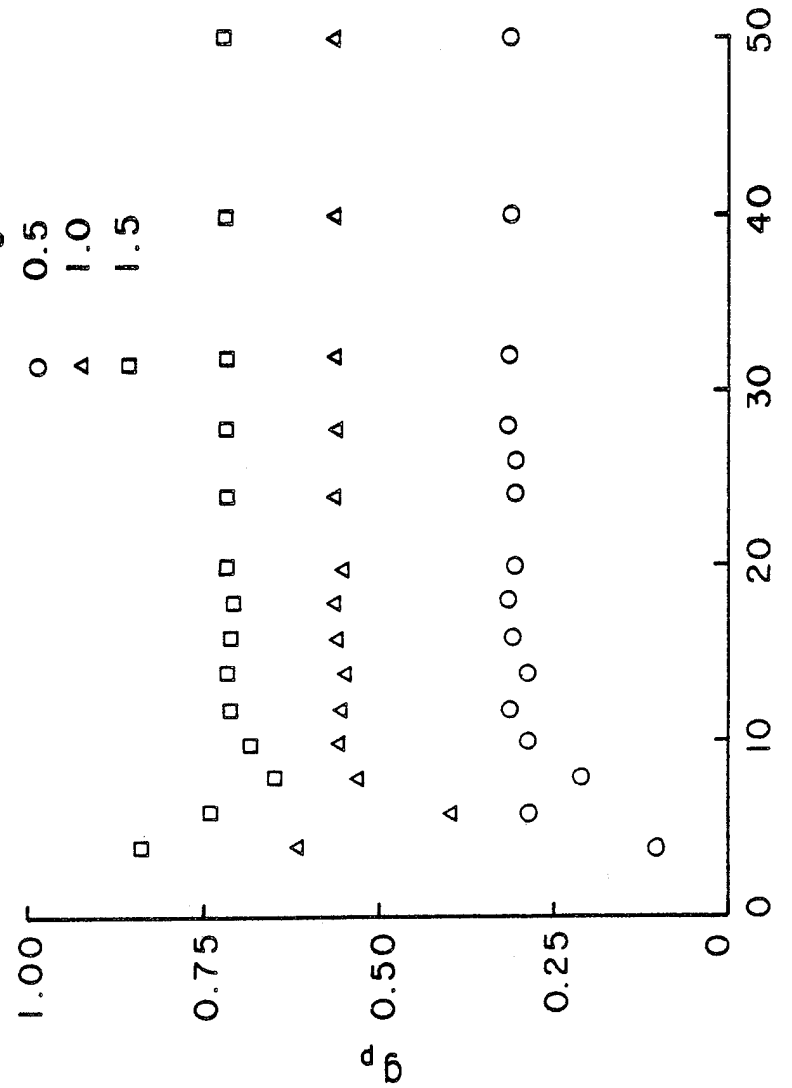

Figure A2.6 Magnified plot of g_p vs. number of fibers